

**Development of Dual Stimuli-responsive Degradable  
Polylactide-based Multifunctional Materials for Drug  
Delivery**

**Kamaljeet Kaur Bawa**

A Thesis  
In the Department  
Of  
Chemistry and Biochemistry

Presented in Partial Fulfillment of the Requirements for the Degree of  
Doctor of Philosophy (Chemistry) at Concordia University  
Montréal, Quebec, Canada

**July 2021**

**© Kamaljeet Kaur Bawa, 2021**

# CONCORDIA UNIVERSITY

## School of Graduate Studies

This is to certify that the thesis prepared By: Kamaljeet Kaur Bawa

Entitled: **Development of Dual Stimuli-responsive Degradable Polylactide-based Multifunctional Materials for Drug Delivery**

and submitted in partial fulfillment of the requirements for the degree of

### Doctor of Philosophy (Chemistry)

complies with the regulations of the University and meets the accepted standards with respect to originality and quality.

Signed by the final examining committee:

\_\_\_\_\_  
Dr. Peter John Darlington Chair

\_\_\_\_\_  
Dr. Michael Serpe External Examiner

\_\_\_\_\_  
Dr. Xia Li External to Program

\_\_\_\_\_  
Dr. Jung Kwon Oh Thesis Supervisor

\_\_\_\_\_  
Dr. Louis Cuccia Examiner

\_\_\_\_\_  
Dr. Chris Wilds Examiner

Approved by

\_\_\_\_\_  
Dr. Yves Gélinas, Graduate Program Director

7/28/2021

\_\_\_\_\_  
Dr. Pascale Sicotte, Dean  
Faculty of Arts and Science

## **Abstract**

### **Development of Dual Stimuli-responsive Degradable Polylactide-based Multifunctional Materials for Drug Delivery**

**Kamaljeet Kaur Bawa, Ph.D. Chemistry  
Concordia University, 2021**

Progress in the synthesis of amphiphilic block copolymers has contributed to promising advances in the construction of smart nanocarriers for anticancer drug delivery systems. Their excellent features such as biodegradability through enzymatic hydrolysis and biocompatibility have led to tremendous applications in the biomedical field. Polylactide (PLA) is a biocompatible and FDA-approved polymer which has been used as hydrophobic core-forming block in drug delivery vehicles. However, hydrophobicity and slow degradation are the two main drawbacks that limits its usage in drug delivery systems. An introduction of stimuli-responsive degradable (SRD) platform into the design of PLA-based polymeric drug delivery systems can overcome these challenges as they can precisely tune drug release kinetics to fit the therapeutic window of the encapsulated drug. However, most of the smart PLA-based block copolymers are designed to respond to a single stimulus and therefore, multi-stimuli responsive degradable systems in which the location, number and type of degradable linkages can be varied needs to be developed.

My PhD research was focused on the studies of dual stimuli-responsive degradation (DSRD) platform to synthesize advanced PLA-based nanomaterials. They were featured with different types and location of labile linkages, that cleaved in response to biological stimuli found in cancer cells and tumor tissues. In this thesis, I had developed robust strategies that allowed for the synthesis of three novel PLA-based SRD copolymers designed with a) reduction-responsive disulfide linkage and b) an acid-labile linkage. These synthetic strategies utilized a combination of ring opening polymerization (ROP), atom transfer radical polymerization (ATRP) and facile coupling reactions. The results demonstrated the feasibility to design and synthesize smart DSRD-based block copolymers which self-assemble to form colloiddally-stable micellar aggregates and encapsulate hydrophobic dyes or drugs in the hydrophobic cores. Furthermore, the SRD-driven enhanced/controlled release of loaded cargoes suggested that DSRD strategy can offer the versatility and hold great potential in the development of intracellular drug delivery nanocarriers.

## Acknowledgements

I would like to express my sincere gratitude to my supervisor, Dr. Jung Kwon (John) Oh for his valuable guidance and encouragement throughout my PhD program. With his great enthusiasm, he continuously taught and motivated me to become a better researcher. I am also thankful to my committee members Dr. Louis Cuccia and Dr. Christopher Wilds for their valuable questions and suggestions in the annual committee meetings. I would like to thank my examination committee, Dr. Michael Serpe and Dr. Xia Li for taking the time to read and evaluate my thesis.

Throughout the five years of PhD, I have been fortunate to work with amazing mentors and colleagues. I would like to thank all the current and former members in OH research group and my friends in Chemistry Department. I would like to specifically extend my gratitude to Arman Moini Jazani, Depannita, Dr. Sungmin Jung, Twinkal Patel, Peter Liu, Zujhar Singh, Newsha Arezi, Chaitra Shetty, Keaton, Xiaolei, Kadambari and Dr. Pothana Gandhi for their help and moral support.

I thank Concordia University, Natural Sciences and Engineering Research Council of Canada (NSERC), Fonds de recherche du Québec - Nature et technologies (FRQNT), Polymer Nanoparticles for Drug Delivery (PoND) for funding this research.

I would like to thank my family and especially acknowledge my parents Mr. Jatinder Singh Bawa and Mrs. Rajnish Kaur Bawa and my brother Kunwardeep Singh Bawa for believing in me and standing by my decisions and celebrating every milestone I ever achieved. I owe my success to you, and I would not be where I am without your endless love. My uncle Dr. Harpreet Sodhi, who always stood with me like rock and believed in me since childhood, thank you so much for believing in me.

My friends Ishika, Kritika, Gaganpreet, Indu, Amanpuneet, Assad, Sonu, Urvi and Bhavpreet uplifted my spirit in the challenging times and made me smile throughout this journey.

Most importantly, this work is dedicated in loving memory of my aunt Dr. Anita Sodhi.

## Contribution of Authors

Most of the research presented in this thesis was conducted by the author of this thesis under the supervision of Prof. Jung Kwon (John) Oh. Chapters 2, 3 and 4 are reproduced in part or whole from original articles with the permission from the publishers. Here are the specific contributions of collaborators.

Chapter 2: Stimuli-responsive degradable polylactide-based block copolymer nanoassemblies for controlled/enhanced drug delivery, *Molecular Pharmaceutics* 2017, 14, 2460-2474.

Chapter 3: PLA-Based Triblock Copolymer Micelles Exhibiting Dual Acidic pH/Reduction Responses at Dual Core and Core/Corona Interface Locations, *Macromolecular rapid communications* 2018, 1800477.

*Contributions:* Arman Moini Jazani (PhD student) synthesized and characterized A1 molecule. Chaitra Shetty (M.Sc. student) conducted the cell viability studies by MTT assay.

Chapter 4: Synthesis of degradable PLA-based diblock copolymers with dual acid/reduction-cleavable junction, *Polymer* 2020, 194, 122391.

*Contributions:* Arman Moini Jazani (PhD student) synthesized and characterized the initiator Br-AC-SS-OH. Dr. Ye helped in data analyses and manuscript preparation.

Chapter 5 (Contributions): Xiaolei Hu (M.Sc. student) and Arman Moini Jazani synthesized and characterized PEG-SS-OH.

## Table of Contents

List of Figures .....	x
List of Tables .....	xv
List of Abbreviations .....	xvi
Chapter 1 .....	1
Introduction and Statement .....	1
1.1. Emergence of drug delivery systems .....	1
1.2. Polymeric NPs as effective drug delivery nanocarriers .....	2
1.3. PLA as promising material .....	3
1.4. Objectives .....	5
Chapter 2 .....	8
Stimuli-responsive degradable PLA-based block copolymer nanoassemblies for controlled/enhanced drug delivery .....	8
2.1. Introduction.....	8
2.2. Conventional PLA and PLA-based ABP assemblies.....	9
2.2.1. Synthesis and properties of PLA.....	9
2.2.2. General strategies to PLA-based ABPs and their assemblies .....	10
2.3. SRD for enhanced release .....	12
2.3.1. General concept of SRD .....	12
2.3.2. General approaches to SRD-exhibiting ABPs and their assemblies.....	14
2.4. Strategies to reduction-responsive PLA-based ABP systems .....	16
2.4.1. Direct polymerization strategy.....	16
2.4.2. Covalent coupling strategy.....	21
2.4.3. Drug-polymer conjugation strategy .....	23
2.5. Strategies to acidic pH-responsive PLA-based ABP systems.....	24
2.5.1. Sheddable and prodrug strategies .....	24
2.5.2. Strategy to acidic pH-responsive volume change .....	26
2.6. Intracellular tumor-targeting drug delivery.....	27
2.7. Summary and outlook .....	30
2.8 Recent literature update .....	31
2.8.1. Reduction-responsive PLA-based systems .....	31
2.8.2. Strategy to synthesize photo-responsive PLA-based ABP systems.....	33
2.8.3. Triple-stimuli responsive PLA-based ABP systems.....	34

2.8.4. Reactive oxygen species (ROS)-responsive PLA-based ABP systems .....	34
2.8.5. Dual pH/reduction-responsive PLA-based polyplexes for siRNA delivery .....	35
2.8.6. SRD-based self-immolative nps for controlled drug release .....	35
Chapter 3.....	36
PLA-based triblock copolymer micelles exhibiting dual acidic pH/reduction responses at dual core and core/corona interface locations .....	36
3.1. Introduction.....	36
3.2. Instrumentation .....	38
3.2.1. Experimental .....	38
3.2.2. Materials .....	39
3.2.3. Synthesis of (co)polymers.....	39
3.2.4. Aqueous micellization.....	40
3.2.5 Studies of dual acidic pH/reduction-responsive degradation.....	41
3.2.6. Dual stimuli-responsive release of NR from NR-loaded micelles.....	41
3.2.7. Cytotoxicity of P4 micelles using MTT assay .....	42
3.3. Results and Discussion .....	42
3.4. Conclusion .....	51
3.5. Supporting figures.....	52
Chapter 4.....	56
Synthesis of degradable PLA-based diblock copolymers with dual acid/reduction-cleavable junction.....	56
4.1. Introduction.....	56
4.2. Experimental .....	58
4.2.1. Instrumentation .....	58
4.2.2. Materials .....	59
4.2.3. General procedure for ATRP .....	59
4.2.4. General procedure for a tin-catalyzed ROP of LA.....	60
4.2.5. Synthesis of P6 by reaction of P5 with SA .....	60
4.2.6. Synthesis of P7 by reaction of P6 with Br-AC-SS-OH.....	60
4.2.7. Determination of critical micellar concentration (CMC).....	61
4.2.8. Aqueous micellization.....	61
4.2.9. Investigation of acidic pH/reduction-responsive degradation.....	61
4.3. Results and discussion .....	61
4.3.1. An initial unsuccessful approach involving a tin-catalyzed ROP initiated with an acetal initiator.....	61

4.3.2. Alternative approach to synthesis of well-controlled PLA-SS-AC-POEOMA block copolymer .....	67
4.3.3. Investigation of aqueous micellization and acid/reduction-responsive degradation.....	70
4.4. Conclusion .....	72
4.5. Supplementary Information .....	72
Chapter 5.....	77
Synthetic method and drug release evaluation of GSH-degradable PEG-SS-PLA block copolymer nanoassemblies .....	77
5.1. Introduction.....	77
5.2. Experimental.....	78
5.2.1. Materials. ....	78
5.2.2. Synthesis of PEG-Cl (A1).....	78
5.2.3. Synthesis of PEG-N3 (A2).....	78
5.2.4. Synthesis of A3.....	79
5.2.5. Synthesis of PEG-SS-OH/I.....	79
5.2.6. Synthesis of monoprotected 2-hydroxyldisulfide (OH-SS-Ketal, B1).....	79
5.2.7. Synthesis of PEG-SS-OH/II.....	79
5.2.8. General procedure for ring opening polymerization (ROP) of LA.....	80
5.2.9. Investigation of reduction-responsive degradation.....	80
5.2.10. Determination of CMC using NR probe method.....	81
5.2.11. Aqueous micellization.....	81
5.2.12. Preparation of PTX-loaded micelles.....	81
5.2.13. Determination of loading of PTX in PTX-loaded micelles.....	81
5.2.14. <i>In vitro</i> PTX release.....	82
5.3. Results and discussion .....	82
5.3.1. Synthesis of PEG-SS-OH.....	82
5.3.2. Synthesis of PEG-SS-PLA.....	86
5.3.3. Reduction-responsive degradation.....	87
5.3.4. Aqueous micellization.....	88
5.3.5. GSH-responsive release of PTX using HPLC technique.....	89
5.4. Conclusion .....	90
5.5. Supporting Figures and Table.....	91
Chapter 6.....	94
Summary and recommendations for future work.....	94
6.1. Summary of thesis.....	94

6.2. Future works .....	95
References.....	97

## List of Figures

<b>Figure 1.1.</b> Types of nanocarriers for drug delivery systems. <sup>4</sup> .....	1
<b>Figure 1.2.</b> Coordination-insertion mechanism of ROP of lactide <sup>14</sup> .....	4
<b>Figure 1.3.</b> Overall objectives of doctoral thesis. X and Y refers to the linkages responsive to different types of stimuli.....	6
<b>Figure 2.1.</b> ROP of LA to synthesize PLA (a) and stereochemistry (tacticity) of PDLA, PLLA, and PDLLA (b). .....	10
<b>Figure 2.2.</b> Schematic illustration of conventionally-designed PLA-based ABPs with hydrophilic blocks such as PEG, poly(amino acid), polysaccharide, and polymethacrylate (a) and their self-assembly to form micellar aggregates with PLA cores surrounded with hydrophilic coronas (b). .....	11
<b>Figure 2.3.</b> Degradable linkages including reduction, enzyme, and acidic pH-responsive cleavable as well as photo-labile linkages. ....	13
<b>Figure 2.4.</b> General approaches to synthesize SRD-exhibiting block copolymers and their self-assembled nanostructures as single location (a), dual location SRD (b), and multiple location multiple SRD (c) approaches. ....	15
<b>Figure 2.5.</b> Synthetic route to a double-head initiator of OH-SS-Br for both ROP of LA and ATRP of methacrylates, well-controlled PLA-SS-Br by ROP of LA, and PLA-SS-based ABPs by ATRP in the presence of PLA-SS-Br macroinitiator.....	17
<b>Figure 2.6.</b> Schematic illustration of synthesis of PLA-SS-based interlayered crosslinked micelles for enhanced colloidal stability and shedding extended coronas for rapid release of encapsulated anticancer drugs, based on PLA-SS-PHMssEt-b-POEOMA triblock copolymers having multiple pendant disulfides in the interlayer and single disulfides at junctions of PHMssEt and POEOMA blocks in aqueous solution. <sup>20</sup> Copyright 2013 Royal Society of Chemistry.....	18
<b>Figure 2.7.</b> Synthetic routes to novel PLA-based mono-cleavable and dual location SRD-exhibiting ABPs functionalized with disulfide linkages.....	20
<b>Figure 2.8.</b> For SS(PLA-SS-POEOMA) triblock copolymer, reduction-responsive cleavage of disulfides in the presence of DL-dithiothreitol (a), dynamic light scattering diagrams and transmission electron microscopy images of the micelles before and after treatment with 10 mM GSH at 1.2 mg/mL (b), and enhanced release of DOX from DOX-loaded micelles in the absence (control) and presence of 10 mM GSH (c). <sup>154</sup> Copyright 2014 American Chemical Society.....	20
<b>Figure 2.9.</b> Schematic illustration of redox-responsive biodegradable polymersomes comprising of PEG-SS-PLA-SS-PLA-SS-PEG-folate triblock copolymer with multiple disulfide linkages as intracellular drug delivery nanocarriers in breast cancer. <sup>158</sup> Copyright 2015 American Chemical Society.....	22
<b>Figure 2.10.</b> Schematic illustration of the strategy to synthesis, micellization, and redox responsiveness of a PEG-PLA diblock copolymer (a) and coupling of PEG-A and PLA-B based on unsymmetrical, reversible disulfide-bond formation instructed by H-bonding (b). <sup>159</sup> Copyright 2014 American Chemical Society. ....	23

<b>Figure 2.11.</b> Synthesis (a) and intracellular delivery (b) of Dox-loaded PEG-BM/CD-PLLA supramolecular aggregates exhibiting triggered release of encapsulated Dox in response to intracellular microenvironment. <sup>168</sup> Copyright 2015 American Chemical Society. ....	25
<b>Figure 2.12.</b> Synthesis of PLA-graft-Dox-PEG. <sup>171</sup> Copyright 2015 Royal Society of Chemistry. ....	26
<b>Figure 2.13.</b> Flow cytometric histograms (a) and CLSM images (b) of HeLa cells only (A) and incubated with DOX-loaded micelles of POEOMA-SS-PLA-SS-PLA-SS-POEOMA triblock copolymer (B), and free DOX (C) for 16 hrs. Scale bar = 20 $\mu\text{m}$ . <sup>154</sup> Copyright 2014 American Chemical Society. ....	28
<b>Figure 2.14.</b> For Dox-loaded micelles self-assembled from hyaluronic acid-cystamine-PLGA block copolymer (HA-SS-PLGA), <i>in vivo</i> combination therapy using orthotopic mammary fat pad tumor growth model; tumor volumes (A, B, D), life survival of tumor-bearing mice (C), photos of excised tumors at the end of the treatment at day 40 (E), and day 75 (F). <sup>179</sup> Copyright 2015 Royal Society of Chemistry. ....	29
<b>Figure 2.15.</b> Schematic diagram of cellular entry routes and intracellular fates of self-assembled mPEG-b-PDLLA micelles and disulfide bonded mPEG-(Cys) <sub>4</sub> -PLA micelles. ....	30
<b>Figure 2.16.</b> Synthetic route of raft copolymer HA-ss-PLA and HA-PLA a), schematic representation of self-assembled process of mixed micelles b). <sup>182</sup> ....	32
<b>Figure 2.17.</b> Synthetic scheme for photo-responsive PLA-NB-PEG-NB-PLA a), schematic illustration of dox-loaded micelles and photo-controlled release at 365 nm irradiation b). <sup>185</sup> .....	33
<b>Figure 3.1.</b> Illustration of aqueous micellization and dual acidic pH/reduction-responsive degradation of a PLA-based triblock copolymer (P4) consisting of a hydrophilic polymethacrylate and PLA blocks with an acidic pH-responsive ketal linkage in the center of PLA block and reduction-responsive disulfides at polymethacrylate/PLA block junctions, thus exhibiting dual responses at dual locations. ....	38
<b>Figure 3.2.</b> Illustration of our strategy to synthesize a dual acidic pH/reduction-responsive degradable PLA-based P4 triblock copolymer at dual locations, utilizing ROP, ATRP, esterification, and coupling reaction. Sn(EH) <sub>2</sub> : tin(II) 2-ethylhexanoate, SA: succinic anhydride, PMDETA: N,N,N',N'',N''-pentamethyldiethylenetriamine, Et <sub>3</sub> N: triethylamine, DMAP: N,N-dimethylaminopyridine, EDC: 1-ethyl-3-(3-(dimethylamino)-propyl)carbodiimide-HCl salt, and DCM: dichloromethane. ....	43
<b>Figure 3.3.</b> GPC diagrams of P4, compared with its precursors of P1, P2 and P3. ....	44
<b>Figure 3.4.</b> <sup>1</sup> H-NMR spectra of P3 (a) and P4 (b) in CDCl <sub>3</sub> . ....	45
<b>Figure 3.5.</b> Overlaid fluorescence spectra (a) and maximum fluorescence intensity (b) of NR in aqueous mixtures containing various amounts of P4 to determine CMC as well as DLS diagram (c), TEM images at high (d) and low (e) magnifications of aqueous micelles of P4 at 1 mg/mL.47	
<b>Figure 3.6.</b> Schematic illustration of dual acidic pH/reduction-responsive degradation of P4 (a) as well as evolution of z-average diameter of empty micelles by DLS (b) and maximum fluorescence intensity of NR-loaded micelles by fluorescence spectroscopy (c), after incubation with and without 10 mM GSH at pH = 7.4 and 5.4. ....	49

<b>Figure 3.7.</b> Cell viability of HeLa cells incubated with empty P4 micelles for 48 hrs determined using MTT assay.....	50
<b>Figure 3.S1.</b> <sup>1</sup> H-NMR spectrum of P1 in CDCl <sub>3</sub> . X denotes residual THF. ....	52
<b>Figure 3.S2.</b> <sup>1</sup> H-NMR spectrum of P2 in CDCl <sub>3</sub> . ....	52
<b>Figure 3.S3.</b> Deconvolution GPC trace of P4. ....	53
<b>Figure 3.S4.</b> GPC diagrams of the degraded products formed after incubation with 10 mM GSH (pH = 7.4) (a), pH = 5.3 (b), and their combination (c). ....	53
<b>Figure 3.S5.</b> Evolution of DLS diagrams of aqueous micelles in the presence of various stimuli. ....	54
<b>Figure 3.S6.</b> DLS diagram and digital image of aqueous NR-loaded micelles. ....	54
<b>Figure 3.S7.</b> Overlaid fluorescence spectra of NR-loaded micelles incubated with various stimuli. ....	55
<b>Figure 4.1.</b> Schematic illustration of a novel diblock copolymer consisting of a PLA block linked with a POEOMA block through disulfide and acetal linkages and its aqueous micellization as well as dual acid/reduction-responsive degradation. ....	58
<b>Figure 4.2.</b> Schematic illustration of an initial unsuccessful approach utilizing combined ATRP and tin-catalyzed ROP techniques in the presence of a double-head initiator (Br-AC-SS-OH) in an attempt to synthesize POEOMA-AC-SS-PLA P2 diblock copolymer (a); possible cleavage of acetal linkages of P1 precursor during ROP of LA with Sn(EH) <sub>2</sub> at 120 °C resulting in the formation of P2-ATRP/ROP product composed of D1P and D2P (b) and its possible reductive degradation with DTT (c). ....	62
<b>Figure 4.3.</b> GPC diagrams of P2-ATRP/ROP product, synthesized by a combination of ATRP of OEOMA with ROP of LA in the presence of Br-AC-SS-OH, before and after being incubated with acid (a) and DTT (b). ....	64
<b>Figure 4.4.</b> Small molecule OH-bearing initiators labeled without an acetal linkage examined under a tin-catalyzed ROP condition. ....	65
<b>Figure 4.5.</b> GPC diagrams of PLA homopolymers (a) and P5-ROP product synthesized by ROP of LA with Br-AC-SS-OH before and after being incubated with DTT in DMF (b). ....	66
<b>Figure 4.6.</b> Schematic illustration of ROP of LA with Br-AC-SS-OH initiator (a) and possible cleavage of acetal linkages on the course of tin-catalyzed ROP of LA, yielding undesired P5-ROP product composed of D3P and D4P (b), and their possible reductive degradation in the presence of DTT (c). ....	66
<b>Figure 4.7.</b> Schematic illustration of an alternative approach designed with the conjugation of Br-AC-SS-OH with a COOH-terminated PLA and subsequent ATRP to synthesize PLA-SS-AC-POEOMA diblock copolymer.....	67
<b>Figure 4.8.</b> <sup>1</sup> H-NMR spectra of Py-PLA-OH (P3), Py-PLA-COOH (P6), Py-PLA-SS-AC-Br (P7), and POEOMA-AC-SS-PLA (P8) in CDCl <sub>3</sub> . Conditions: [LA] <sub>0</sub> /[Py-OH] <sub>0</sub> /[Sn(EH) <sub>2</sub> ] <sub>0</sub> = 70/1/0.05 with LA/toluene = 1.9/1 wt/wt at 120 °C for ROP and [OEOMA] <sub>0</sub> /[P7] <sub>0</sub> /[CuBr] <sub>0</sub> /[PMDETA] <sub>0</sub> = 50/1/0.4/0.42 with OEOMA/anisole = 1.4/1 wt/wt at 50 °C for ATRP. ....	69

<b>Figure 4.9.</b> GPC diagrams of P8 before and after treatment with HCl and DTT, compared with P3 (Py-PLA-OH) precursor (a) and schematic illustration of degraded products of P8 upon the cleavage of the junction acetal and disulfide linkages in response to acid and reduction (b). ....	70
<b>Figure 4.10.</b> For P8-based nanoaggregates, DLS intensity distributions (a, c) and TEM images (b, d, scale bar = 1 $\mu$ m and e-f, scale bar = 200 nm) before (a-b) and after (c-f) treatment with pH = 5.4 and 10 mM GSH in aqueous solution.....	71
<b>Figure 4.S1.</b> Reaction scheme to synthesize A2. ....	72
<b>Figure 4.S2.</b> $^1\text{H-NMR}$ spectrum of Br-AC-SS-OH in $\text{CDCl}_3$ .....	73
<b>Figure 4.S3.</b> $^1\text{H-NMR}$ spectra of POEOMA-AC-SS-OH (P1) precursor (a) and P2-ATRP/ROP product (b) in $\text{CDCl}_3$ .....	73
<b>Figure 4.S4.</b> GPC traces of POEOMA-AC-SS-OH precursor (P1) and P2-ATRP/ROP product (b).....	74
<b>Figure 4.S5.</b> Maximum fluorescence intensity of NR over concentration of the formed P2-ATRP/ROP product to determine CMC with a NR probe.....	75
<b>Figure 4.S6.</b> $^1\text{H-NMR}$ spectrum in $\text{CDCl}_3$ of P3 synthesized by ROP of LA with Py-OH.....	75
<b>Figure 4.S7.</b> $^1\text{H-NMR}$ spectrum in $\text{CDCl}_3$ of P4 synthesized by ROP of LA with Br-SS-OH. ..	76
<b>Figure 4.S8.</b> $^1\text{H-NMR}$ spectrum of Br-AC-SS-OH incubated with $\text{Sn}(\text{EH})_2$ for 4 hrs at 100 $^\circ\text{C}$ , compared with those of $\text{Sn}(\text{EH})_2$ and Br-AC-SS-OH in toluene- $d_8$ . ....	76
<b>Figure 5.1.</b> Route I exploring azido-alkyne cycloaddition reaction to synthesize PEG-SS-OH/I. ....	83
<b>Figure 5.2.</b> Overlaid $^1\text{H-NMR}$ spectra of PEG-Cl a), PEG- $\text{N}_3$ b), Alkyne-SS-OH, and PEG-SS-OH/I in $\text{CDCl}_3$ .....	84
<b>Figure 5.3.</b> Route II utilizing the protection-deprotection chemistry with acid-labile ketal group to synthesize PEG-SS-OH/II.....	85
<b>Figure 5.4.</b> Overlaid $^1\text{H-NMR}$ spectra of B1, B2 and PEG-SS-OH/II in $\text{CDCl}_3$ . EA refers to traces of ethyl acetate.....	85
<b>Figure 5.5.</b> Synthetic scheme (a), $^1\text{H-NMR}$ spectrum in $\text{CDCl}_3$ (b) of PEG-SS-PLA (P1) by ROP of LA in the presence of PEG-SS-OH/II. Conditions: $[\text{LA}]_0/[\text{I}]_0/[\text{Sn}(\text{EH})_2]_0 = 70/1/0.08$ ; $\text{LA}/\text{toluene} = 0.43/1$ and GPC diagram of P1, compared with PEG-SS-OH, its macroinitiator c). ....	87
<b>Figure 5.6.</b> Schematic illustration of reduction-responsive degradation a) and GPC traces of P2 before and after incubation with DTT b). ....	88
<b>Figure 5.7.</b> DLS diagram of empty a) and PTX-loaded P1 micelles b). ....	89
<b>Figure 5.8.</b> <i>In vitro</i> release profiles of PTX from PTX-loaded micelles incubated with and without 10 mM GSH in PBS solution.....	90
<b>Figure 5.S1.</b> $^1\text{H-NMR}$ of P1C in $\text{CDCl}_3$ a), GPC diagram of P1C, compared with PEG-OH, its macroinitiator b).....	91

<b>Figure 5.S2.</b> DP of PLA block over the amount of LA as batch size for the synthesis of P1C block copolymers [Inset; P2C block copolymers].	92
<b>Figure 5.S3.</b> Maximum fluorescence intensity of NR over concentration of P1 to determine CMC with a NR probe.	92
<b>Figure 5.S4.</b> Calibration curve for PTX generated using different concentrations of PTX using HPLC.	93

## List of Tables

<b>Table 4.1.</b> Characteristics and properties of functional PLA homopolymers synthesized by ROP of LA with small molecule OH-bearing initiators with no acetal linkage. <sup>a)</sup> .....	65
<b>Table 5.S1.</b> Characterization data for all control block copolymers synthesized. (P1C and P2C refers to block copolymers synthesized using PEG5000-OH and PEG2000-OH macroinitiators respectively).....	91

## List of Abbreviations

ABPs	Amphiphilic block copolymers
ATRP	Atom transfer radical polymerization
BBB	Blood-brain barrier
CCM	Core crosslinked micelles
CDI	Carbonyldiimidazole
CLSM	Confocal laser scanning microscopy
CMC	Critical micelle concentration
CSC	Cancer stem cell
CuBr	Copper (I) bromide
CYC	Cyclopamine
DCC	N,N'-dicyclohexylcarbodiimide
DCM	Dichloromethane
DDS	Drug delivery system
DLS	Dynamic light scattering
DL-SRD	Dual location stimuli-responsive degradation
DMAP	4-(Dimethylamino)pyridine
DOX	Doxorubicin
DP	Degree of polymerization
DTT	Dithiothreitol
EDC	1-ethyl-3-(3-(dimethylamino)-propyl)carbodiimide-HCl salt
Et <sub>3</sub> N	Triethylamine

EPR	Enhanced permeability and retention effect
FRET	Fluorescence resonance energy transfer
GPC	Gel permeation chromatography
GSH	Glutathione
HA	Hyaluronic acid
LA	Lactide
LCST	Lower critical solution temperature
LDA	Lithium diisopropylamide
LDLR	Low-density lipoprotein receptor
MDR	Multidrug resistance
ML-SRD	Multi location stimuli-responsive degradation
MSNPs	Mesoporous silica nanoparticles
MTX	Methotrexate
NaN <sub>3</sub>	Sodium azide
Nps	Nanoparticles
NR	Nile red
OEOMA	Oligo(ethylene glycol) monomethyl ether methacrylate
PAAs	Polyamino acids
PAE	Poly( $\beta$ -amino ester)
PCL	Polycaprolactone
PEI	Polyethyleneimine
PEG	Poly(ethylene glycol)

PEtG	Poly(ethylglyoxylate)
PGA	Polyglycolide
PLA	Poly lactide
PMDETA	N,N,N',N'',N''-pentamethyldiethylenetriamine
PNIPAM	Poly(N-isopropylacrylamide)
POEOMA	Poly(oligo(ethylene glycol) monomethyl ether methacrylate)
PPTS	Pyridinium p-toluenesulfonate
PTX	Paclitaxel
RES	Reticuloendothelial system
ROP	Ring opening polymerization
RSV	Resveratrol
SA	Succinic anhydride
SL-SRD	Single location stimuli-responsive degradation
SRD	Stimuli-responsive degradable
Sn(EH) <sub>2</sub>	Tin-2-ethylhexanoate
THP	Tetrahydropyran
TEM	Transmission electron microscopy
THF	Tetrahydrofuran

# Chapter 1

## Introduction and Statement

### 1.1. Emergence of drug delivery systems

During the past several decades, the drug delivery field has been revolutionized by the emergence of nanotechnology where nanomedicines have been explored extensively in cancer diagnosis and treatment. Commonly used small anticancer drugs such as doxorubicin (DOX) and paclitaxel (PTX) are associated with various pitfalls such as low solubility, rapid renal clearance, no specific targeting and systemic toxicity.<sup>1,2</sup> Thus to circumvent these challenges, drug delivery systems (DDS) primarily comprising of nanometer-sized particles (NPs) came into picture, enhancing the solubility and bioavailability of poorly water-soluble drugs.<sup>3</sup> Furthermore, these NPs enable passive targeting to the tumors by the Enhanced Permeability and Retention (EPR) effect, resulting in a higher drug concentration targeted at the tumor site.<sup>4</sup> Different nanostructures such as nanocapsules, nanodendrimers, quantum dots, gold NPs, liposomes and polymeric structures have been developed for the encapsulation and delivery of drugs (Figure 1.1).

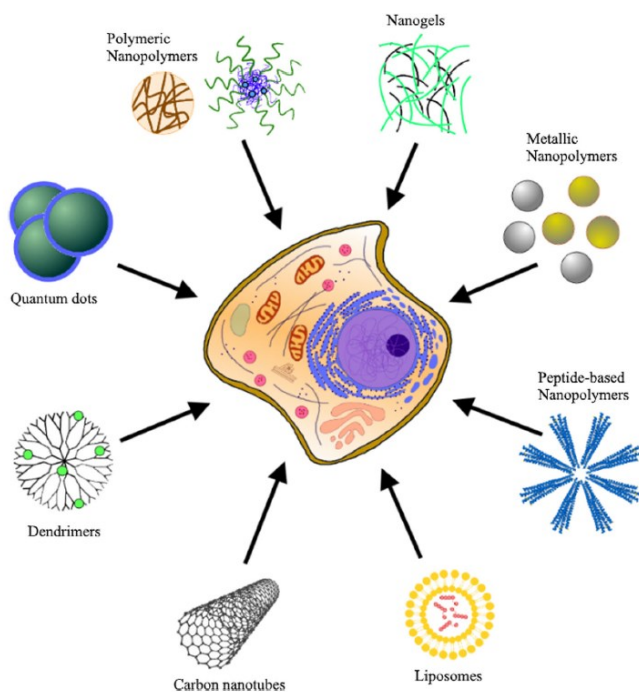


**Figure 1.1.** Types of nanocarriers for drug delivery systems.<sup>5</sup>

These drug molecules can be physically encapsulated inside NPs or covalently conjugated to NPs, leading to improved pharmacokinetic and pharmacodynamic properties, prolonged circulation times and sustained drug release kinetics.<sup>6</sup> Among various approaches, polymeric NPs (PNPs) have emerged as effective DDS with the underlying potential.<sup>7</sup>

## **1.2. Polymeric NPs as effective drug delivery nanocarriers**

Polymeric nanomaterials have gained significant attention in the field of drug delivery due to large solubilization power, increased loading capacity and higher stability in the blood stream. Polymeric micelles can be built by self-assembly of amphiphilic block copolymers (ABPs) with a hydrophilic outer shell and a hydrophobic core, thus enabling the transport of water insoluble drugs to their specific target. The hydrophilic shell of the micelles provides colloidal stability and stealth and avoids its uptake by reticuloendothelial system (RES), resulting in prolonged circulation in the blood.<sup>8</sup> The hydrophobic cores are able to encapsulate hydrophobic drugs and offer increased drug loading capacity.<sup>9</sup> Mostly used polymers for the hydrophobic core formation include polyesters, polyethers and poly(amino acids). The most frequently used core forming molecules are poly(D,L-lactide) (PLA), poly( $\epsilon$ -caprolactone) (PCL) and poloxamers.

Conventional ABP-based micelles rely on diffusion gradient to release payload via diffusion outside the micelles.<sup>10,11</sup> Despite their preferential accumulation in tumors due to passive targeting, they are still associated with adverse effects attributed to the nonspecific biodistribution and uncontrolled drug release. To overcome these barriers, stimuli-responsive degradable (SRD) polymers have been developed which are equipped with environment-sensitive modalities within their structures.<sup>12,13</sup> In general, these stimuli can be divided into two categories: internal stimuli such as pH, temperature, redox potential and enzymes; and external stimuli which are triggered externally such as electromagnetism, light, radiation and ultrasound.<sup>14</sup> The underlying principle in the development of such polymers lies in the chemical structure of the polymers. These so-called smart polymers undergo rapid changes in their shape, solubility, surface characteristics and dissociation triggered by changes in their environment. The benefits of internal stimuli-responsive nanoformulations are more pronounced as the stimuli exist specifically in inherent physiological sites.<sup>3</sup> Such specificity enables the nanoformulations to release encapsulated drugs precisely at

target sites in a tailored manner with reduced adverse effects. This ultimately helps in achieving controlled drug release pattern.

### 1.3. PLA as promising material

Amongst other polymerizations, ring opening polymerization (ROP) is the most widely used polymerization techniques for the synthesis of industrially important polymers such as polynorbornene, poly(ethylene oxide), polyphosphazene and polysiloxane. The driving force for most ROPs is the release of ring strain and steric hinderance. PLA is a commonly used term for polylactide and poly(lactic acid), however, both are produced using different methods. Poly(lactic acid) is synthesized via polycondensation of lactic acid which is a chiral molecule and exists in the form of two enantiomers: L-(+)-lactic acid or (S)-lactic acid and D-(-)-lactic acid or (R)-lactic acid.<sup>15</sup>

PLA is a biodegradable polyester derived from renewable resources such as potato cassava, corn and beet sugar.<sup>15</sup> It is vastly preferred over conventional or non-biodegradable polymers for drug delivery because it decomposes into naturally occurring metabolites by hydrolysis or enzymatic processes. It has been extensively studied for wide variety of applications such as orthopedics, food packaging, drug delivery, bioresorbable devices and scaffolds.<sup>16</sup> The most efficient method to synthesize aliphatic polyesters is the ROP of cyclic esters in the presence of catalysts. Certain drawbacks of PLA include hydrophobicity, poor elasticity and slow degradation.<sup>17, 18</sup> These can be addressed by copolymerization with hydrophilic monomers<sup>19, 20</sup> and introduction of stimuli-responsive cleavable linkages.<sup>21, 22</sup>

To synthesize high molecular weight PLA, ROP of a cyclic monomer called lactide (LA) is performed, which gives better control over the chemistry and thus properties of the resulting polymers. LA, a cyclic dimer is synthesized from thermal cracking of low molecular weight PLA oligomer at high temperature and low pressure in the presence of catalysts. There are three stereoisomeric forms: D-LA, L-LA and D,L-LA. ROP of LA can be classified into three different reaction mechanisms: anionic,<sup>23, 24</sup> cationic<sup>25</sup> and coordination-insertion<sup>26</sup> mechanisms. The most widely studied method for synthesis of high molecular weight PLA is coordination -insertion mechanism, with the use of metal oxide-based catalysts. As illustrated in Figure 1.2, in the first step of this mechanism, the exocyclic oxygens of the LA temporarily coordinates with the metal

atom of the initiator. The coordination enhances the nucleophilicity of the alkoxide part of the initiator as well as the electrophilicity of the LA carbonyl group. In the second step, the acyl-oxygen bond (between the carbonyl group and the endocyclic oxygen) of LA is broken and the LA chain produced is inserted into the metal–oxygen bond of the initiator.

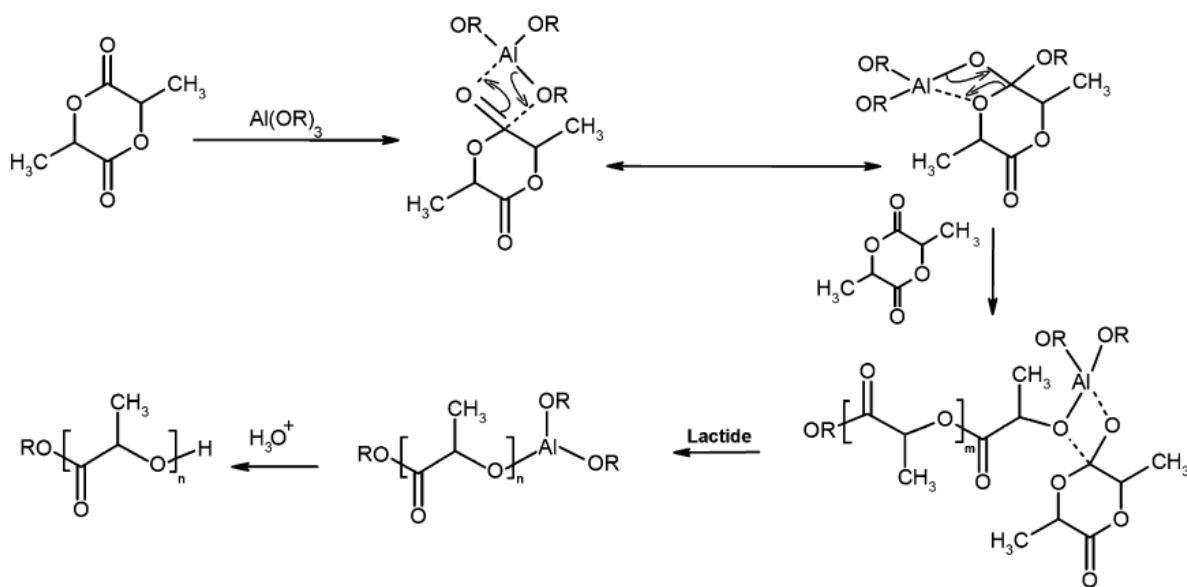


**Figure 1.2.** Coordination-insertion mechanism of ROP of lactide,<sup>15</sup> where *m* and *n* are degree of polymerizations of lactide, R stands for alkyl groups.

Different catalysts have been studied for ROP of LA which includes metal powders, Lewis acids, Lewis bases, organometallic compounds and different metal salts. Most commonly used catalysts includes iron<sup>27</sup>, tin-2-ethylhexanoate ( $\text{Sn}(\text{EH})_2$ ),  $\text{SnCl}_4$ ,  $\text{Sn}(\text{C}_6\text{H}_6)_4$ <sup>28</sup>, Zinc lactate [ $(n\text{-C}_4\text{H}_9\text{O}_2)\text{AlO}]_2\text{Zn}$ <sup>29, 30</sup>, oxyethyl methacrylate aluminium trialkoxides, cyclic tin alkoxide<sup>31</sup>, butyl lithium and butylmagnesium<sup>32</sup>, complexes of Cu, Zn, Co and Ni schiff base<sup>33</sup>, yttrium, and yttrium (III) complexes<sup>34</sup>. Among these catalysts,  $\text{Sn}(\text{EH})_2$  is the standard catalyst used for the synthesis of high molecular weight polylactides.<sup>35</sup> It is approved by FDA to synthesize polymers for food packaging and biomedical applications.<sup>36</sup> The acceptable content of tin (II) residue ranges between 20-50 ppm and hence adequate purification methods are required for its removal.<sup>37</sup> Of a number of different procedures reported for the purification of  $\text{Sn}(\text{EH})_2$  containing materials<sup>38, 39</sup>, the most efficient procedure is the extraction with an aqueous solution of an acid.<sup>37</sup> It was reported that after

treatment of PLLA organic solution with HCl gas, the residual amount of tin was significantly reduced from 500 to 20 ppm.

*Properties and applications of PLA.* Properties of PLA depends on the presence of a pendant methyl group on the alpha carbon atom, which is responsible for the chirality at alpha carbon of lactic acid and thus different isomers can be obtained. Homochiral PLA (PLLA or PDLA) is isotactic, stereoregular and semicrystalline polymer with the melting point ( $T_m$ ) of 170-183 °C and a glass transition temperature ( $T_g$ ) of 55-65 °C.<sup>40</sup> Similarly, the polymerization of racemic mixture of L- and D- lactides leads to the synthesis of atactic poly-DL-lactide, which is amorphous in nature with a  $T_g$  of 59 °C.<sup>41</sup> Polylactide with defined chirality can be obtained using optically active catalysts or mixtures of D,D-lactide and L,L-lactide with defined stoichiometry. Due to the non-toxic degradation products, PLA and its copolymers are used typically in the field of drug delivery,<sup>42</sup> protein encapsulation and delivery<sup>43</sup>, development of microspheres and hydrogels<sup>44</sup> and tissue engineering<sup>45</sup> etc. The main focus of this thesis work is the use of PLA for drug delivery applications.

#### **1.4. Objectives**

The overall objectives of my doctoral research aim to explore new strategies that allows for the synthesis of novel PLA-based block copolymers containing acid-labile acetal and reduction-responsive disulfide linkages as potential candidates for drug delivery. As illustrated in Figure 1.3, my particular interest lies in developing a method to integrate those linkages in well-controlled block copolymers in terms of their numbers and locations of self-assembled micelles. It is very well established that glutathione (GSH, 0.1-10 mM) is found at a higher concentration in cytosol than in the extracellular fluids (<10  $\mu$ M). Such a large concentration gradient between the intracellular and extracellular environment and its elevated concentration in cancer cells offers new opportunities for the development of polymers that selectively degrade after their uptake by the cell.<sup>46, 47</sup> Similarly, compared to the constant extracellular and intracellular pH values of blood and healthy tissues (pH 7.4 and 7.2, respectively), the extracellular pH of tumor tissues range from 6.0 to 7.2. Furthermore, after endocytosis of extracellular material by host tumor cells, the intracellular pH of the endosomal compartments can drop substantially, to as low as 6.5 in early endosomes, 5.0-6.0 in late endosomes and 4.0-5.0 in lysosomes.<sup>48, 49</sup> Thus, incorporating both

these endogenous stimuli triggers in one system could potentially lead to synergistic release of encapsulated payload.

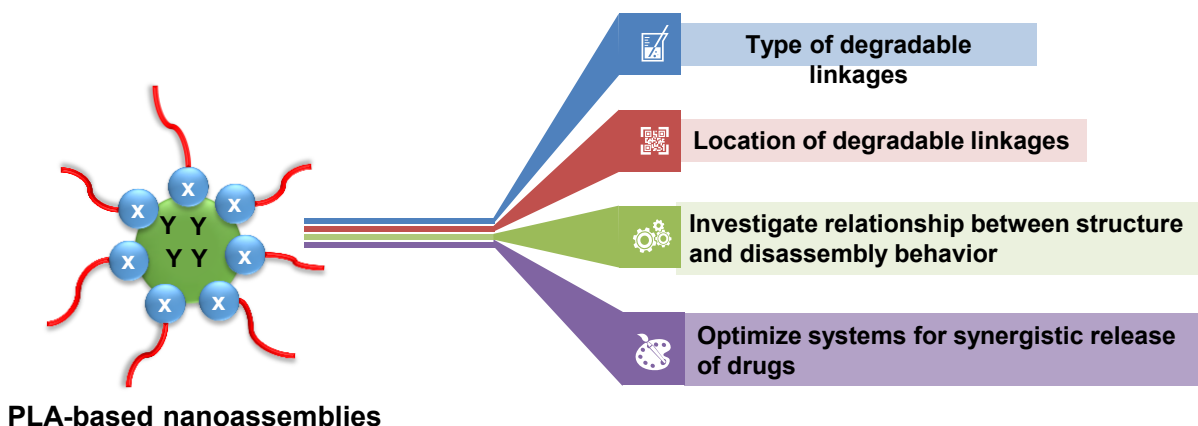


**Figure 1.3.** Overall objectives of doctoral thesis. X and Y refers to the linkages responsive to different types of stimuli.

Well-established synthetic methods including ROP of LA, controlled radical polymerization of vinyl monomers, and facile organic coupling reactions have been employed to synthesize block copolymers exhibiting both acid and reduction-degradable responses. In addition, the proposed PLA-based nanoassemblies were evaluated for their drug release and cytotoxicity using biological assays.

This thesis consists of six chapters, namely the preface, review literature encapsulating the recent development of novel PLA-based ABPs, three research projects, conclusion and future works.

**Chapter 2** entails the literature overview of SRD-based PLA block copolymer nanoassemblies for controlled drug delivery. This review highlights the recent development in the area of novel PLA-based ABPs and their self-assembled nanostructures for SRD-induced enhanced drug release. This chapter begins with an introduction to the concept of conventional PLA-based ABP assemblies and then focuses on various strategies used to design such systems.

**Chapter 3** describes the synthetic design and evaluation of novel PLA-based triblock copolymer labelled with acidic pH-responsive ketal linkages in the core and reduction-responsive disulfide linkages at the junction of hydrophobic and hydrophilic interfaces. This triblock

copolymer was then evaluated for the micellization studies and dye loading and release studies to explore the qualitative and quantitative degradation kinetics.

**Chapter 4** describes the initially adopted synthetic route using an initiator labelled with both disulfide and acetal linkages for the PLA-based diblock copolymer, which led to the degradation of acetal linkages. Furthermore, it discusses an alternative route which was adopted to synthesize the diblock copolymer followed by its characterization as self-assembled nanoassemblies.

**Chapter 5** describes the development of reduction-responsive disulfide labelled polyethylene glycol-poly lactide (PEG-SS-PLA) based block copolymers as potential candidates for PTX delivery. This block copolymer was synthesized using a PEG based OH-terminated macroinitiator consisting of reduction-responsive disulfide linkages (PEG-SS-OH). Furthermore, this diblock copolymer was explored for the micellization, PTX-loading and release studies.

**Chapter 6** describes the summary and conclusion of the research conducted during the program and proposed future works for each research project.

## Chapter 2

### Stimuli-responsive degradable PLA-based block copolymer nanoassemblies for controlled/enhanced drug delivery

#### 2.1. Introduction

Polymer-based DDS have been extensively explored as a promising platform in pharmaceutical science and medicine for the transportation of therapeutics to targeted diseased sites. Anticancer therapeutics as small drugs or macromolecules (therapeutic proteins and nucleic acids such as DNA and RNA) are either covalently conjugated to polymeric chains or physically encapsulated inside DDS. This feature can improve the biodistribution of encapsulated therapeutics, thus enhancing therapeutic efficacy while minimizing undesired side effects common to small drugs.<sup>50-55</sup> Among numerous examples of typical polymer-based DDS, self-assembled micellar aggregates have gained significant attention as promising candidates for effective polymer-based DDS.<sup>56-59</sup> The micelles are generally formed by aqueous micellization through self-assembly of ABPs in aqueous solution. They consist of a hydrophobic core, capable of encapsulating a variety of bioactive molecules including anticancer drugs, surrounded with hydrophilic coronas, ensuring colloidal stability and biocompatibility.<sup>60-62</sup> Upon intravenous injection into blood stream, drug-loaded micellar nanoassemblies (or nanocarriers) circulate in the blood to target tumor tissues.<sup>60, 63-66</sup> Through the process known to be EPR effect, they are extravasated into tumor tissues from prolonged blood circulation.<sup>67-69</sup> Once the nanocarriers are internalized into cancer cells through endocytosis, the encapsulated drugs can be released from the nanocarriers.<sup>70</sup> A number of ABP-based self-assembled nanocarriers have been developed and effective systems rely on the choice of building blocks, particularly hydrophobic blocks, to synthesize novel ABPs.

PLA is a class of hydroxyalkanoic acid-based hydrophobic aliphatic polyesters, along with PCL and polyglycolide (PGA). PLA and its copolymers are biocompatible and FDA-approved for clinical use. They are slowly degraded by hydrolysis or enzymatic reaction in physiological conditions to the corresponding water-soluble oligomers and lactic acids. In mammalian physiology, lactic acid is naturally produced as a by-product of anaerobic respiration (a form of

respiration using electron acceptors other than oxygen). It is then metabolized into carbon dioxide and water. These unique features have made PLA-based materials valuable for extensive applications in biomedical fields, including sutures, bone fixation implants, and stents as well as tissue scaffolds and drug delivery carriers.<sup>71-74</sup> Toward the successful biomedical applications of conventionally-designed PLA and PLA-based nanomaterials, a critical challenge to be addressed is associated with the slow biodegradation of PLA and thus slow and uncontrolled release of encapsulated drugs. Such slow release is attributed to delayed diffusion through the hydrophobic PLA core due to both hydrophobic interactions as well as the slow hydrolysis of the ester linkages of the PLA backbones. An introduction of stimuli-responsive degradation (SRD) into the design of novel PLA-based ABPs has been explored as a promising platform enabling the controlled/enhanced release of encapsulated therapeutics for cancer therapy.

This review summarizes the recent development of novel PLA-based ABPs and their self-assembled nanostructures for SRD-induced enhanced drug release, with a focus on their design, synthesis, and evaluation as intracellular drug delivery nanocarriers. Further, conventional PLA and PLA-based ABP assemblies as well as general concept and typical strategies of SRD are described in this review.

## **2.2. Conventional PLA and PLA-based ABP assemblies**

### **2.2.1. Synthesis and properties of PLA**

Well-controlled PLA with narrow molecular weight distribution is generally synthesized by ROP of LA in the presence of hydroxyl (OH) or amine (NH<sub>2</sub>)-bearing initiators at elevated temperatures<sup>75, 76</sup> (Figure 2.1a). The fundamentals and kinetics of ROP of cyclic monomers including LA are described in literature.<sup>73, 77-80</sup> Furthermore, recent reports describe elegant strategies that allow for the synthesis of a variety of functional PLAs. Interesting strategies utilize functional LA monomers bearing vinyl/then azide group<sup>81</sup> as well as functional initiators bearing disulfide,<sup>82</sup> pyridiyl disulfide,<sup>83</sup> and a peptide linkage with a sequence of Pro-Leu-Gly-Leu-Ala-Gly.<sup>84, 85</sup>

Given stereospecific characteristics as illustrated in Figure 2.1b, PDLA from D-LA and PLLA from L-LA are semi-crystalline with a melting transition (>150 °C), while PDLLA from DL-LA

is amorphous with a glass transition at  $\approx 45$  °C. Hereinafter, note that “PLA” presents amorphous PDLLA. Both PDLA and PLLA have great mechanical properties due to the presence of crystalline domains. Furthermore, PDLA and PLLA form physically crosslinked networks through stereocomplexation. Such feature has been explored for supramolecular micellization for drug delivery.<sup>86, 87</sup>

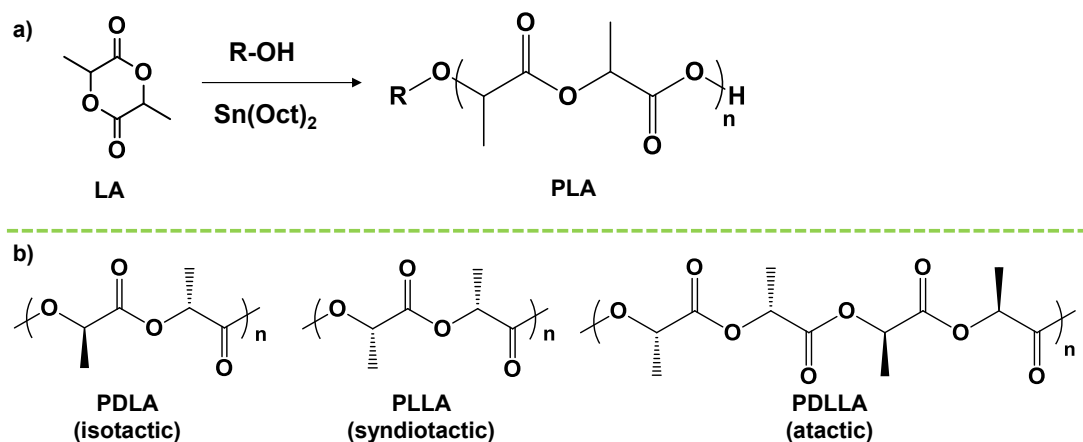


**Figure 2.1.** ROP of LA to synthesize PLA (a) and stereochemistry (tacticity) of PDLA, PLLA, and PDLLA (b).

### 2.2.2. General strategies to PLA-based ABPs and their assemblies

One of the challenges for clinical uses of PLA involves its hydrophobicity that causes short residence time in blood by undesired elimination through opsonization. The hydrophobicity of PLA also presents its incompatibility with biological systems, leading to decreased therapeutic efficacy. Significant efforts have been made over the past years to address the challenge of hydrophobicity of PLA. A promising solution is to introduce water-soluble or hydrophilic blocks into the design of PLA-containing ABPs. Typically explored hydrophilic blocks include PEG, PAAs, polysaccharides, and polymethacrylates. The resultant ABPs tend to self-assemble toward micellar aggregation in aqueous solution, consisting of hydrophobic PLA block residing in core and hydrophilic block forming outstretched coronas (Figure 2.2). The development of PLA-based ABPs and their self-assembled structures is summarized in a review article.<sup>20</sup> This section describes recent strategies to synthesize PLA-based ABPs, particularly with PEG and polypeptide, since 2010.

PEG is FDA-approved and has been extensively used as a hydrophilic polymer in biomedical field. A general approach to synthesize PLA-based PEG block copolymers involves the direct ROP of LA in the presence of PEG as an initiator. Various PEG initiators have been examined to synthesize novel copolymers. They include a monofunctional methoxy PEG having a terminal OH group (mPEG-OH) for the synthesis of mPEG-b-PLA diblock copolymer, a difunctional PEG having both terminal OH groups (HO-PEG-OH) for PLA-PEG-PLA triblock copolymer, and multifunctional PEGs for highly-branched copolymers.<sup>88-92</sup>

Synthetic polypeptide based on amino acid or poly(amino acid) is biocompatible and biodegradable.<sup>93</sup> Most diblock copolymers consisting of PLA and poly(amino acid) blocks have been synthesized by ROP of an  $\alpha$ -amino acid N-carboxyanhydride from  $\text{NH}_2$ -terminated polymer, followed by the hydrolysis for deprotection of groups to the corresponding amino acids. A diblock copolymer of PLA-b-poly(L-lysine) was synthesized by ROP of N-carboxylbenzoxy-L-lysine in the presence of  $\text{NH}_2$ -PLA initiator.<sup>94</sup> The synthesis of a triblock copolymer of PEG-b-poly(L-serine) grafted with PLA has been reported. The approach involves the ROP of o-(t-butyl)-L-serine in the presence of PEG- $\text{NH}_2$ , followed by the hydrolytic cleavage of pendant t-butoxy groups to the corresponding OH groups. The resultant PEG-b-P(L-serine) was used as a macroinitiator for the ROP of LA, yielding the designed product.<sup>95</sup>

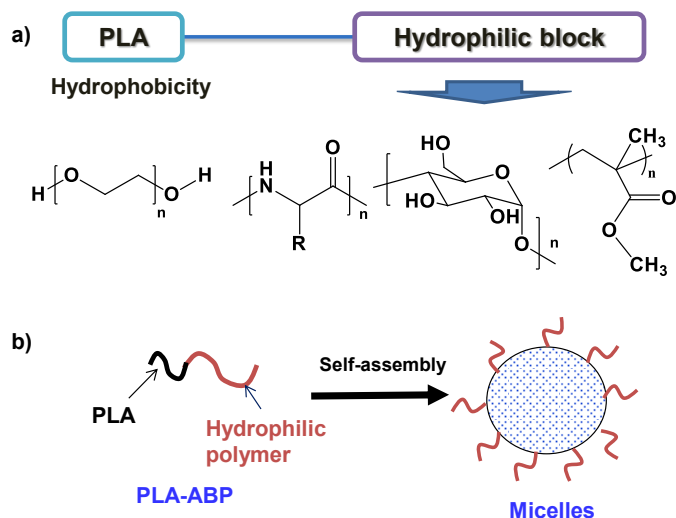


**Figure 2.2.** Schematic illustration of conventionally-designed PLA-based ABPs with hydrophilic blocks such as PEG, poly(amino acid), polysaccharide, and polymethacrylate (a) and their self-assembly to form micellar aggregates with PLA cores surrounded with hydrophilic coronas (b).

## 2.3. SRD for enhanced release

### 2.3.1. General concept of SRD

Stimuli-responsive (or smart) (co)polymers undergo a chemical or physical transition in response to external stimuli (or triggers).<sup>96-99</sup> Most of these transitions, particularly utilized in biological and biomedical applications, result in a change in hydrophobic/hydrophilic balance of the smart polymers. Physical transition causes a volume change through either a coil-globular or conformational transition when physical stimuli are applied. Of physical stimuli including pH, magnetic, and electric fields, a typical example is temperature change. PNIPAM is a typical thermoresponsive polymer. It undergoes coil-globular transition at LCST.<sup>100-103</sup> At below LCST, PNIPAM is hydrophilic and becomes soluble in water; however, it turns to be hydrophobic, forming aggregates, at above LCST. Due to such temperature-responsive transition, PNIPAM-based block copolymer nanoassemblies have been extensively utilized for drug delivery exhibiting a size-controlled drug release.

In contrast, chemical transition involves the degradation (or disintegration) through the cleavage of degradable (or labile) covalent bonds in the presence of chemical or biological stimuli such as glutathione, acidic pH, light, or enzyme.<sup>104-108</sup> Such chemical transition is known to be “stimuli-responsive degradation (SRD)”, which involves the introduction of cleavable linkages (covalent bonds) into the design of nanomaterials, particularly self-assembled ABP-based micellar nanoaggregates. Later, these labile linkages are cleaved in the presence of chemical and biological stimuli when needed. Consequently, the SRD property allows for controlled/enhanced release of encapsulated drugs from drug-loaded nanocarriers. It is ideal that when degradable linkages are cleaved in response to biological components of targeted cells or tissues. As summarized in Figure 2.3, the promising degradable linkages include reduction-responsive disulfides;<sup>109-112</sup> acid-labile linkages such as acetals, ketals, orthoesters, hydrazones, and imines;<sup>113, 114</sup> and enzyme-responsive linkages such as specific peptide linkages, ester, and amide bonds;<sup>115-117</sup> as well as photo-cleavable linkages such as coumarin dimers, pyrenylmethyl and o-nitrobenzyl group.<sup>118-120</sup> Disulfide linkages are cleaved to the corresponding thiols in reducing environments. In biological systems, GSH (a tripeptide containing cysteine) is found at a higher concentration in intracellular environments ( $\approx 10$  mM) than extracellular environments ( $\approx 10$   $\mu$ M), and even at elevated levels in

cancer cells.<sup>121, 122</sup> Covalent ester linkages in the presence of esterase enzymes and specific peptide linkages are cleaved by enzymatic reactions. Similarly, acid-labile linkages are cleaved in response to acidic conditions. In biological systems, acidic pH is present in tumor tissue (pH = 6.5-6.9) as well as in endosomes and lysosomes (pH = 5.0-6.5). Photo-labile linkages are cleaved on demand upon irradiation with light in targeted sites.

It is imperative that drug-loaded nanocarriers are able to release encapsulated anticancer drugs in a rapid and controlled fashion after being taken up by cancer cells after extravastion into tumor tissues from blood circulation. Self-assembled nanocarriers designed with cleavable linkages are stable under physiological conditions; however, they can be dissociated in a controlled fashion upon appropriate stimuli in tumor tissues/cancer cells. Consequently, SRD has been extensively explored as a promising platform in the design and development of a variety of SRD-exhibiting block copolymers and their self-assembled nanostructures for tumor-targeting drug delivery applications.<sup>123-126</sup>

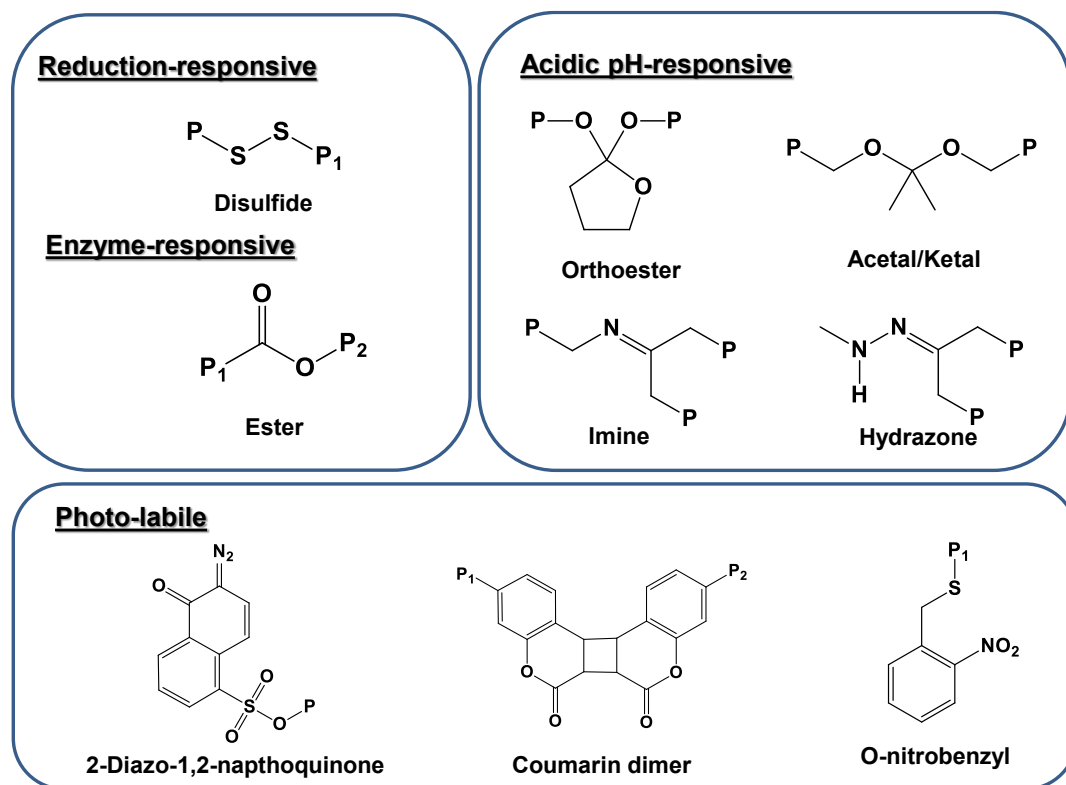


**Figure 2.3.** Degradable linkages including reduction, enzyme, and acidic pH-responsive cleavable as well as photo-labile linkages, P refers to the different polymeric chains.

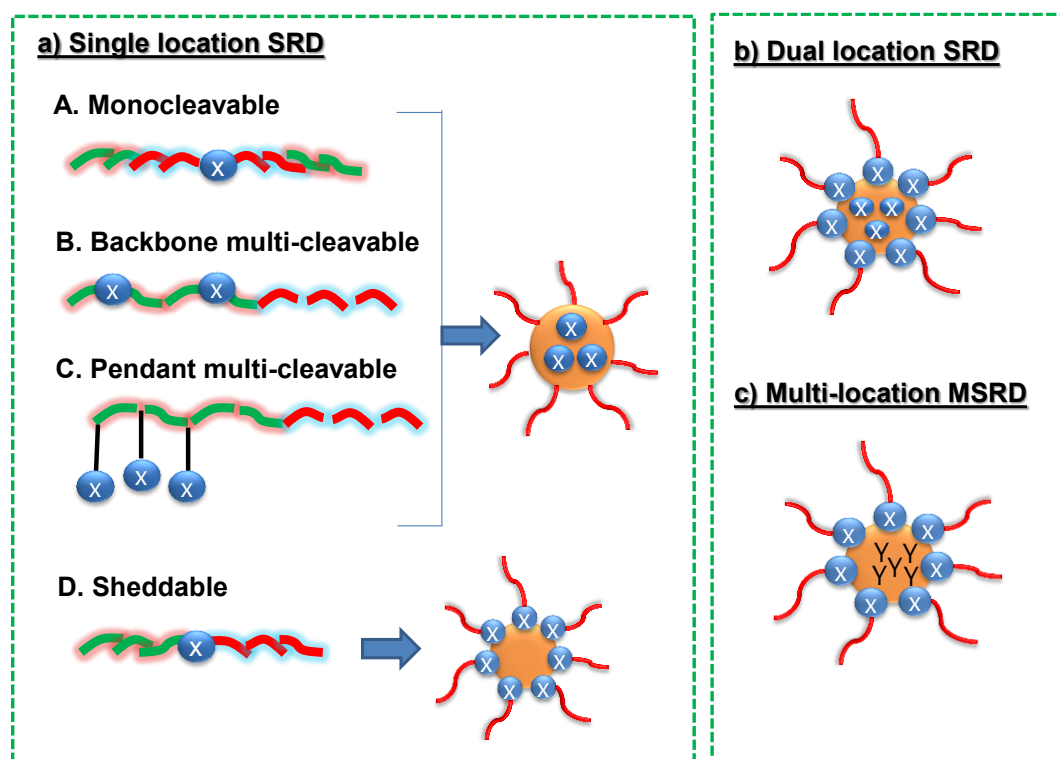
### 2.3.2. General approaches to SRD-exhibiting ABPs and their assemblies

Figure 2.4 summarizes the general approaches that allow for the synthesis of SRD-exhibiting block copolymers and their self-assembled nanostructures, which are based on the number, position, and location of single or multiple (or dual) cleavable linkages.<sup>127, 128</sup> Figure 2.4a illustrates “single location SRD approach (SL-SRD)”. Four distinct strategies can be categorized with the number and position of the cleavable linkages in single locations, as in micellar cores or at core/corona interfaces of self-assembled micelles. They respond to either single stimulus or multiple stimuli. Pendant multi-cleavable ABPs are designed with multiple linkages positioned in the pendent chains of hydrophobic blocks (strategy A). Backbone multi-cleavable ABPs have multiple cleavable linkages positioned on the main chains of hydrophobic blocks (strategy B). Typical examples of backbone multi-cleavable blocks include step-growth polymers, typically polyesters labeled with disulfides<sup>129, 130</sup> as well as polyurethanes with o-nitrobenzyl<sup>131</sup> and SeSe linkages.<sup>132</sup> Mono-cleavable ABPs involve single cleavage linkages in the middle of single triblock copolymers (strategy C). The strategies A, B, and C feature the position of cleavable linkages in hydrophobic cores of self-assembled micelles. In response to external stimuli, the pendant multi-cleavable micelles (strategy A) are disintegrated (or destabilized) by a change of hydrophobic/hydrophilic balance upon the cleavage of pendant cleavable linkages. Other micelles (strategy B and C) are dissociated by main chain degradation upon the cleavage of cleavable linkages positioned on backbones. Strategy D involves the synthesis of ABPs with cleavable linkages at the junction of hydrophilic and hydrophobic blocks. These Strategy D ABPs self-assemble to form micelles with cleavable linkages positioned at the interfaces of hydrophobic cores and hydrophilic coronas. In the presence of triggers, hydrophilic coronas are shed from the micellar cores upon cleavable linkages at the interfaces (thus, called sheddable micelles).

For the preparation of reduction-responsive disulfide-containing ABPs, typical examples of pendant multi-cleavable hydrophobic blocks include polymethacrylates having pendant alkyl disulfide<sup>133, 134</sup> or pyridiyl disulfide groups.<sup>135-137</sup> The design of these ABPs presents an additional benefit that allows for the synthesis of disulfide-induced core crosslinked micelles (CCMs). The pendant disulfides are further involved in insitu disulfide-thiol exchange crosslinking reactions in micellar cores when being treated with a residual reducing agent. The resulting disulfide-CCMs exhibit enhanced colloidal stability during blood circulation as well as reduction-responsive enhanced release of encapsulated drugs.<sup>138-140</sup>

Dual location SRD (DL-SRD) approach centers on the synthesis of new intracellular nanocarriers having disulfide linkages in dual locations (Figure 2.4b). The locations of the disulfides can be in the micellar core, in the interlayered corona, or at the core/corona interface. The placement of reduction-responsive linkages in dual locations provides desirable synergistic release kinetics and therapeutic effects. Recent examples include novel ABP nanoassemblies having disulfides at core/interface and core/interlayered corona.<sup>141, 142</sup>

As illustrated in Figure 2.4c, multiple location multiple SRD (ML-MSRD) approach has been exploited to develop new intracellular nanocarriers possessing multiple stimuli-responsive cleavable linkages at multiple or dual locations. This new route offers considerable versatility in respect that responses to each stimulus can independently and precisely regulate drug release at several locations. A few reports describe dual systems such as reduction (interface)/pH (core)<sup>143, 144</sup> and pH (interface)/reduction (core),<sup>145</sup> and reduction (interface)/light (core).<sup>146</sup>



**Figure 2.4.** General approaches to synthesize SRD-exhibiting block copolymers and their self-assembled nanostructures as single location (a), dual location SRD (b), and multiple location multiple SRD (c) approaches.

## 2.4. Strategies to reduction-responsive PLA-based ABP systems

### 2.4.1. Direct polymerization strategy

This direct polymerization strategy begins with the design and synthesis of multifunctional initiators bearing three distinct functional groups: one for ROP of LA, one for controlled/living radical polymerization, and a disulfide linkage for reduction-responsive degradation. In the presence of the initiators, the sequential polymerizations allowed for the formation of PLA-based ABP functionalized with disulfide linkages. As a consequence, this strategy enables one to overcome the complexity caused by the covalent coupling strategy (described in the next section) that requires extra separation steps of excess homopolymers from targeted PLA-based ABPs for purification.

One elegant approach involves the synthesis of sheddable ABPs and their nanoassemblies. As summarized in Figure 2.5, this approach centers on the synthesis of a double-head initiator of HO-SS-Br by a facile coupling reaction of 2-hydroxyethyl disulfide with  $\alpha$ -bromoisobutyryl bromide. The initiator was used to initiate the ROP of LA catalyzed with  $\text{Sn}(\text{EH})_2$  in toluene at 120 °C, yielding well-defined PLA-SS-Br homopolymers with narrow molecular weight distribution as  $M_w/M_n < 1.0$ . The detailed studies indicate that initial mole ratio of  $[\text{Sn}(\text{EH})_2]_0/[\text{HO-SS-Br}]_0$  and polymerization time are important parameters that significantly influence low and high molecular weight PLA-SS-Br synthesis.<sup>147, 148</sup> Next, atom transfer radical polymerization (ATRP) was employed for various hydrophilic methacrylate monomers in the presence of the PLA-SS-Br macroinitiator to synthesize a variety of novel PLA-SS-based ABPs bearing a disulfide linkage at the block junction between PLA and polymethacrylate. These ABPs formed sheddable micelles having disulfides at PLA core/corona interfaces.

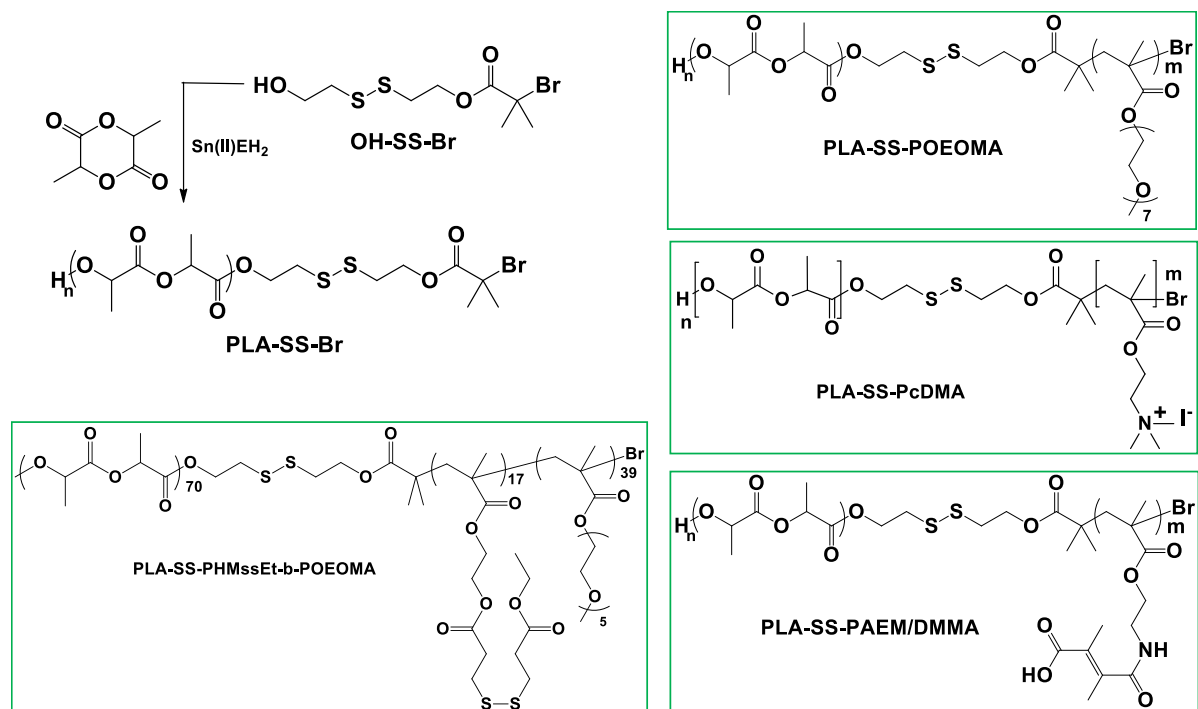


**Figure 2.5.** Synthetic route to a double-head initiator of OH-SS-Br for both ROP of LA and ATRP of methacrylates, well-controlled PLA-SS-Br by ROP of LA, and PLA-SS-based ABPs by ATRP in the presence of PLA-SS-Br macroinitiator.

A report describes the synthesis of PLA-SS-based poly(quarternized N,N-dimethylaminoethyl methacrylate) (PcDMA). The resultant PLA-SS-PcDMA self-assembled to form PLA cores, encapsulating anticancer drugs, surrounded with PcDMA cationic coronas, enabling the formation of complementary complexes with nucleic acids. Such sheddable-type micelloplexes exhibit enhanced release of both anticancer drugs and nucleic acids upon reductive response, suggesting great potential for dual chemotherapy and gene therapy.<sup>149</sup> Other reports also describe the synthesis of PLA-SS-based poly(oligo(ethylene oxide) monomethyl ether methacrylate)<sup>150</sup> and poly(aminoethyl methacrylate)/2,3-dimethylmaleic anhydride<sup>151</sup> for drug delivery.

Further, the DL-SRD approach was explored to synthesize a new PLA-SS-based triblock copolymer possessing disulfide linkages at dual locations, thus PLA-SS-PHMssEt-b-POEOMA. As illustrated in Figure 2.6, the self-assembly of the triblock copolymer allowed for the formation of micellar aggregates having multiple pendant disulfide linkages in a hydrophobic interlayer as well as single disulfides at interfaces of the interlayer and PLA core, surrounded with hydrophilic coronas. Through thiol-responsive cleavage of these dually located disulfide linkages, novel

interlayer-crosslinked micelles with a crosslinkable and sheddable extended corona were formed, thus combining enhanced colloidal stability, along with controlled release of encapsulated anticancer drugs to promote the inhibition of cell proliferation after internalization into cancer cells.<sup>21</sup>

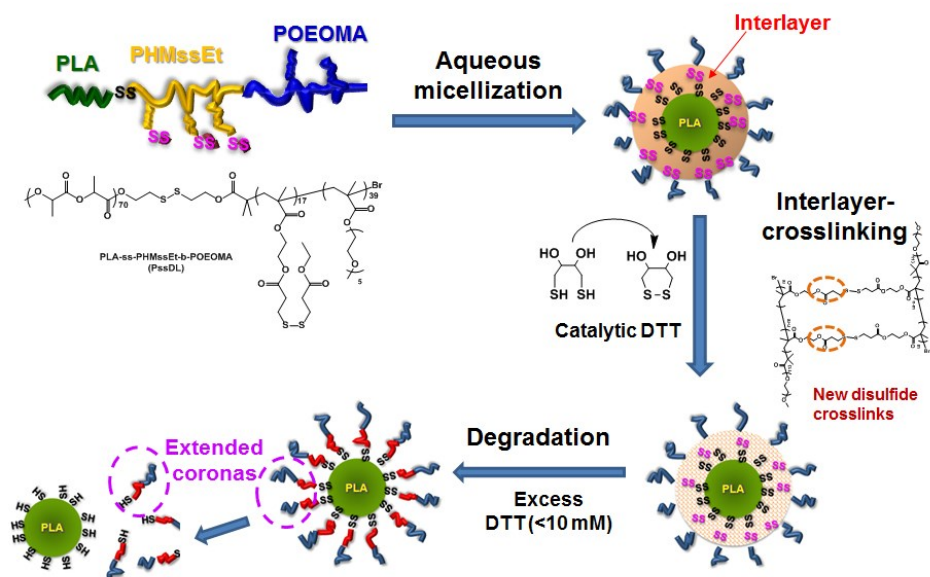


**Figure 2.6.** Schematic illustration of synthesis of PLA-SS-based interlayered crosslinked micelles for enhanced colloidal stability and shedding extended coronas for rapid release of encapsulated anticancer drugs, based on PLA-SS-PHMssEt-b-POEOMA triblock copolymers having multiple pendant disulfides in the interlayer and single disulfides at junctions of PHMssEt and POEOMA blocks in aqueous solution.<sup>21</sup> Copyright 2013 Royal Society of Chemistry.

Another approach involves the synthesis of PLA-based mono-cleavable and dual location SRD-exhibiting ABPs and their nanoassemblies. As illustrated in Figure 2.7, this approach began with the synthesis of functional PLA having a disulfide in the center (OH-PLA-SS-PLA-OH, i.e., SS(PLA-OH)<sub>2</sub>) by ROP of LA in the presence of 2-hydroxyethyl disulfide. For the synthesis of mono-cleavable SS(PLA-b-POEOMA)<sub>2</sub> triblock copolymer, ATRP of OEOMA was followed by the esterification of the resultant SS(PLA-OH)<sub>2</sub> to SS(PLA-Br)<sub>3</sub>. At concentrations above the CMC (5 µg/mL), this mono-cleavable ABP formed self-assembled micellar aggregates with disulfide-containing PLA cores. Thiol-triggered degradation exhibit enhanced release of encapsulated anticancer drug; however, thiol-responsive drug release kinetics was slower, compared to multi-cleavable ABP systems. Such slow release from mono-cleavable micelle systems is presumably

attributed to the amphiphilicity of the degraded products (HS-PLA-b-POEOMA and HS-PLA-b-PEG) with a half of molecular weight of their original ABPs (i.e., SS(PLA-b-POEOMA)<sub>2</sub> and SS(PLA-SS-PEG)<sub>2</sub>). These degraded products appeared to form smaller-sized aggregates which can also encapsulate drugs released from original mono-cleavable micelles.<sup>152</sup> In addition to the combination of ROP and ATRP, the combined ROP and esterification has been also explored to synthesize a triblock copolymer containing PLA and PEG, thus SS(PLA-b-PEG)<sub>3</sub>.<sup>153, 154</sup>

To explore a DL-SRD, a novel triblock copolymer having triple disulfide linkages in the center and at the junction of PLA and POEOMA blocks (SS(PLA-SS-POEOM)<sub>2</sub>) was synthesized by a combination of facile coupling reactions and ATRP from SS(PLA-OH)<sub>3</sub>. As illustrated in Figure 2.8, the ABP enabled the formation of micelles with disulfides positioned both in the hydrophobic PLA core and at the core/corona interface. The reductive response to glutathione as a cellular trigger resulted in the cleavage of the disulfide linkages both at the interface shedding hydrophilic coronas as well as in the PLA core causing disintegration of PLA cores. Such dual disulfide degradation process led to a synergistically enhanced release of encapsulated anticancer drugs in cellular environments.<sup>155</sup>

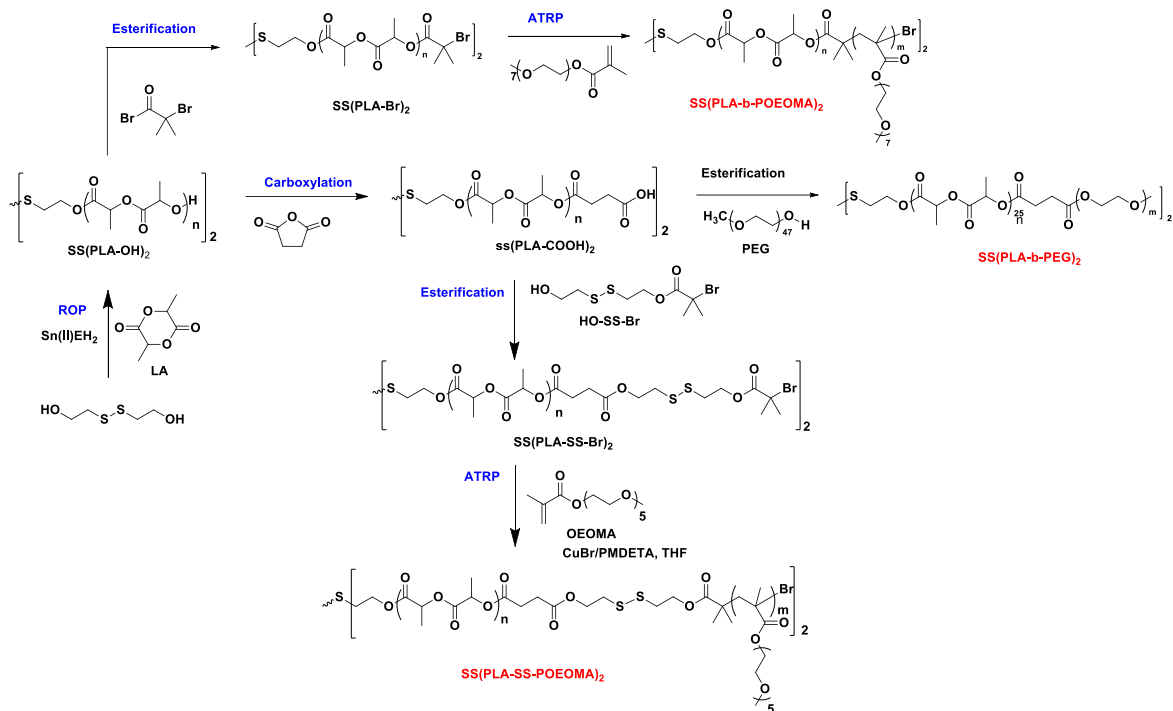


**Figure 2.7.** Synthetic routes to novel PLA-based mono-cleavable and dual location SRD-exhibiting ABPs functionalized with disulfide linkages.

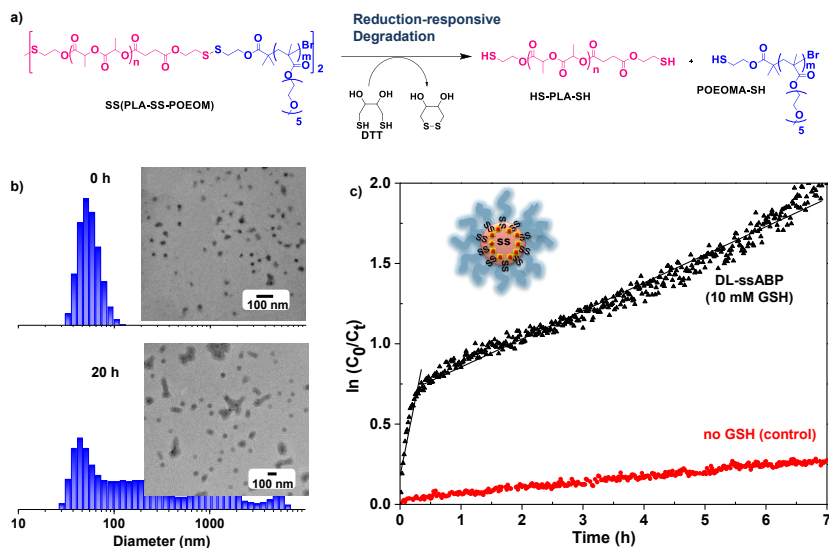


**Figure 2.8.** For SS(PLA-SS-POEOMA) triblock copolymer, reduction-responsive cleavage of disulfides in the presence of DL-dithiothreitol (a), dynamic light scattering diagrams and transmission electron microscopy images of the micelles before and after treatment with 10 mM GSH at 1.2 mg/mL (b), and enhanced release of DOX from DOX-loaded micelles in the absence (control) and presence of 10 mM GSH (c).<sup>155</sup> Copyright 2014 American Chemical Society.

### 2.4.2. Covalent coupling strategy

This strategy utilizes facile coupling reactions of functional PLA and hydrophilic polymer, either of which contains disulfide groups, thus yielding reduction-responsive PLA-based ABPs. One of the drawbacks of this strategy involves the extra separation steps to remove excess homopolymers from targeted ABPs because it requires the use of excess of either PLA or hydrophilic polymer. A report describes the reaction of poly(2-ethoxy-2-oxo-1,3,2-dioxaphospholane) (PEP) synthesized by ROP of EP with 3,3'-dithiodipropionic acid. The formed PEP-SS-COOH was then coupled with a hyperbranched Bolton H40-PLA-OH to yield H40-star-PLA-SS-PEP.<sup>156</sup> Other reports describe the synthesis of D- $\alpha$ -tocopherol (TPGS)-conjugated PEG-SS-PLA<sup>157</sup> and folate-conjugated PEG-PLA-SS-polyethyleneimine (PEI).<sup>158</sup> The formed PLA-based ABPs having disulfide linkages at the block junctions allowed for the formation of sheddable micelles having disulfide linkages located at hydrophobic PLA cores/coronas (SL-SRD).

Another approach shown in Figure 2.9 involves the synthesis of a folic acid-conjugated triblock copolymer comprising of PEG and PLA with multiple disulfide linkages (PEG-SS-PLA-SS-PLA-SS-PEG-folate) by multiple steps of coupling reactions (DL-SRD). Through nanoprecipitation method of the copolymer, redox-responsive folic acid and trastuzumab functionalized polymersomes with diameter = 150 nm were formed, with disulfides in the PLA cores and at core/corona interfaces. The presence of multiple redox responsive disulfide linkages led to complete disintegration of polymersomes in redox rich environment of cancer cells resulting in enhanced doxorubicin release. Folic acid and trastuzumab mediated active targeting resulted in improved cellular uptake and enhanced apoptosis in invitro studies. Further, *in vivo* studies in Ehrlich ascites tumor bearing Swiss albino mice exhibit enhanced antitumor efficacy and minimal cardiotoxicity of polymersomes.<sup>159</sup>

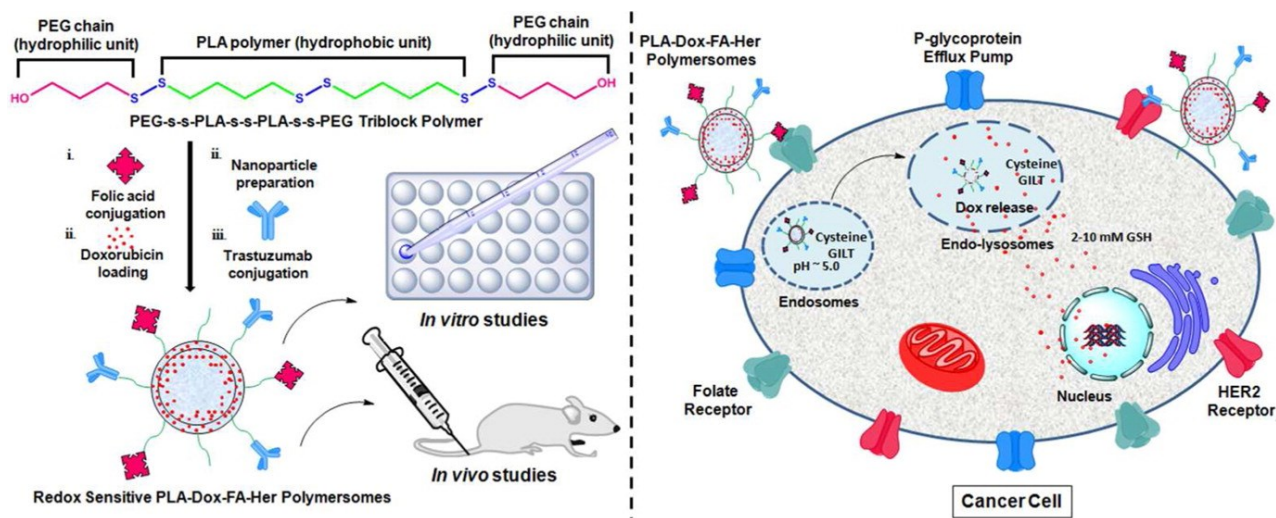


**Figure 2.9.** Schematic illustration of redox-responsive biodegradable polymersomes comprising of PEG-SS-PLA-SS-PLA-SS-PEG-folate triblock copolymer with multiple disulfide linkages as intracellular drug delivery nanocarriers in breast cancer.<sup>159</sup> Copyright 2015 American Chemical Society.

Shen and coworkers have reported an interesting approach that involves reversible and unsymmetrical disulfide bond formation directed by hydrogen bonding association. Consequently, this strategy requires the synthesis of functional homopolymers with oligoamide strands having complementary H-bonding sequences (i.e., arrays of H-bond acceptor and donor). As illustrated in Figure 2.10, PEG and PLA chains were end-modified with amide units A and B which are hydrogen bonding donor and acceptor. Further, they were functionalized with S-trityl groups capable for the formation of a double disulfide linkage by oxidation. The resultant PEG-A and PLA-B treated with iodine resulted in connection of PEG and PLA blocks, yielding PEG-SS-PLA diblock copolymer, while minimizing self-coupling. The resulting diblock copolymer self-assembled to form sheddable micelles having unsymmetrical disulfide linkages at PLA core/PEG corona interfaces. When the self-assembled micelles were treated with DTT, they were dissociated to PLA and PEG chains in aqueous solution.<sup>160</sup> Further, this disulfide and supramolecular H-bonding strategy has been explored to synthesize novel block copolymers and their nanoassemblies. They include PEG-SS-PLA-SS-PEI triblock copolymer for gene delivery<sup>161</sup> as well as PEG-grafted chitosan oligosaccharide,<sup>162</sup> PLA-SS-PEG-SS-PLA triblock,<sup>163</sup> and (PLA-SS-PEG) multi-block copolymer<sup>164</sup> for drug delivery.

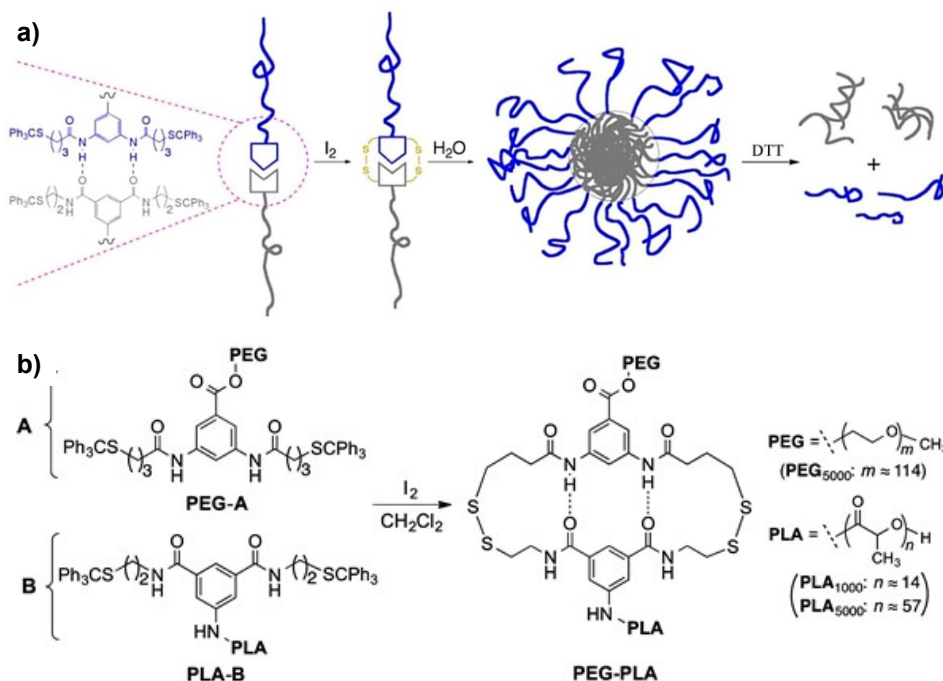


**Figure 2.10.** Schematic illustration of the strategy to synthesis, micellization, and redox responsiveness of a PEG-PLA diblock copolymer (a) and coupling of PEG-A and PLA-B based on unsymmetrical, reversible disulfide-bond formation instructed by H-bonding (b).<sup>160</sup> Copyright 2014 American Chemical Society.

### 2.4.3. Drug-polymer conjugation strategy

This strategy (called polymer prodrug strategy) involves the conjugation of anticancer drug molecules to PEG-b-PLA block copolymer through disulfide linkages through multiple steps of organic coupling reactions. The drug molecules were conjugated to PLA blocks of the copolymers, thus yielding reduction-responsive PEG-b-PLA-drug conjugates (i.e., prodrugs). Due to the amphiphilicity, these prodrugs self-assemble to form drug-conjugated nanoassemblies. After extravasation into tumor tissues and further internalization into cancer cells, anticancer drugs can be released from these prodrugs upon the cleavage of disulfide linkages in a reducing environment. Reports describe the synthesis and reduction-responsive drug release of curcumin-conjugated PLA-b-PEG prodrug (Cur-SS-PLA-b-PEG)<sup>165</sup> and docetaxel-conjugated poly(lactide-co-glycolide)-b-PEG (DTX-SS-PLGA-b-PEG)<sup>166</sup> and its self-assembled micellar aggregates.

## 2.5. Strategies to acidic pH-responsive PLA-based ABP systems

Inherently, PLA slowly degrades to the corresponding oligomers or LA species through the cleavage of backbone ester groups in a physiological condition. This hydrolysis process can be promoted in acidic conditions. Such process called acidic hydrolysis can facilitate the degradation process of PLA-based nanoparticles, inducing the enhanced release of encapsulated drugs. Further to enhance the degradation kinetics, several approaches have been proposed to synthesize acidic pH-responsive PLA-based nanoassemblies.

### 2.5.1. Sheddable and prodrug strategies

For the strategy to develop PLA-based sheddable systems, acidic pH-cleavable covalent tetrahydropyran (THP) chemistry was explored for the synthesis of PEO-THP-PLA block copolymer.<sup>167</sup> The copolymer self-assembled to form micellar aggregates having THP linkages at the interfaces of PLA cores and PEG coronas. In acidic pH, THP linkages were cleaved at the interfaces. The process enabled shedding PEG coronas from PLA cores, leading to enhanced release of encapsulated Dox. In addition, the preparation of pH-responsive nanoparticles having covalent phenylboronic-catechol ester linkages at the interfaces of PLA cores with poly(ethyleneimine) coronas was reported.<sup>168</sup> More interestingly, supramolecular host-guest chemistry was employed for the design of sheddable PLA systems. As illustrated in Figure 2.11, terminal benzimidazole-functionalized PEG (PEG-BM) and terminal  $\beta$ -cyclodextrin-functionalized PLLA (PLA-CD) were synthesized. Supramolecular self-assembly of these polymers enabled the formation of colloidally-stable aggregates having supramolecular CD-BM linkages at the interfaces of PLA cores and PEG coronas. TEM analysis indicates the diameter = 274 nm for the aggregates prepared at pH = 7.4. As pH decreased to 5.5, the diameter by TEM increased to 590 nm, due to pH-responsive dissociation of supramolecular CD-BM linkages. Such acidic pH response allows for enhanced release of encapsulated Dox, confirmed by in vitro and in vivo studies.<sup>169</sup>

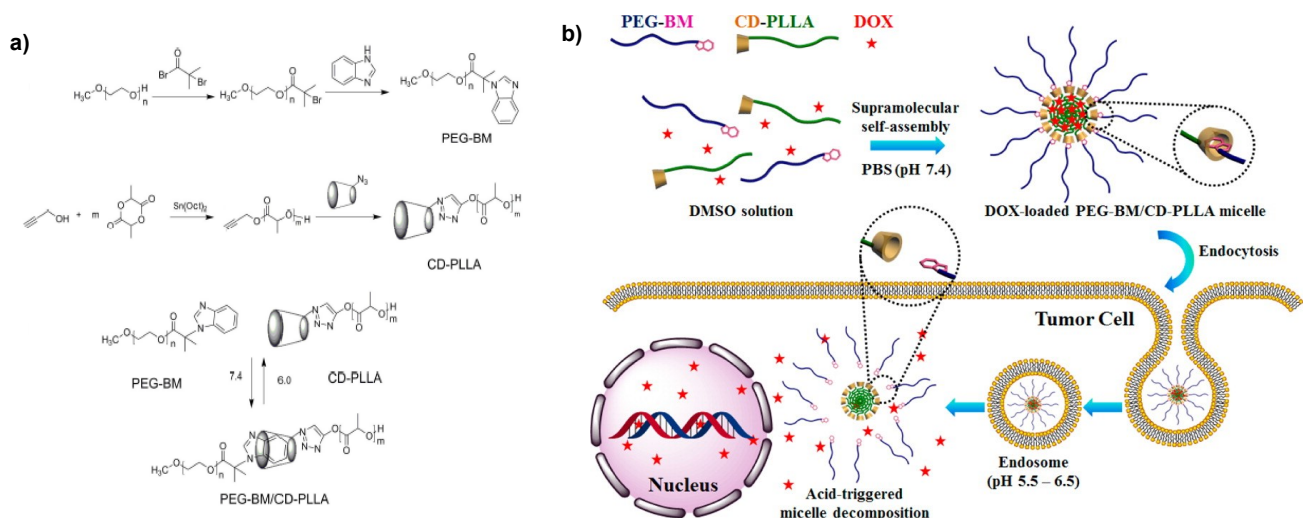


**Figure 2.11.** Synthesis (a) and intracellular delivery (b) of Dox-loaded PEG-BM/CD-PLLA supramolecular aggregates exhibiting triggered release of encapsulated Dox in response to intracellular microenvironment.<sup>169</sup> Copyright 2015 American Chemical Society.

For the strategy to develop acidic pH-responsive prodrugs, various anticancer drugs have been conjugated covalently through acidic pH-cleavable linkages with PLA-based ABPs as multiple steps of organic coupling reactions have been employed. Due to amphiphilic nature, the resultant ABP-drug conjugates self-assembled to form nanoassemblies containing drugs covalently conjugated to hydrophobic cores. Upon the cleavage of pH-responsive linkages, anticancer drugs were released from nanoassemblies.

Reports describe the synthesis of “linear” PLA-drug conjugates by simple conjugation of drugs with terminal PLA blocks of PLA-b-PEG, typically Dox conjugated with acetal linkage<sup>170</sup> and docetaxel conjugated with hydrazone linkage.<sup>171</sup> Other reports also describe the synthesis of “grafted” PLA-drug conjugates (PLA-graft-drug conjugates) by conjugation of drugs such as particularly Dox with pendant functional groups on PLA backbones through acid pH-cleavable linkages such as hydrazones. Yu and coworkers have reported the synthesis of amphiphilic PLAs grafted with Dox and PEG pendants (PLA-graft-Dox-PEG).<sup>172</sup> As illustrated in Figure 2.12, the synthetic route involves 1) ring opening polymerization to synthesize PLA functionalized with alkyne pendants (PLA-alkyne), 2) alkyne-azide cycloaddition to conjugate PEG-N<sub>3</sub> and 6-azidohxyl-4-formylbenzoate, and 3) coupling reaction of Dox with the aldehyde groups through hydrazone linkage formation. Similarly, Ganivada et al have synthesized PEG-based

PLA/polycarbonate copolymer that has biotin conjugated to PEG and pendant Dox grafted to polycarbonate through hydrazone linkages.<sup>173</sup> Initially, biotin-labeled PEG (biotin-PEG) and a cyclo-carbonate monomer functionalized with di-alkynes were synthesized by coupling reactions. Then, a ROP of LA and the monomer in the presence of biotin-PEG allowed for the synthesis of biotin-labeled PEG-b-(PLA-co-polycarbonate) with pendant alkynes. Their alkyne-azido cycloaddition with azido-functionalized Dox was followed.

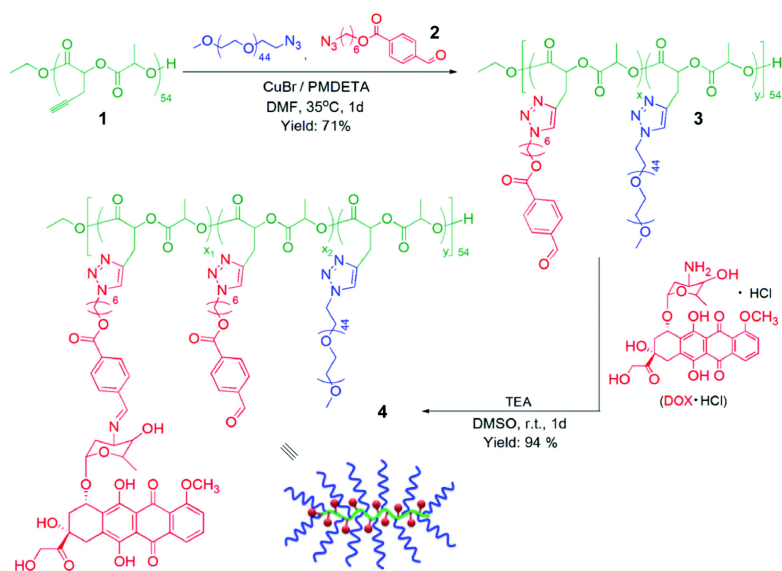


**Figure 2.12.** Synthesis of PLA-graft-Dox-PEG.<sup>172</sup> Copyright 2015 Royal Society of Chemistry.

### 2.5.2. Strategy to acidic pH-responsive volume change

This strategy involves the introduction of acidic pH-responsive groups such as  $\beta$ -amino ester (AE), oxazoline, and histidine into the design of PLA-based ABPs.<sup>174-178</sup> Upon change to acidic environments, these groups induce the assemblies undergoing changes in their polarities and eventually their volumes or dimensions, leading to enhanced release of encapsulated drugs.

Zhang et al has reported the synthesis and acidic pH-responsive drug release of poly( $\beta$ -amino ester) (PAE)-based ABP, thus (PEO-b-P(PLA-co-PAE)), by copolymerization of 4,4'-trimethylene (TDP) with vinyl-functionalized PLA and PEO through a Michael-addition reaction of diamines to vinyl groups.<sup>174</sup> PAE is soluble at pH < 6.5, but insoluble at pH > 6.5 because of its tertiary amine with  $pK_b = 6.5$ . At a physiological pH, the ABP assembled to form Dox-loaded nanoassemblies

consisting of (PLA-co-PAE) cores surrounded with PEO coronas. At mild acidic pH (5.0-6.5), the polarity of hydrophobic PLA cores could be changed to be relatively hydrophilic due to protonation of PAE groups. This process caused the loss of integrity of the formed nanoaggregates, exhibiting sustainable release of encapsulated Dox. Qiao and coworkers have reported the synthesis of a triblock copolymer consisting of PEG, PLA, and poly(L-histidine) blocks, thus PEG-b-PLA-b-PHis, with different degrees of polymerization of PLA and PHis blocks.<sup>175</sup> At pH = 8.5, the ABP formed micellar aggregates consisting of (PLA-b-PHis) cores surrounded with PEG coronas. Upon a change of pH to 4.5, PHis blocks were protonated, which resulted in reassembly of the micellar aggregates into micelles of PLA cores and PEG and protonated PHis coronas. Such pH-induced reassembly triggered enhanced release of encapsulated Dox, confirmed by cytotoxicity and CLSM results. In addition, reports describe the preparation of acidic pH-responsive nanoassemblies through co-micellization of acidic pH-responsive ABP with peptide-conjugated PEG-b-PLA for drug delivery with active targeting to specific tumors.<sup>177, 178</sup>

## 2.6. Intracellular tumor-targeting drug delivery

Most PLA-based ABP micelles having SRD elements, particularly disulfides and acidic pH-labile groups, have been designed with hydrophilic coronas, typically PEG or POEOMA. They are nontoxic to mammalian cells, and thus biocompatible. Anticancer drugs such as Dox and PTX were encapsulated physically in hydrophobic PLA cores. The resultant drug-loaded SRD-exhibiting micelles were degraded or disintegrated upon the cleavage of the cleavable linkages in response to glutathione or acidic pH (5-6.5). Such SRD enabled the enhanced release of encapsulated drugs.

Drug-loaded PLA-based micelles exhibiting SRD-induced enhanced drug release were further evaluated as effective intracellular drug delivery nanocarriers for cancer therapy. *In vitro* intracellular trafficking of drugs from the micelles were studied using flow cytometry and confocal laser scanning microscopy (CLSM). As an example, Dox-loaded micelles from POEOMA-SS-PLA-SS-PLA-SS-POEOMA triblock copolymer were incubated with HeLa cancer cells.<sup>155</sup> As illustrated in Figure 2.13, compared with HeLa cells, the flow cytometric histogram of HeLa cells incubated with Dox-loaded micelles presented a noticeable shift in the direction of high fluorescence intensity. CLSM images also show that HeLa cells incubated with Dox-loaded

micelles display strong Dox fluorescence in their nuclei. These results confirm that Dox-loaded micelles enable the delivery and release of Dox into nuclei of cancer cells.

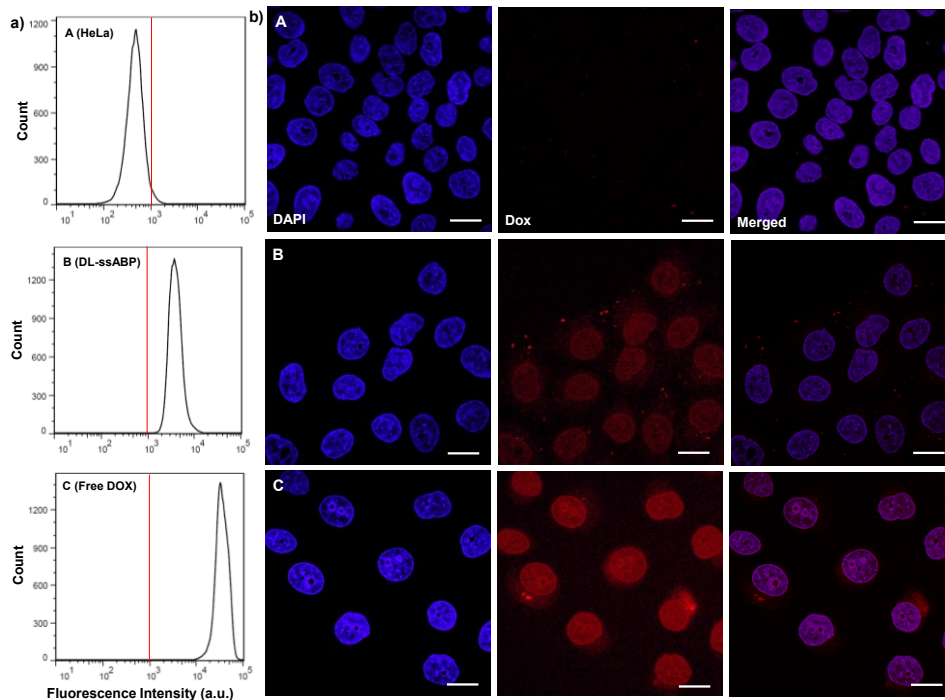


**Figure 2.13.** Flow cytometric histograms (a) and CLSM images (b) of HeLa cells only (A) and incubated with DOX-loaded micelles of POEOMA-SS-PLA-SS-PLA-SS-POEOMA triblock copolymer (B), and free DOX (C) for 16 hrs. Scale bar = 20  $\mu\text{m}$ .<sup>155</sup> Copyright 2014 American Chemical Society.

Further to *in vitro* studies, reductive PLA-based micelles were evaluated *in vivo* (animal models).<sup>157, 159, 161, 179</sup> Typically, a report describes the synthesis of hyaluronic acid-cystamine-PLGA block copolymer (HA-SS-PLGA) and self-assembly to construct sheddable micelles encapsulated with both Dox) and cyclopamine (CYC, a primary inhibitor of the hedgehog signaling pathway of cancer stem cells).<sup>180</sup> Dual drug-loaded particles potently diminished the number and size of tumorspheres and HA showed a targeting effect towards breast CSCs. As illustrated in Figure 2.14, *in vivo* combination therapy further demonstrated a remarkable synergistic anti-tumor effect and prolonged survival compared to mono-therapy using the orthotopic mammary fat pad tumor growth model. The co-delivery of drug and the CSC specific

inhibitor towards targeted cancer chemotherapeutics provides an insight into anticancer strategy with facile control and high efficacy.

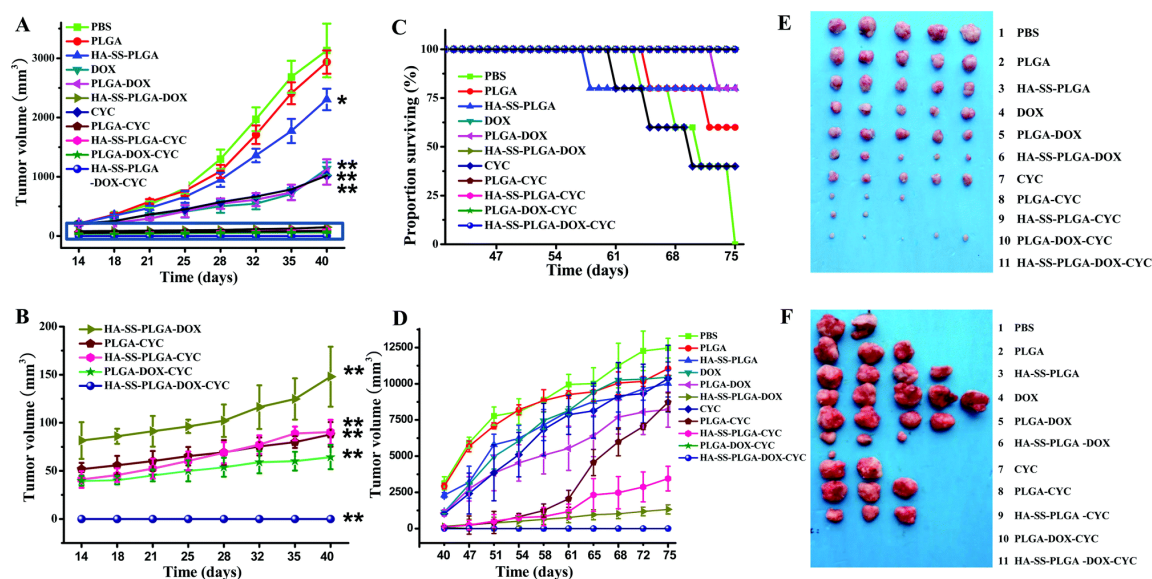


**Figure 2.14.** For Dox-loaded micelles self-assembled from hyaluronic acid-cystamine-PLGA block copolymer (HA-SS-PLGA), *in vivo* combination therapy using orthotopic mammary fat pad tumor growth model; tumor volumes (A, B, D), life survival of tumor-bearing mice (C), photos of excised tumors at the end of the treatment at day 40 (E), and day 75 (F).<sup>180</sup> Copyright 2015 Royal Society of Chemistry.

An interesting study has been reported for different intracellular drug delivery routes of self-assembled and disulfide bonded micelles using physically loading hydrophobic FRET probes (Figure 2.15). The former was made of mPEG-b-PLA (no disulfide), while the latter was made of mPEG-(Cys)<sub>4</sub>-PLA block copolymer synthesized by coupling reaction of oligocysteine (Cy<sub>4</sub>) with PEG and PLA blocks. The self-assembled micelles were structurally dissociated by micelle-membrane interactions, and the hydrophobic probes were distributed on the plasma membrane. However, intact disulfide bonded micelles carrying hydrophobic probes were internalized into cancer cells via multiple endocytic pathways. Following internalization, disulfide bonded micelles were decomposed in early endosomes by glutathione-mediated disulfide bond reduction, exposing the probes to intracellular organelles.<sup>181</sup> Further, disulfide bonded micelles stably retained doxorubicin in the bloodstream and efficiently delivered the drug to a tumor, with a 7-fold increase of the drug in the tumor and 1.9-fold decrease in the heart, as compared with non-crosslinked self-

assembled micelles. With a Dox dose as low as 2 mg/kg, disulfide bonded micelles almost completely suppressed tumor growth in mice.<sup>182</sup>

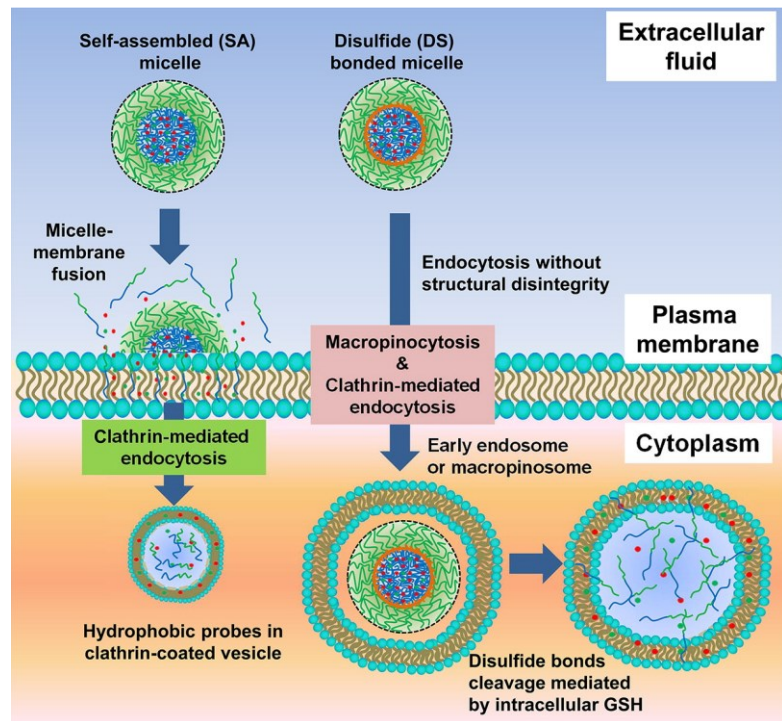


**Figure 2.15.** Schematic diagram of cellular entry routes and intracellular fates of self-assembled mPEG-b-PDLLA micelles and disulfide bonded mPEG-(Cys)<sub>4</sub>-PLA micelles.

## 2.7. Summary and outlook

The recent advances in the development of PLA-based ABPs and their self-assembled nanostructures exhibiting SRD-induced enhanced drug release is summarized, with an emphasis on their design, synthesis, and evaluation as intracellular drug delivery nanocarriers for cancer therapy. A number of novel strategies have been reported to synthesize various self-assembled stimuli-responsive degradable PLA-based micellar aggregates having the different numbers, positions, and locations of single or multiple (or dual) cleavable linkages, particularly disulfide and acid-labile linkages. Covalent coupling, direct polymerization, and drug-polymer conjugation strategies to synthesize reduction-responsive PLA-based nanoassemblies as well as sheddable and prodrug strategies to acidic pH-responsive PLA-based nanoassemblies have explored. Most of these PLA-ABPs were designed with disulfide and acid-labile linkages positioned in the junctions

of PLA and hydrophilic blocks or PLA and drug, in the center of triblock copolymers, or in the dual locations. Further to SRD-induced enhanced/controlled release profiles of encapsulated drugs to kill cancer cells, *in vitro* (cells) and *in vivo* studies suggest that the development of novel SRD-exhibiting PLA-based nanoassemblies is the promising platform for tumor-targeting drug delivery. Current and future design and development of more effective SRD PLA-based nanoassemblies require a high degree of control to their degradation kinetics for precise release of encapsulated anticancer drugs. Further to the design and development of new nanoassemblies, more efforts should be made for *in vivo* and clinical studies.

## **2.8 Recent literature update**

In addition to the sections discussed above, following reports regarding PLA-based SRD systems for drug delivery applications, were published after 2017.

### **2.8.1. Reduction-responsive PLA-based systems**

Du et al. designed a redox-responsive mixed micelle system, by combining reduction-sensitive hyaluronic acid-poly(lactide) (HA-ss-PLA) conjugates and D- $\alpha$ -tocopheryl polyethylene glycol 1000 succinate (TPGS, a PEGylated-vitamin E, well-known as a P-gp efflux inhibitor, capable of reversing multidrug resistance (MDR) in tumor cells.<sup>183</sup> As illustrated in Figure 2.16a, PLA was first synthesized using ROP and was then subject to end chain acid-amine coupling reactions with hyaluronic acid (HA), yielding HA-ss-PLA.

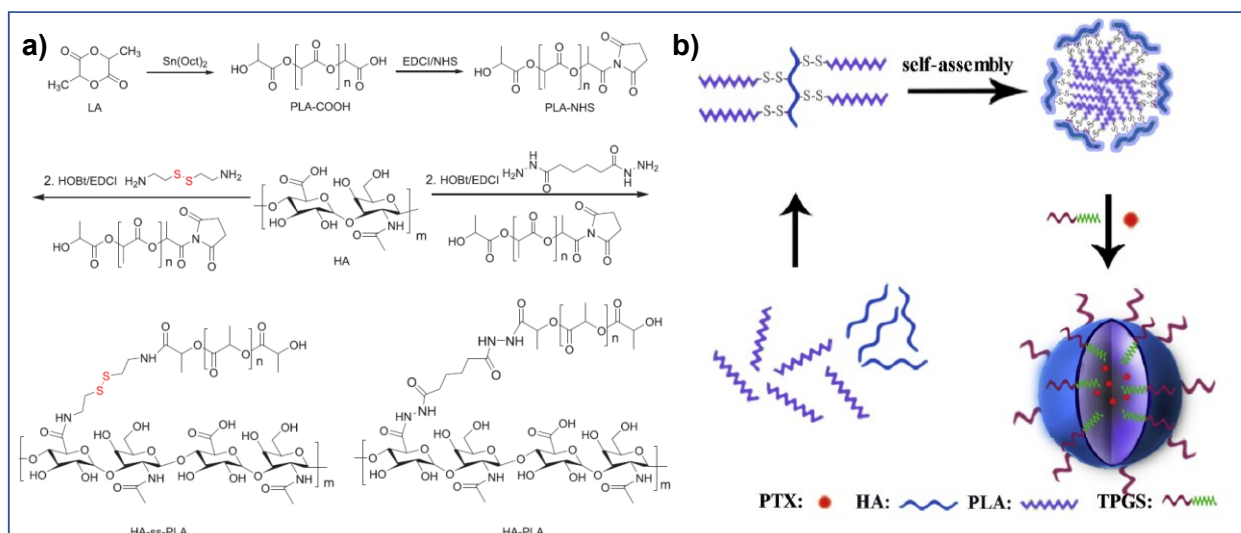


**Figure 2.16.** Synthetic route of raft copolymer HA-ss-PLA and HA-PLA a), schematic representation of self-assembled process of mixed micelles b).<sup>183</sup>

This copolymer, therefore, falls under the coupling strategy to synthesize PLA-based ABPs. The blank and PTX loaded mixed micelles with HA-ss-PLA and TPGS were prepared using a film dispersion-ultrasonic method, which possessed particle diameter of 124 nm and showed an entrapment efficiency of 87.9 % (Figure 2.16b). The micelles showed reduction-responsive release of PTX in intracellular reductive environment. In addition, they demonstrated an enhanced drug accumulation to the tumor site via reversal of MDR and inhibited growth of tumor cells, thus being a potential candidate in treating MDR tumors in the future. In another report, Gaspar et al. designed redox-responsive triblock copolymer micelles based on poly(2-ethyl-2-oxazoline)-poly(L-lactide) grafted with bioreducible polyethylenimine (PEOZ-PLA-g-PEI-SS).<sup>184</sup> This synthesis was performed by modifying the PEI with CBA first to synthesize PEI-CBA. In a separate reaction, PEOZ-PLA was synthesized by cationic ROP, whose terminal hydroxyl groups were activated using carbonyldiimidazole and further conjugated to PEI-CBA to yield PEOZ-PLA-g-PEI-SS. This triblock copolymer comprised of non-fouling oxazolines, hydrophobic PLA block for drug encapsulation and PEI-SS for minicircle DNA (mcDNA) complexation and triggered release. These micelleplexes not only showed higher cellular uptake but also demonstrated enhanced gene expression in comparison to non-bioreducible control nanocarriers.

### 2.8.2. Strategy to synthesize photo-responsive PLA-based ABP systems

Photo-responsive polymeric systems typically consist of moieties that undergo photocleavage with subsequent disruption of the nanocarrier and payload release.<sup>185</sup> Photo-responsive systems have gained significant attention as the high spatial and temporal resolution of light enables precise control over the degradation kinetics and hence drug delivery. In a novel approach, flower like micelles were fabricated using triblock copolymers composed of polylactide-block-o-nitrobenzyl-poly (ethylene glycol)-o-nitrobenzyl-block-polylactide (PLA-NB-PEG-NB-PLA).<sup>186</sup> Under UV irradiation at 365 nm, the NB groups in backbone of the polymer cleaved leading to the hydrophobic aggregates (Figure 2.17).

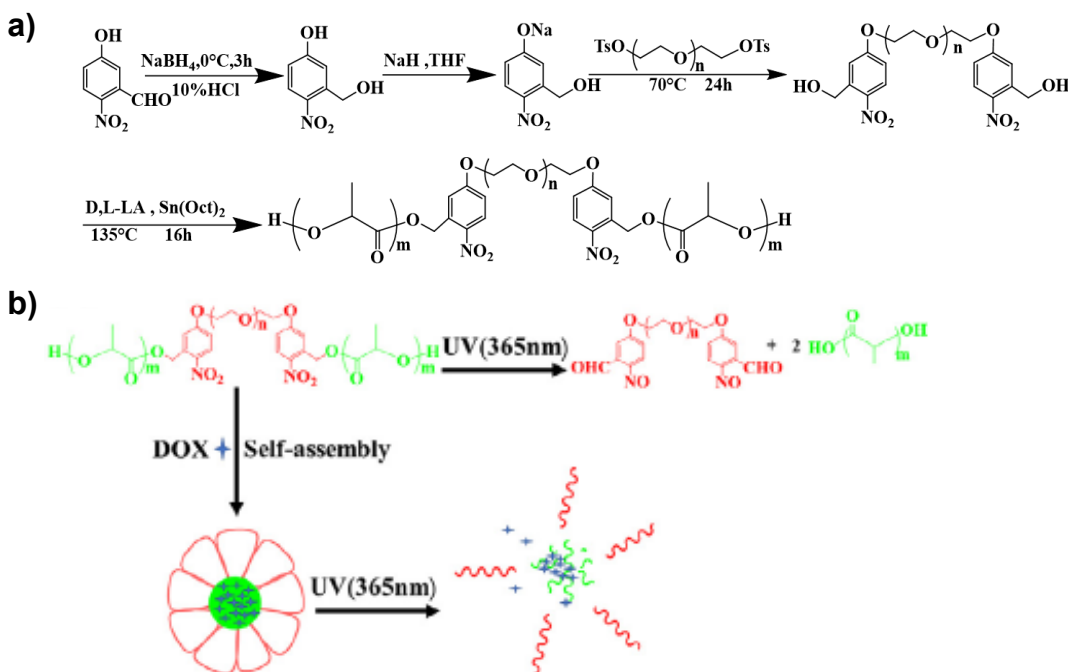


**Figure 2.17.** Synthetic scheme for photo-responsive PLA-NB-PEG-NB-PLA a), schematic illustration of dox-loaded micelles and photo-controlled release at 365 nm irradiation b).<sup>186</sup>

Different chain lengths of PEG and PLA were tested to understand the effect on photolysis rate and loading efficiency of Dox, with shorter lengths leading to higher photolysis rates and increased loading efficiencies.

### 2.8.3. Triple-stimuli responsive PLA-based ABP systems

Sadr et al. prepared novel Fe<sub>3</sub>O<sub>4</sub> conjugated PLA grafted-poly(2-hydroxyethyl methacrylate (HEMA)-co-(N-isopropylacrylamide)(NIPAAm)-co-methacrylic acid (MAA)-co-3-(trimethoxysilyl) [Fe<sub>3</sub>O<sub>4</sub>@PLA-g-P(NIPAAm-co-HEMA-co-MAA-co-TMSPMA)] polymer by ROP and free radical polymerization method.<sup>187</sup> These nanoparticles (nps) were designed for combination cancer therapy by synthesizing paramagnetic, thermoresponsive and pH-responsive grafted copolymers. Cationic Dox and anionic methotrexate (MTX) anticancer drugs were loaded simultaneously with higher encapsulation efficiencies of 95.04 % and 97.29 % respectively. Different assays such as MTT assay, DAPI staining, cell cycle and real time PCR analysis demonstrated higher antitumor activity of DOX/MTX loaded nanocomposite in comparison to free drugs, thus proving its potential for targeted drug delivery for *in vivo* uses.

### 2.8.4. Reactive oxygen species (ROS)-responsive PLA-based ABP systems

To address the challenges of PEG dilemma, an innovative molecule, amphiphilic mPEG bridged to the photosensitizer Ce6 via a thioketal bond (mPEG-TK-Ce6), was synthesized and used to achieve the PEGylation of PLA-based nanoparticles to encapsulate the prodrug Pt(IV).<sup>188</sup> Upon subject to 660 nm radiation, Ce6 generated ROS which led to the degradation of TK bonds and dePEGylation, thus enhancing tumor cell internalization and subsequent anticancer effect. In another report, PLA coated mesoporous silica nanoparticles (MSNPs), conjugated with a ligand peptide of low-density lipoprotein receptor (LDLR) which is known to increase the transcytosis of MSNPs and enable blood-brain barrier (BBB) crossing were developed.<sup>189</sup> These MSNPs were designed to encapsulate antioxidant resveratrol (RSV) for delivery to central nervous system to target oxidative stress. It was shown that ROS can potentially accelerate the degradation of PLA hence releasing RSV, with PLA acting as a gatekeeper.

### **2.8.5. Dual pH/reduction-responsive PLA-based polyplexes for siRNA delivery**

Zhu et al. designed a dual pH/redox-responsive system comprising of methoxy-poly(ethylene glycol)-polylactide-polyhistidine-ss-polyethylenimine (PEG-b-PLA-PHis-ssPEI1.8 k) which consisted of pH-responsive histidine segment linked to branched PEI through a redox-responsive disulfide bond.<sup>190</sup> This copolymer demonstrated excellent siRNA complexation and protection. FRET test was used to investigate the disassembly extent of siRNA from the copolymer and accelerated release of siRNA was observed until the N/P ratio was increased above 10.

### **2.8.6. SRD-based self-immolative nps for controlled drug release**

In this study, hybrid nps composed of self-immolative poly(ethylglyoxylate) (PEtG) and slowly degrading PLA were synthesized with an aim of observing a rapid release of drug from PEtG domains and a slower release from PLA domains.<sup>191</sup> 6-Nitroveratryl carbonate capped PEtG and disulfide-capped PEtG were selected for UV light-responsive and thiol-responsive systems and their degradation was studied by dynamic light scattering (DLS) and release of NR as a probe. Upon appropriate stimuli, the PEtG blocks degraded faster as anticipated, with dependence on PEtG:PLA ratio used.

## Chapter 3

### PLA-based triblock copolymer micelles exhibiting dual acidic pH/reduction responses at dual core and core/corona interface locations

#### 3.1. Introduction

PLA, along with PCL and PGA, belongs to a class of hydrophobic aliphatic polyesters of hydroxyalkanoic acids, and is known to be biocompatible, biodegradable, and FDA-approved for clinical use.<sup>71, 73, 77</sup> Due to these features, PLA and its copolymers have been extensively used as a promising choice of hydrophobic blocks to synthesize amphiphilic block copolymers (ABPs).<sup>20</sup> Designed with hydrophilic blocks such as PEG,<sup>192</sup> well-controlled PLA-based ABPs self-assemble in aqueous solution to form aqueous micellar aggregates (or nanoassemblies). The hydrophobic PLA cores surrounded with PEG coronas are capable of the encapsulation of small molecule hydrophobic anticancer drugs. Upon intravenous injection into the blood, the drug-loaded micelles could be extravasated into tumor tissues through the EPR effect.<sup>67-69</sup> Inside targeted tissues and cells, it is anticipated that drugs can be released in a controlled fashion. However, a drawback associated with conventionally designed PLA-based micellar nanocarriers is the slow-release rate of encapsulated drugs, which could be mainly due to the slow degradation of PLA backbones in physiological or slightly acidic pH environments.

To improve the drug release kinetics, SRD has been explored as a promising platform in the development of smart ABP-based nanoassemblies. SRD involves the incorporation of labile linkages into the design of ABPs and their nanoassemblies. Later, the linkages can be cleaved in response to external stimuli.<sup>105, 111, 193</sup> The stimuli-responsive cleavage causes the destabilization or disintegration of micelles, thus leading to enhanced/controlled release of encapsulated drugs.<sup>128</sup> Of external stimuli, the reductive reaction is promising because disulfide bonds can be cleaved to the corresponding thiols in a reducing environment (in the presence of reducing agents). In biological systems, intracellular level of GSH (which acts as a reducing agent) is known to be 100–1000 fold higher than extracellular level. Further, the concentration of GSH is 4-5 times greater in cancer cells, compared with normal cells.<sup>109-112, 194</sup>

Given the promising disulfide chemistry, early efforts have been made to synthesize reduction-responsively degradable PLA-based ABPs with disulfide linkages positioned either at the junction of PLA/hydrophilic blocks or in the center of triblock copolymer. Consequently, the self-assembled micelles from these PLA-ABPs have disulfides positioned at single location, as at core/corona interfaces (shedtable micelles)<sup>149-151, 161, 162</sup> or in PLA cores (monocleavable micelles).<sup>152-154</sup> Further efforts led to the synthesis of advanced reduction-responsive PLA-based micelles with disulfides positioned at dual locations, as interface/core or interface/interlayered core.<sup>21, 155, 159, 163</sup> These dual location reduction-responsive micelles appeared to be more effective as disulfide linkages degraded in dual locations, leading to the accelerated release of encapsulated drugs.<sup>195</sup> In addition to GSH-driven reduction, acidic pH is another promising endogenous trigger found in biological systems because of the presence of slightly acidic pH = 6.5-6.9 in tumor tissues and further pH = 4.5-5.5 in endosomes and lysosomes.<sup>113, 196</sup> Acetal and hydrazone groups have been incorporated into the synthesis of acidic pH-responsive PLA-based micelles.<sup>170, 171, 197</sup> Despite these advances, most of the smart PLA-based micelles have been designed to respond to single stimulus (reduction or acidic pH). Developing smart PLA-based micelles exhibiting dual stimuli-responses at dual locations (core, interlayer, and core/corona interface) is highly beneficial. These micelles designed with DL-DSRD could offer the versatility in that dual-stimuli responses to each stimulus can independently regulate the release of encapsulated molecules and can facilitate synergistic/accelerated release at dual locations.<sup>146, 198</sup>

This chapter describes our initial effort to develop a novel strategy that allows for the synthesis of an ABA-type PLA-based triblock copolymer consisting of a hydrophilic polymethacrylate (A) and PLA (B) blocks (P4). The P4 copolymer contains two reduction-responsive disulfide (ss) linkages positioned to link A and PLA blocks and acidic pH-responsive ketal linkage in the center of PLA block, thus A-ss-PLA-ketal-PLA-ss-A. The strategy utilizes a combination of two polymerization techniques, esterification, and coupling reaction. As illustrated in Figure 3.1, the P4 self-assembled to nanoassemblies with ketal in PLA cores and disulfide at the PLA core/corona interfaces, thus retaining DL-DSRD. The cleavage of interfacial disulfide in the presence of GSH (a cellular reducing agent) resulted in shedding coronas from micelles, while the cleavage of core ketal linkages in acidic pH resulted in the disruption of the micelle cores. Compared with those single responses, dual responses in the presence of GSH at acidic pH at dual locations (both cores

and interfaces) resulted in synergistic regulation of micelle destabilization, thus leading to accelerated release.

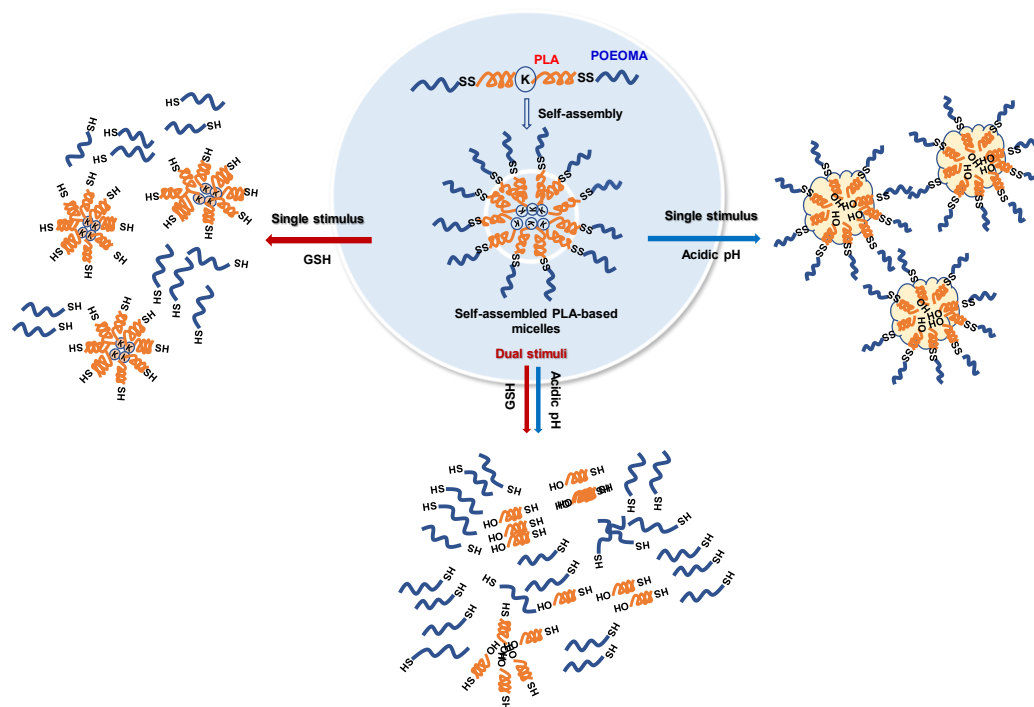


**Figure 3.1.** Illustration of aqueous micellization and dual acidic pH/reduction-responsive degradation of a PLA-based triblock copolymer (P4) consisting of a hydrophilic polymethacrylate and PLA blocks with an acidic pH-responsive ketal linkage in the center of PLA block and reduction-responsive disulfides at polymethacrylate/PLA block junctions, thus exhibiting dual responses at dual locations.

## 3.2. Instrumentation

### 3.2.1. Experimental

$^1\text{H-NMR}$  spectra were recorded using a 500 MHz Varian spectrometer. The  $\text{CDCl}_3$  singlet at 7.26 ppm was selected as the reference standard. Molecular weight and molecular weight distribution were determined by gel permeation chromatography (GPC). An Agilent GPC was equipped with a 1260 Infinity Isocratic Pump and a RI detector. Two Agilent PLgel mixed-C and mixed-D columns were used with DMF containing 0.1 mol % LiBr at 50 °C at a flow rate of 1.0 mL/min. Linear poly(methyl methacrylate) standards from Fluka were used for calibration. Aliquots of the polymer samples were dissolved in DMF/LiBr. The clear solutions were filtered using a 0.45  $\mu\text{m}$  PTFE filter to remove any solvent-insoluble species. A drop of anisole was added

as a flow rate marker. Monomer conversion was determined using  $^1\text{H}$  NMR spectroscopy. The size of micellar aggregates in hydrodynamic diameter was measured by dynamic light scattering (DLS) at a fixed scattering angle of  $175^\circ$  at  $25^\circ\text{C}$  with a Malvern Instruments Nano S ZEN1600 equipped with a 633 nm He-Ne gas laser. Fluorescence spectra on a Varian Cary Eclipse Fluorescence spectrometer and UV/Vis spectra on an Agilent Cary 60 UV/Vis spectrometer were recorded using a 1 cm wide quartz cuvette.

*Transmission Electron Microscopy (TEM)* images were obtained using a Philips Tecnai 12 TEM, operated at 120 kV and equipped with a thermionic LaB6 filament. An AMT V601 DVC camera with point-to-point resolution and line resolution of 0.34 nm and 0.20 nm respectively was used to capture images in 2048 by 2048 pixels. To prepare specimens, the micellar dispersions were dropped onto copper TEM grids (400 mesh, carbon coated), blotted and then allowed to air dry at room temperature.

### 3.2.2. Materials

Triethylamine ( $\text{Et}_3\text{N}$ ,  $\geq 99.5\%$ ), succinic anhydride (SA, 99%), 4-(N,N-dimethylamino)pyridine (DMAP,  $\geq 99\%$ ), 3,6-dimethyl-1,4-dioxane-2,5-dione (DL-lactide, LA, 99%), copper (I) bromide ( $\text{CuBr}$ ,  $>99.99\%$ ), N,N,N',N'',N''-pentamethyldiethylenetriamine (PMDETA,  $>98\%$ ), tin(II) 2-ethylhexanoate ( $\text{Sn}(\text{EH})_2$ , 95%), Nile Red (NR), and glutathione (GSH, a reduced form) from Aldrich, 1-ethyl-3-(3-(dimethylamino)-propyl)carbodiimide-HCl salt (EDC) from Matrix Innovation and DL-dithiothreitol (DTT, 99%) from Acros Organics were purchased and used as received. Oligo(ethylene glycol) monomethyl ether methacrylate (OEOMA) with MW = 300 g/mol and EO units = 5 purchased from Aldrich, was purified by passing through a column filled with basic alumina to remove the inhibitors. A double-head initiator (HO-ss-Br) and a ketal-labeled diamine (A1) were synthesized as described in our publications.

### 3.2.3. Synthesis of (co)polymers

**PI by ROP.** HO-ss-Br (45.9 mg, 0.3 mmol), LA (5 g, 34 mmol),  $\text{Sn}(\text{EH})_2$  (10.0 mg, 24  $\mu\text{mol}$ ), and toluene (3 mL) were placed in a 10 mL Schlenk flask. The resulting mixture was deoxygenated by four freeze-pump-thaw cycles. The reaction flask was filled with nitrogen, thawed, and then immersed in an oil-bath preheated at  $120^\circ\text{C}$  to start the polymerization. After 3 hrs, the

polymerization was stopped and cooled to room temperature. The resulting PLA was precipitated from cold MeOH, and then dried in vacuum oven overnight.

**P2 by ATRP.** The purified P1 (4.0 g, 0.40 mmol), OEOMA (3.62 g, 12.0 mmol), PMDETA (35  $\mu$ L, 0.16 mmol), and THF (3 mL) were mixed in a 10 mL Schlenk flask. The resulting mixture was deoxygenated by four freeze-pump-thaw cycles. The reaction flask was filled with nitrogen and CuBr (23.1 mg, 0.16 mmol) was then added to the frozen solution. The flask was sealed, purged with vacuum, and backfilled with nitrogen once. The mixture was thawed, and the flask was then immersed in an oil-bath preheated to 50 °C to start the polymerization. The polymerization was stopped after 1.5 hrs by exposing the reaction mixture to air.

For purification, as-synthesized polymer solutions were added dropwise into hexane (800 mL) under magnetic stirring. The resulting precipitates were dissolved in THF and passed through a column filled with basic aluminum oxide to remove copper species two times. After the solvent was removed by rotary evaporation, the formed polymers were dried in a vacuum oven at room temperature overnight.

**P3 by esterification.** The purified, dried P2 (1.4 g, 47  $\mu$ mol), SA (0.11 g, 1.19 mmol), and DMAP (2.8 mg, 23  $\mu$ mol) were dissolved in THF (10 mL). The resulting solution was kept at room temperature for 12 hrs and then was dialyzed against PBS solution (pH 7.4) to remove excess SA and DMAP for 12 hrs. Then, the resulting P3 was collected by lyophilization.

**P4 by EDC mediated coupling reactions.** A solution of A1 (2.2 mg, 14  $\mu$ mol) dissolved in chloroform (10 mL) was added dropwise to a solution consisting of P3 (0.6 g, 27  $\mu$ mol), EDC (0.05 g, 0.27 mmol), and DMAP (3.3 mg, 27  $\mu$ mol) in chloroform (10 mL) under stirring at room temperature for 24 hrs. The resulting mixture was then dialyzed over PBS solution (pH = 7.4) to remove excess EDC and DMAP for 12 hrs. The mixture was lyophilized to collect the purified, dried P4 polymer.

### 3.2.4. Aqueous micellization

**Determination of CMC using a NR probe.** A stock solution of NR in THF at 1 mg/mL and a stock solution of P4 in THF at 1 mg/mL were prepared. PBS solution at pH 7.4 (10 mL) was then added dropwise into different vials containing the same amount of NR (0.5 mL, 0.5 mg NR)

and varying amounts of P4. The resulting mixtures were stirred for 12 hrs to remove THF and were then subjected to filtration using 0.45 $\mu$ m PES filters to remove excess NR. A series of NR-loaded micelles at various concentrations of P4 ranging from 10<sup>-6</sup> to 0.1 mg/mL were formed. Their fluorescence spectra were recorded at  $\lambda_{\text{ex}} = 480$  nm.

**Preparation of aqueous micelles.** PBS at pH = 7.4 (10 mL) was added dropwise into a solution of P4 (10 mg) dissolved in THF (10 mL). The resulting mixture was stirred for 24 hrs to remove THF, yielding aqueous micellar dispersions at 1 mg/mL.

### 3.2.5 Studies of dual acidic pH/reduction-responsive degradation

**P4 in DMF.** A solution of P4 (20 mg, 1.3  $\mu$ mol) dissolved in DMF (4 mL) was mixed with a stock solution of DTT in DMF (3 mg/mL, 1.6 mL, 13.2  $\mu$ mol) for reductive response under magnetic stirring at room temperature. The equivalent solution of P4 was mixed with HCl (5  $\mu$ L) for acidic pH response. Aliquots were taken periodically for GPC analysis.

**P4 micelles in water.** Aliquots of aqueous empty micellar dispersion were mixed with PBS (pH = 7.4) with and without 10 mM GSH as well as aqueous acetate buffer at pH = 5.4 with and without 10 mM GSH under stirring.

### 3.2.6. Dual stimuli-responsive release of NR from NR-loaded micelles

For preparation of NR-loaded micelles, a stock solution of NR in THF (5 mg/mL, 0.5 mL) was mixed with a solution of P4 (10 mg) dissolved in THF (2.0 mL). After a PBS solution at pH = 7.4 (10 mL) was added, the resulting mixture was stirred for 24 hrs to remove THF. Free (not encapsulated) NR was removed by filtration using a 0.45  $\mu$ m PES filter to form aqueous NR-loaded micellar dispersion at 0.8 mg/mL.

For release experiments, the formed dispersions were divided into equivalent aliquots (0.5 mL each) in 20 mL vials. They were mixed with 10 mM GSH in PBS (pH = 7.4), acetate buffer at pH = 5.4, 10 mM GSH in acetate buffer at pH 5.4 and PBS with pH 7.4 as control. Their fluorescence spectra were recorded at given times to follow the fluorescence intensity at maximum wavelength.

### 3.2.7. Cytotoxicity of P4 micelles using MTT assay

HeLa cells were cultured in DMEM supplemented with 10% FBS and 1% antibiotic (penicillin and streptomycin) solution. Then, cells were incubated at 37 °C, 95% relative humidity, and 5% CO<sub>2</sub> till they reached more than 80% confluency. The cells were then harvested with 0.25% trypsin-EDTA solution and seeded in each well of a 96-well plate at a density of 6000 cells in DMEM (100 μL). After 24 hrs of incubation at 37 °C, media was replaced with fresh media (100 μL) containing various concentrations of empty micelles. For negative and positive controls, the media was replaced with fresh media (100 μL) with and without 1% sodium dodecyl sulfate. After 48 hrs, the media was replaced with fresh media (100 μL) containing 10% MTT dye. After 4 hrs, the media was discarded, and the formazan crystals were dissolved in DMSO (200 μL). Absorbance was recorded at 570 nm using a plate reader (Tecan Infinite 200 Pro). Each concentration was replicated 3 times. Cell viability was calculated as the percent ratio of absorbance of mixtures with nanoparticles to control (cells only without micelles).

### 3.3. Results and Discussion

Figure 3.2 illustrates our approach with multiple steps to synthesize a novel, dual acidic pH/reduction-responsive degradable PLA-based triblock copolymer (P4). The first step is the synthesis of PLA-ss-Br homopolymer (P1). ROP of LA was initiated by a double-head initiator (HO-ss-Br) in toluene at 120 °C, with the initial mole ratio of  $[LA]_0/[OH-ss-Br]_0 = 70$  as the degree of polymerization of PLA. The detailed procedure for ROP of LA is described in our previous publication.<sup>147</sup> After precipitation from MeOH, the product was analyzed for the structure using <sup>1</sup>H-NMR spectroscopy and molecular weight by GPC. <sup>1</sup>H-NMR spectrum in Figure 3.S1 shows the peak at 5.2 ppm corresponding to methine protons of LA units and the peak at 1.9 ppm corresponding to two methyl protons of the initiator (HO-ss-Br). From their integral ratio, the degree of polymerization (DP) of LA was calculated to be 65. GPC analysis indicates the molecular weight as a number average molecular weight ( $M_n$ ) = 11 kg/mol with  $M_w/M_n = 1.25$  (Figure 3.3).

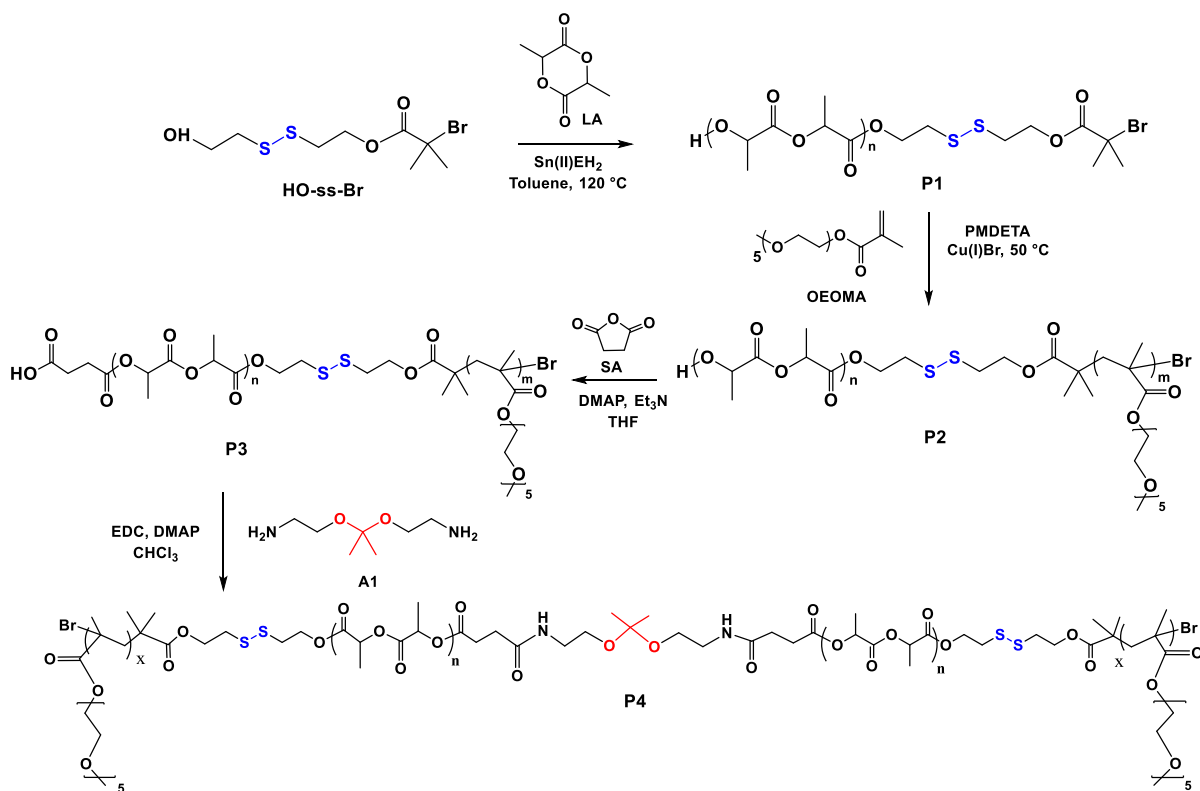


**Figure 3.2.** Illustration of our strategy to synthesize a dual acidic pH/reduction-responsive degradable PLA-based P4 triblock copolymer at dual locations, utilizing ROP, ATRP, esterification, and coupling reaction. Sn(EH)<sub>2</sub>: tin(II) 2-ethylhexanoate, SA: succinic anhydride, PMDETA: N,N,N',N'',N''-pentamethyldiethylenetriamine, Et<sub>3</sub>N: triethylamine, DMAP: N,N-dimethylaminopyridine, EDC: 1-ethyl-3-(3-(dimethylamino)-propyl)carbodiimide-HCl salt, and DCM: dichloromethane.

The second step is the chain extension of P1 with hydrophilic block POEOMA to synthesize well-defined diblock copolymer having a disulfide linkage at the block junction, thus PLA-ss-POEOMA-Br (P2). ATRP<sup>199</sup> of OEOMA was examined in the presence of P1 macroinitiator in tetrahydrofuran (THF) at 50 °C. Conditions include the initial mole ratio of [OEOMA]<sub>0</sub>/[P1]<sub>0</sub>/[CuBr]<sub>0</sub>/[PMDETA]<sub>0</sub> = 30/1/0.4/0.42. When monomer conversion reached 64 %, the polymerization was stopped and purified by precipitation from hexane. <sup>1</sup>H-NMR spectrum of the purified product in Figure 3.S2 shows the presence of EO moieties at 3.4-3.6 ppm and LA units at 5.2 ppm. Using the integral ratio of these peaks, the DP of POEOMA block was calculated to be 24. Its GPC diagram was clearly shifted to high molecular weight region with an

increase in  $M_n = 20$  kg/mol from 11 kg/mol and with  $M_w/M_n = 1.30$  (Figure 3.3). These results suggest the successful synthesis of P2 diblock polymer with a disulfide linkage at block junction.

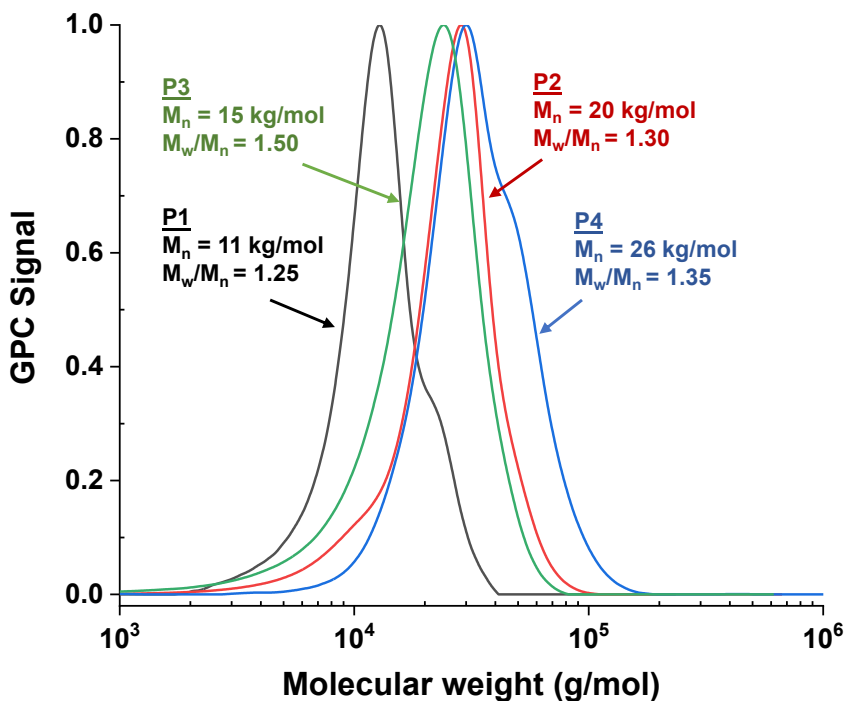


**Figure 3.3.** GPC diagrams of P4, compared with its precursors of P1, P2 and P3.

The third step is the esterification of the resultant P2 to the corresponding carboxylated P3. A terminal hydroxyl group of P2 reacts with excess of succinic anhydride under basic conditions. The resulting P3 was purified by dialysis against distilled water. The esterification was followed by  $^1\text{H-NMR}$  showing the appearance of the new peak at 2.7 ppm corresponding to two methylene groups in succinic acid moieties as well as the disappearance of the peak at 4.4 ppm corresponding to a terminal methine proton in PLA blocks (Figure 3.4). Interestingly, the resultant P3 had the  $M_n = 15$  kg/mol, which is smaller than its precursor P2 (Figure 3.3). The plausible reason is the presence of a terminal carboxylic acid groups of P3 block copolymers, which could be interacting with the stationary phase of the GPC column.

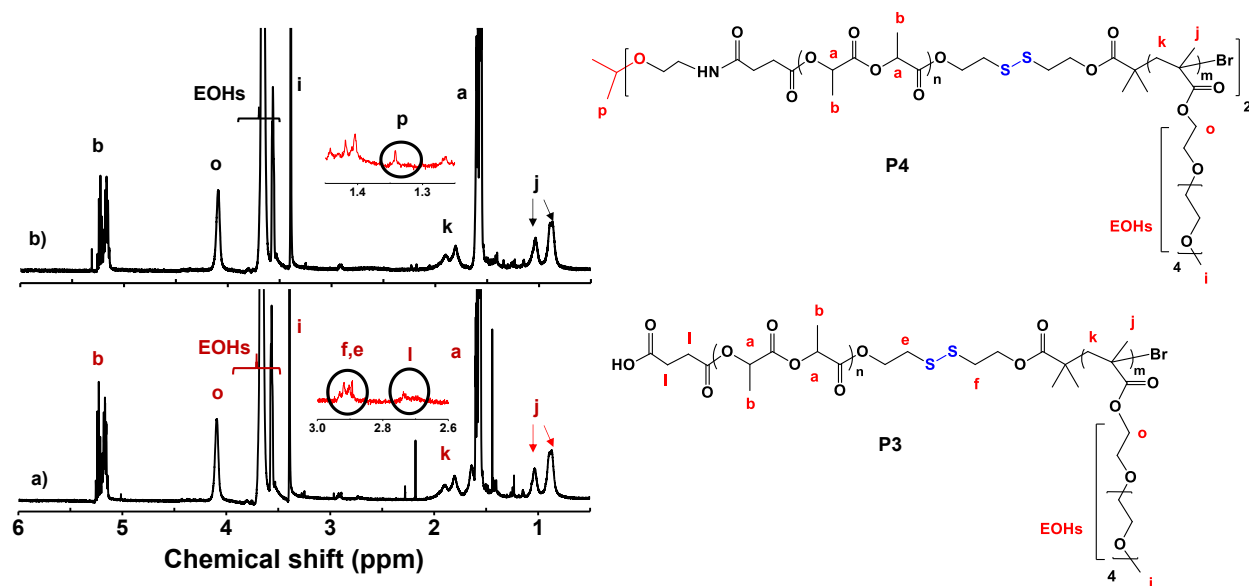


**Figure 3.4.**  $^1\text{H-NMR}$  spectra of P3 (a) and P4 (b) in  $\text{CDCl}_3$ .

The last step is the facile carbodiimide-mediated coupling reaction of the P3 with a ketal-labeled diamine (A1) in the presence of 1-ethyl-3-(3-(dimethylamino)-propyl)carbodiimide-HCl salt (EDC), with the initial mole ratio of  $[\text{P3}]_0/[\text{A1}]_0/[\text{EDC}]_0 = 2/1/20$ . The resulting product was purified by dialysis over PBS at  $\text{pH} = 7.4$  to remove excess EDC and residual A1, followed by lyophilization.  $^1\text{H-NMR}$  spectrum of the purified product in Figure 3.4 shows the appearance of the new peak at 1.35 ppm corresponding to two methyl groups in the ketal moieties. Its GPC diagram shows the bimodal distribution with  $M_n = 26$  kg/mol, which is larger than its P2 and P3 precursors (Figure 3.3). These results suggest the formation of the P4 through the EDC-coupling reaction of P3 and A1. To get insight into the nature of the product, the bimodal GPC diagram was further analyzed using deconvolution method (Figure 3.S3). Of two peaks, one peak in high molecular weight region is estimated to be 60% by the peak analysis, suggesting the formation of 60% of P4 triblock copolymer. Given the other peak in the low molecular weight region overlapped with the GPC diagrams of P2+P3 precursors, the product could contain ca. 40% of P2+P3 precursors.

The resulting P4 is an ABA-type triblock copolymer consisting of hydrophilic POEOMA blocks and a central hydrophobic PLA block labeled with an acidic pH-labile ketal linkage in the center of PLA block and two disulfide linkages at POEOMA/PLA junctions, thus POEOMA-ss-

PLA-ketal-PLA-ss-POEOMA. The P4 copolymer is amphiphilic; thus its CMC was determined using fluorescence spectroscopy with a Nile Red (NR) probe. This method utilizes the low fluorescence intensity of NR in aqueous environment because of its low solubility in water. However, the NR fluorescence intensity increases when NR stays in hydrophobic environment, such as hydrophobic cores of micellar aggregates. Here, a series of mixtures consisting of a given amount of NR with an increasing amount of P4 were prepared in THF. After the removal of THF by evaporation and excess NR by filtration (0.45  $\mu\text{m}$  PES filter), their fluorescence spectra were recorded (Figure 3.5a). As seen in Figure 3.5b, the fluorescence intensity of NR remained low and unchanged at lower concentrations of P4 whereas it gradually increased upon the increase in the amount of P4. Note that the maximum fluorescence emission was shifted to lower wavelength, suggesting the entrapment of NR in hydrophobic PLA micellar cores. From the linear regressions of fluorescence intensity at maximum  $\lambda_{\text{em}}$  (582-587 nm), the CMC of P4 was determined to be 50  $\mu\text{g}/\text{mL}$ , which is somewhat larger,<sup>152, 179, 200</sup> but in the typical range for ABPs.<sup>164, 201, 202</sup>

At concentrations above the CMC, P4 formed self-assembled micellar aggregates consisting of hydrophobic PLA cores surrounded with hydrophilic POEOMA coronas. As an example, with a micellar dispersion at 1 mg/mL, the average diameter was determined to be 29 nm for micelles in aqueous dispersion by DLS technique (Figure 3.5c), while  $35 \pm 6$  nm for dehydrated micelles by transmission electron microscopy (TEM) analysis (Figure 3.5d-2e). Interestingly, the diameter by DLS is somewhat smaller than that by TEM.

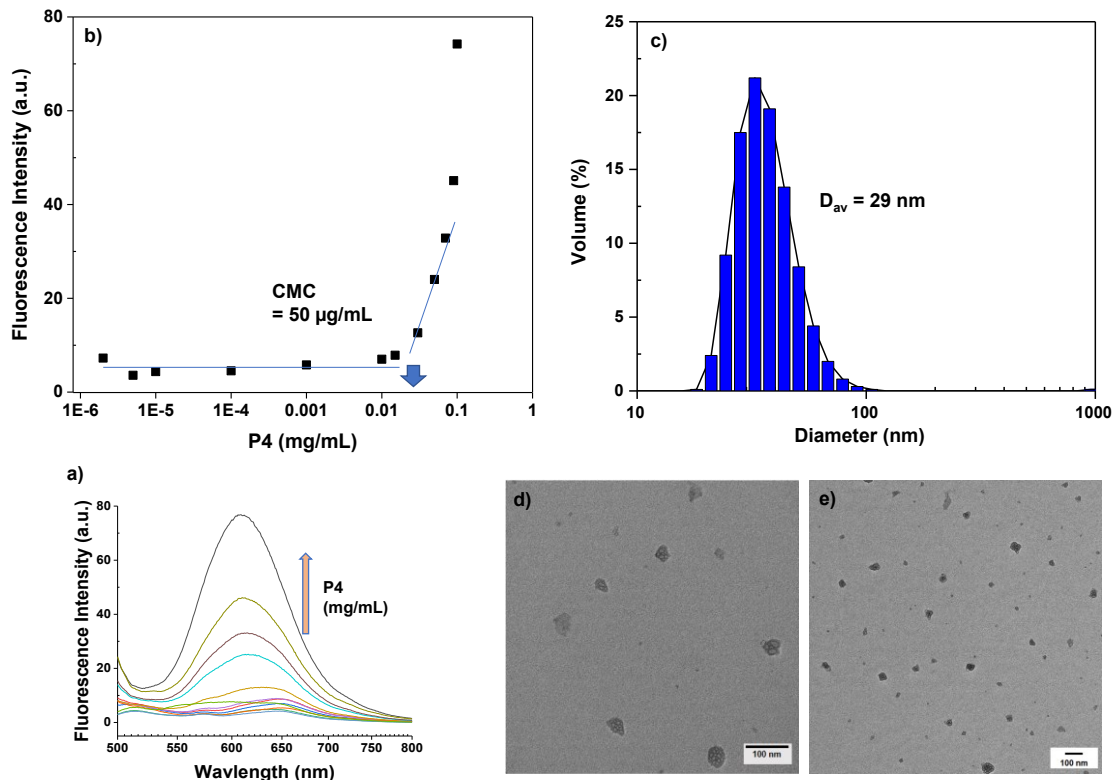


**Figure 3.5.** Overlaid fluorescence spectra (a) and maximum fluorescence intensity (b) of NR in aqueous mixtures containing various amounts of P4 to determine CMC as well as DLS diagram (c), TEM images at high (d) and low (e) magnifications of aqueous micelles of P4 at 1 mg/mL.

Next, P4 micelles were characterized for dual acidic pH/reduction-responsive degradation and drug release. First, dual responses were investigated with P4 fully dissolved in DMF at molecular level. Figure 3.6a shows the schematic illustration of single response and dual responses of P4 to acidic pH/reduction stimuli. A ketal linkage in the center of PLA block and two disulfides at POEOMA/PLA junctions could be cleaved in response to acidic pH and in the presence of a reducing agent. GPC was used to follow the degradation (Figure 3.S4). In the presence of DTT as a typical reducing agent (5 equivalents to the disulfide linkages of P4), the possible degraded products upon the cleavage of disulfide linkages at POEOMA/PLA block junctions could include POEOMA-SH and HS-PLA-ketal-PLA-SH. This reductive cleavage process led to the reduction of molecular weight. As seen in Figure 3.S4a, the  $M_n$  of the degraded products decreased from 26 to 13 kg/mol with the shift of their GPC trace in between P4 and P1 (PLA homopolymer). At pH = 5.4 (mimic to the pH in endo/lysosomes in intracellular compartments), the cleavage of the ketal

linkage led to the formation of degraded products of POEOMA-ss-PLA-OH and acetone. This process resulted in the disappearance of high molecular weight species (i.e. triblock copolymer) and decrease in molecular weight (Figure 3.S4b). In the combination of acidic pH/reduction, shift of GPC trace is observed with the decrease in molecular weight and disappearance of high molecular weight species (Figure 3.S4c).

With our investigation with P4 in homogeneous organic solution, dual acidic pH/reduction-responsive degradation then was examined with aqueous micelles. Empty micelles were incubated under various conditions: pH = 7.4 and acidic pH = 5.3, with and without 10 mM GSH, denoting as acidic pH, GSH, a combination, and a control (pH = 7.4 with no GSH). DLS was used to follow changes in the size distribution of micelles (Figure 3.S5). As seen in Figure 3.6b showing the evolution of z-average diameter over the incubation time, the size distribution remained unchanged for control, which is attributed to colloidal stability of micelles at pH = 7.4. However, the size distribution became bimodal with the occurrence of aggregation in the presence of single and combined stimuli.

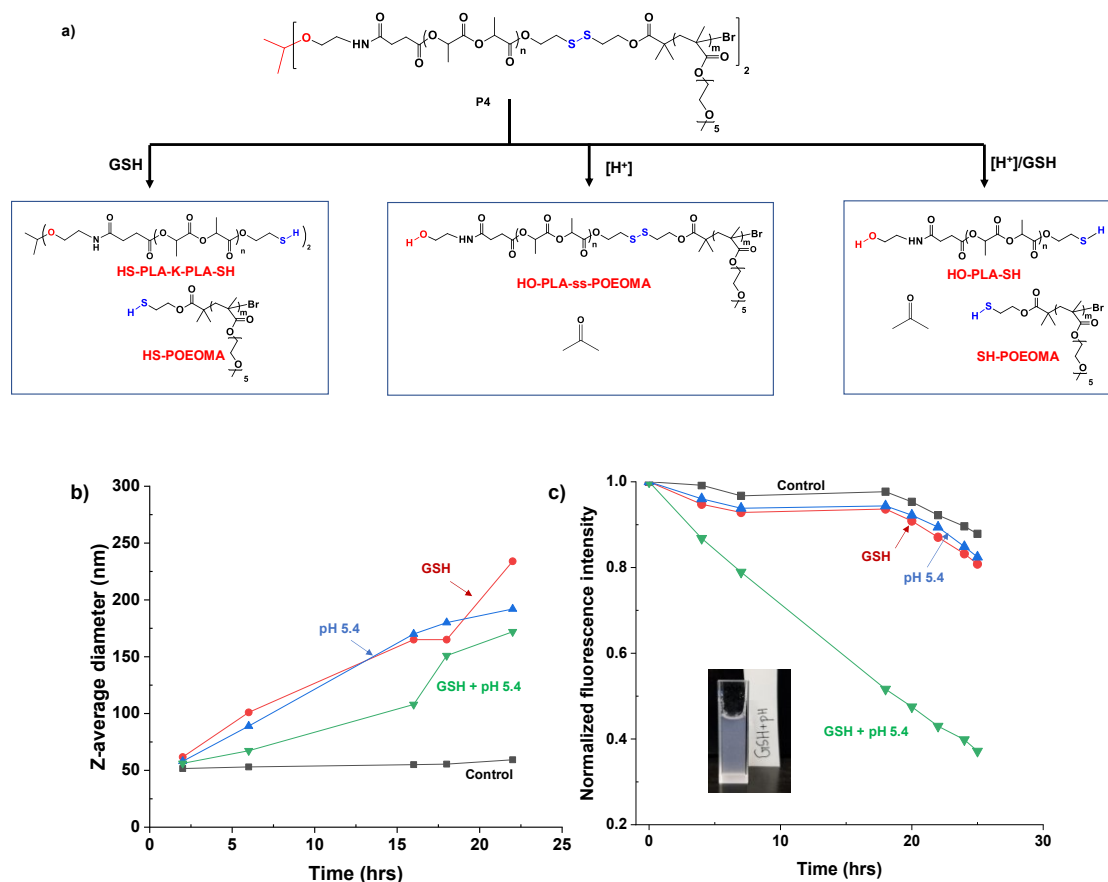


**Figure 3.6.** Schematic illustration of dual acidic pH/reduction-responsive degradation of P4 (a) as well as evolution of z-average diameter of empty micelles by DLS (b) and maximum fluorescence intensity of NR-loaded micelles by fluorescence spectroscopy (c), after incubation with and without 10 mM GSH at pH = 7.4 and 5.4.

Given our comprehensive analysis to dual responses, we then investigated the release of encapsulated drugs with a hydrophobic model drug in response to dual stimuli. Solvent evaporation method was used to prepare NR-loaded micellar dispersions. The formed NR-loaded micelles had the diameter of 32 nm by DLS (Figure 3.S6), which is similar to that of empty micelles. Aliquots of the dispersion (3 mL) were incubated with and without 10 mM GSH at pH = 5.4 and 7.4. Their fluorescence spectra were recorded over the incubation time (Figure 3.S7) to follow their maximum intensities. As summarized in Figure 3.6c, the normalized fluorescence intensity for control remained unchanged, suggesting no important degradation of micelles and thus no NR release. Interestingly, no significant change in fluorescence intensity was observed in response to single stimulus: acidic pH or 10 mM GSH. The response to GSH results in the cleavage

of disulfides at the PLA cores/POEOMA coronas of micelles; as a consequence, POEOMA coronas will shed from the cores, and the resultant cores will be destabilized. The response to acidic pH results in the cleavage of ketal linkages in micellar cores. However, due to the presence of only one linkage in each P4 chain, the cleavage would not be significant to drug release. Similar observation is reported for monocleavable micelles of a PLA-triblock copolymer with one disulfide linkage in the center of triblock copolymer.<sup>152</sup> Promisingly, dual and combined responses in the presence of 10 mM GSH at pH = 5.4 exhibit rapid and synergistic degradation and NR release. Therefore, micelle dispersion became turbid. Furthermore, significant amount of precipitates were detected when it was subjected to centrifugation under mild condition, while none was observed for the control (no GSH and pH = 7.4).

With the promising enhanced degradation and release to dual acidic pH/reduction-responsive degradation, the empty P4 micelles were evaluated for *in vitro* cytotoxicity with HeLa cancer cell line using MTT assay. HeLa cells were incubated without (control) and with P4 micelles at different concentrations for 48 hrs. To verify our results, cells were incubated with negative and positive controls under similar conditions. Figure 3.7 suggests >80% viability of HeLa cells in the presence of P4 micelles up to 100  $\mu\text{g/mL}$ .

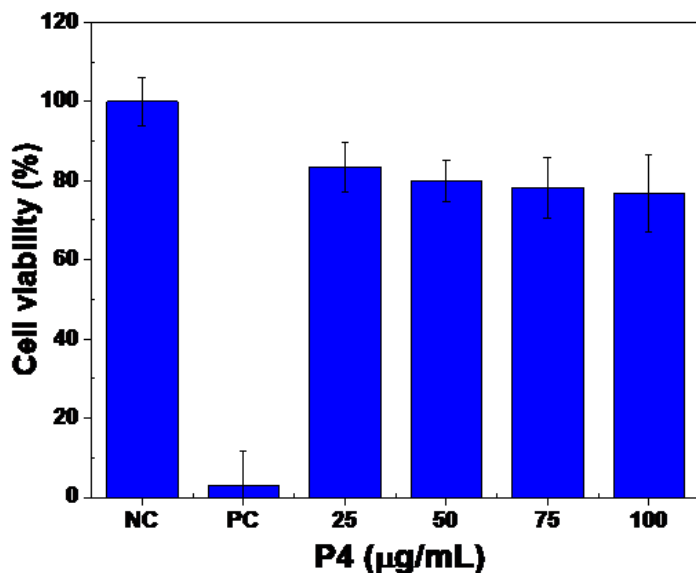


**Figure 3.7.** Cell viability of HeLa cells incubated with empty P4 micelles for 48 hrs determined using MTT assay.

### 3.4. Conclusion

A new strategy utilizing a combination of ROP, ATRP, esterification, and facile coupling reaction was investigated to synthesize a novel ABA-type PLA-based triblock copolymer (P4) consisting of POEOMA and PLA blocks. Both disulfide linkages between POEOMA and PLA blocks and a ketal linkage in the center of PLA block were successfully labeled to form POEOMA-ss-PLA-ketal-PLA-ss-POEOMA. Its amphiphilic nature resulted in the fabrication of nanoassemblies with ketal linkages located in hydrophobic PLA cores and disulfides at PLA core/POEOMA corona interfaces, thus retaining DL-DSRD. Given the cleavage of these labile linkages in response to each stimulus or to dual stimuli, confirmed by GPC analysis, the cleavage of interfacial disulfides and ketal linkages in response to dual glutathione/acidic pH resulted in shedding POEOMA coronas and caused destabilization of micelles. Such dual acidic pH/reduction responses led to the synergistic and accelerated release of encapsulated model drugs from nanoassemblies, compared with the corresponding single stimulus. Promisingly, the P4 micelles were not cytotoxic, confirmed by cell viability measurements.

### 3.5. Supporting figures

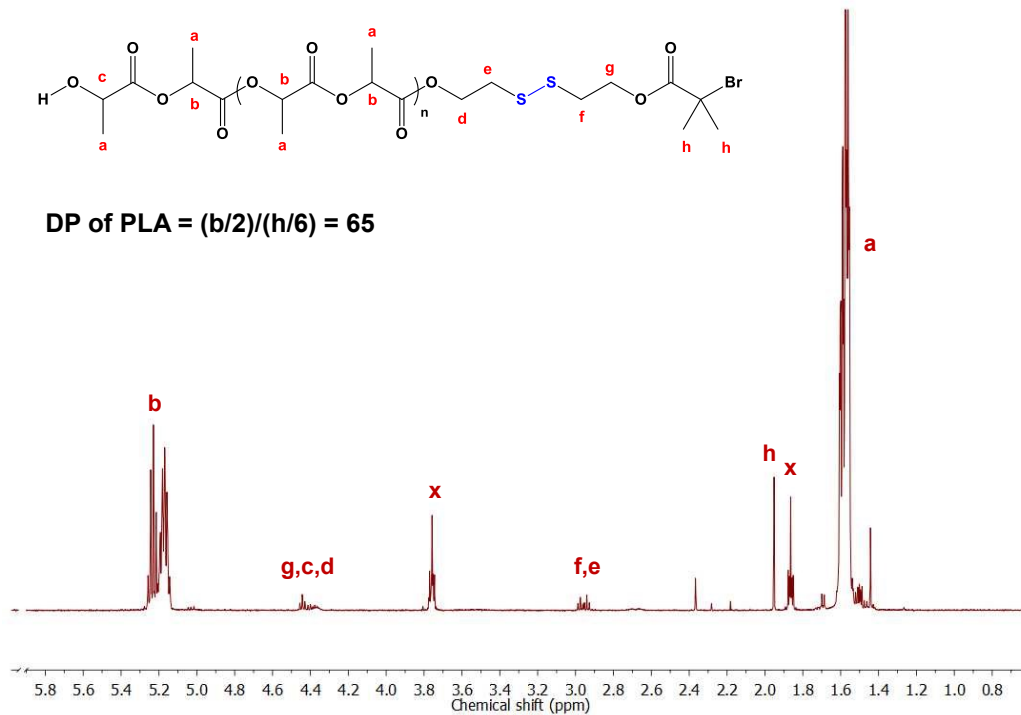


**Figure 3.S1.** <sup>1</sup>H-NMR spectrum of P1 in CDCl<sub>3</sub>. X denotes residual THF.

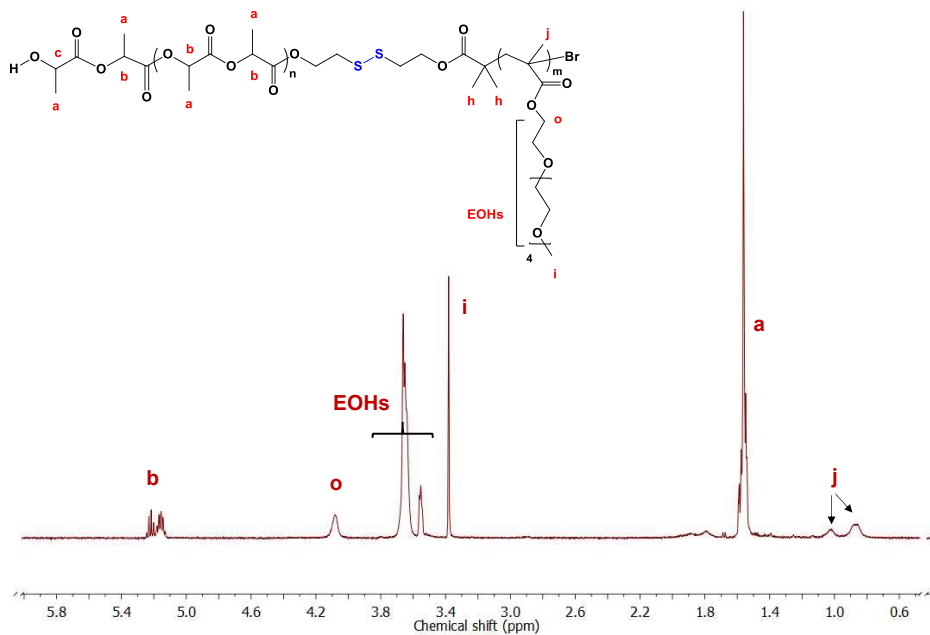


**Figure 3.S2.** <sup>1</sup>H-NMR spectrum of P2 in CDCl<sub>3</sub>.

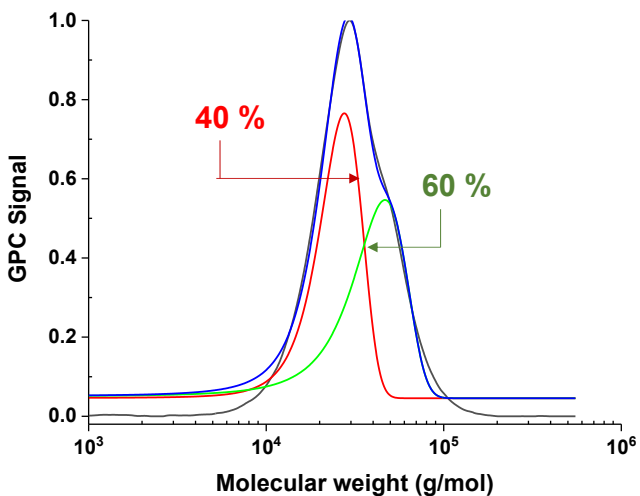


Figure 3.S3. Deconvolution GPC trace of P4.

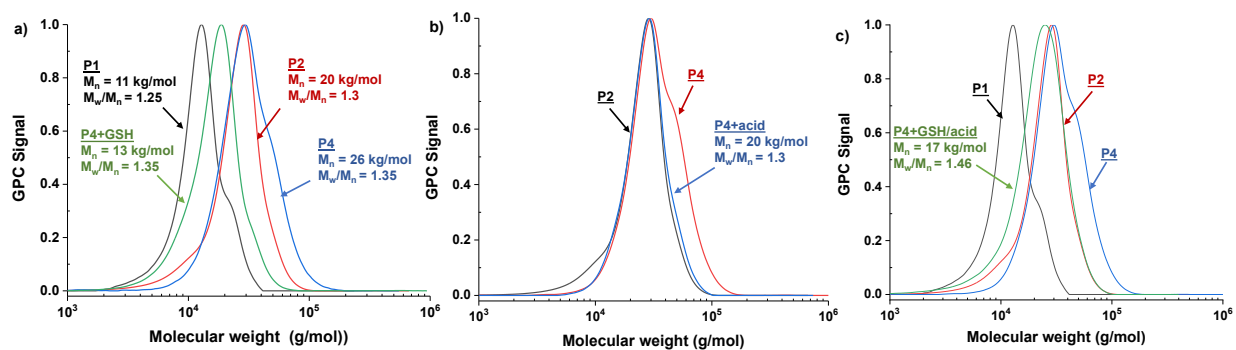
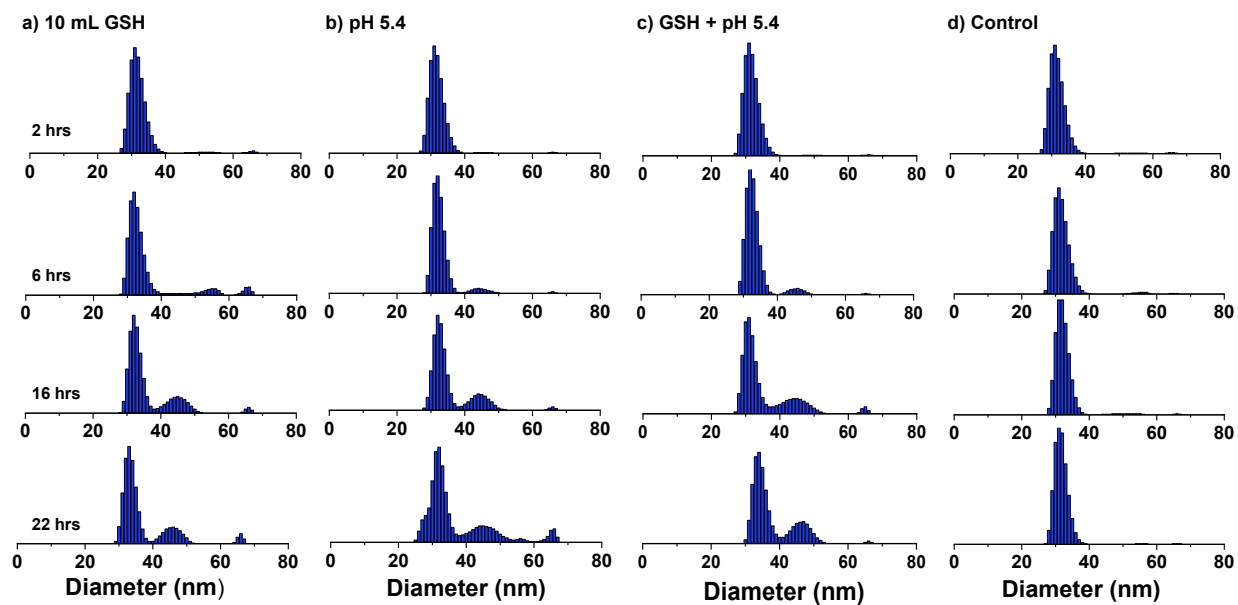
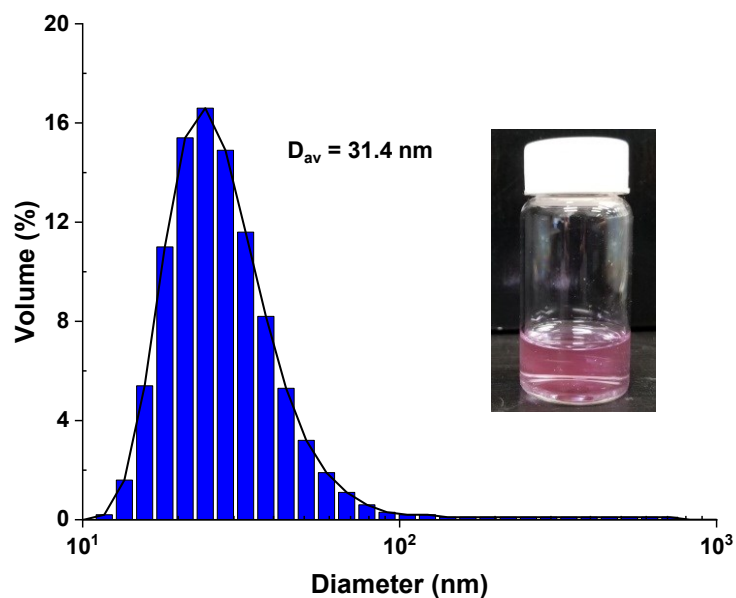


Figure 3.S4. GPC diagrams of the degraded products formed after incubation with 10 mM GSH (pH = 7.4) (a), pH = 5.3 (b), and their combination (c).



**Figure 3.S5.** Evolution of DLS diagrams of aqueous micelles in the presence of various stimuli.



**Figure 3.S6.** DLS diagram and digital image of aqueous NR-loaded micelles.

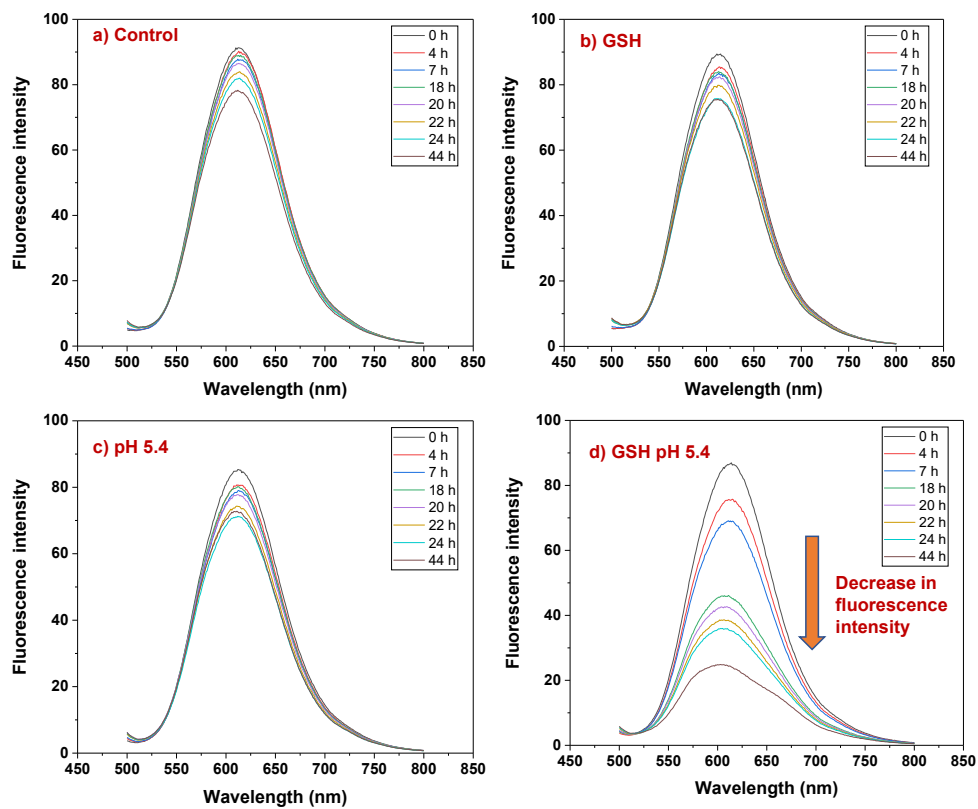


**Figure 3.S7.** Overlaid fluorescence spectra of NR-loaded micelles incubated with various stimuli.

## Chapter 4

### Synthesis of degradable PLA-based diblock copolymers with dual acid/reduction-cleavable junction

#### 4.1. Introduction

Well-defined block copolymers, particularly amphiphilic block copolymers consisting of both hydrophobic and hydrophilic blocks, have been considered as effective building blocks in constructing self-assembled micellar nanoaggregates for various applications in pharmaceutical and materials science.<sup>56-58, 61, 62, 203</sup> In particular, PLA is a promising class of hydrophobic aliphatic polyesters of hydroxyalkanoic acids; PLA is FDA-approved and biocompatible as well as exhibits low immunogenicity.<sup>71, 73</sup> Due to these features, PLA and its copolymers have been widely used as a core-forming hydrophobic block, along with a hydrophilic poly(ethylene glycol) (PEG) or its analog, poly(oligo(ethylene oxide) monomethyl ether methacrylate) (POEOMA) block, in the design of amphiphilic block copolymers.<sup>20</sup> Various di- and tri-block copolymers consisting of PLA and PEG (alternatively POEOMA) blocks have been synthesized for sustainable drug delivery.<sup>88-92</sup> However, their nanoassemblies have often shown the slow release profile of encapsulated molecules. This is mainly attributed to their slow degradation that poses a serious challenge to the design of highly efficient PLA-based delivery nanocarriers.

To address this issue, stimuli-responsive degradation (SRD) through chemical transition involving the cleavage of labile linkages in response to external stimuli has been explored as a promising platform for the enhanced/controlled release of encapsulated drugs.<sup>104-108, 128, 193, 204</sup> In particular, SRD that responds to endogenous stimuli such as GSH<sup>194, 205, 206</sup> and acidic pH<sup>196</sup> found in targeted cells (cancer cells and tumor tissues) are highly desired to attain biodegradation. Reports describe several approaches that allow for the synthesis of smart PLA-based nanoassemblies to be destabilized in the presence of GSH (reductive degradation) or at acidic pH (acid-responsive degradation).<sup>21, 152, 153, 168, 171-173, 180, 195, 207</sup> Among the various approaches reported to date, we<sup>147-150, 155</sup> and others<sup>151, 159, 162-164</sup> have investigated the incorporation of a reduction-cleavable disulfide linkage at the junction of PLA and hydrophilic blocks. This design can be achieved by utilizing ring opening polymerization (ROP) of lactide (LA) as a robust means for the synthesis of well-defined PLA.<sup>76, 77</sup> The resulting PLA-based block copolymers self-assemble to

form shell-sheddable nanoassemblies labeled with disulfides at the core/corona interfaces. Upon the reductive cleavage of the disulfide linkage in response to GSH, hydrophilic coronas are shed from PLA cores. The detachment of coronas generates hydrophilic SH groups at PLA chain ends, resulting in partial swelling of precipitated PLA cores, causing the destabilization of nanoassemblies. The destabilization can promote the enhanced release of encapsulated therapeutics. Recently, the versatility of reductive shell-sheddable nanoassemblies toward tumor-targeting intracellular drug delivery has been evaluated in vivo (mouse model).<sup>208</sup> Similarly, the design of block copolymers through the incorporation of acid-labile linkages into the block junction yields acid-cleavable shell-sheddable nanoassemblies.<sup>209, 210</sup> Compared with these shell-sheddable nanoassemblies labeled with only one labile linkage, the advanced systems labeled with both disulfide and acid-labile linkages at core/corona interfaces can be beneficial to attain both reductive degradation in GSH-rich cytosols and acid-responsive degradation in endosomes/lysosomes (pH = 4.5–5.5). To our best knowledge, no PLA-based shell-sheddable systems exploring dual acid/reduction responses at block junctions and core/corona interfaces have been reported.

In this work, we have explored the synthesis of a new diblock copolymer having a PLA block connected with a POEOMA block through dual reduction-cleavable disulfide and acid-labile acetal linkages, thus PLA-SS-AC-POEOMA or POEOMA-AC-SS-PLA (SS denoted as disulfide and AC as a methylacetal linkage). As illustrated in Figure 4.1, the targeted copolymer self-assembles to form micellar aggregates with disulfide and acetal linkages at the interfaces of PLA cores and POEOMA coronas. In the presence of GSH and acidic pH, the nanoassemblies are destabilized in consequence of the cleavage of those linkages. Our exploration is centered on the use of a double-head initiator functionalized with both acetal and disulfide linkages as well as both OH and bromine terminal groups (OH-AC-SS-Br) for ROP and atom transfer radical polymerization (ATRP) combined with facile coupling reactions. We have further investigated the unexpected instability of the acetal linkage under ROP condition with a tin catalyst at an elevated temperature.

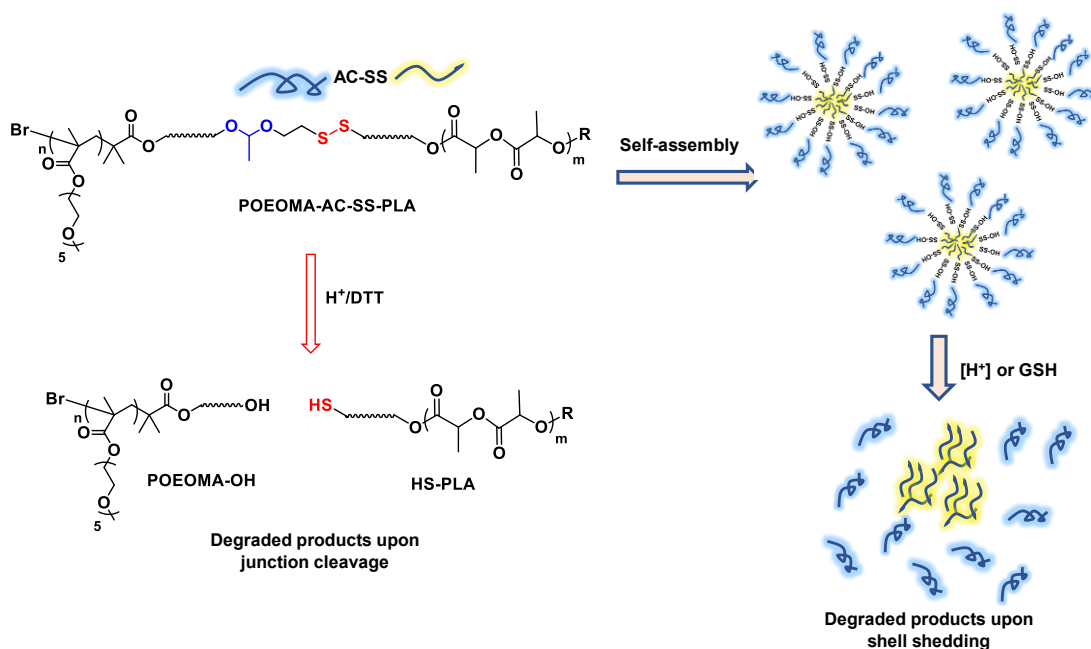


**Figure 4.1.** Schematic illustration of a novel diblock copolymer consisting of a PLA block linked with a POEOMA block through disulfide and acetal linkages and its aqueous micellization as well as dual acid/reduction-responsive degradation.

## 4.2. Experimental

**4.2.1. Instrumentation.**  $^1H$ -NMR spectra were recorded using a 500 MHz Varian spectrometer with  $CDCl_3$  a singlet at 7.26 ppm and toluene- $d_8$  a singlet at 2.08 selected as the reference standard. Monomer conversion was determined using  $^1H$ -NMR technique. Molecular weight and molecular weight distribution were determined by gel permeation chromatography (GPC). An Agilent GPC was equipped with a 1260 Infinity Isocratic Pump and a RI detector. Two Agilent PL gel mixed-C and mixed-D columns were used with DMF containing 0.1 mol% LiBr at 50 °C at a flow rate of 1.0 mL/min. Linear polystyrene (PSt) standards from Fluka were used for column calibration. Aliquots of the polymer samples were dissolved in DMF/LiBr. The clear solutions were filtered using a 0.45  $\mu m$  PTFE filter to remove any DMF-insoluble species. A drop of anisole was added as a flow rate marker. Size and morphology analysis of self-assembled nanoaggregates were conducted with dynamic light scattering (DLS). DLS diagrams were obtained at a fixed scattering angle of 175° at 25 °C with a Malvern Instruments Nano S ZEN1600 equipped with a 633 nm He-Ne gas laser.

#### 4.2.2. Materials

2-Hydroxy ethyl disulfide (99.5%), copper(I) bromide (CuBr, >99.99%), N,N,N',N'',N''-pentamethyldiethylenetriamine (PMDETA, >98%), tin(II) 2-ethylhexanoate (Sn(EH)<sub>2</sub>, 95%), toluene-d<sub>8</sub>, 1-pyrenemethanol (Py-OH, 98%), Nile red (NR), triethylamine (Et<sub>3</sub>N, ≥99.5 %), 4-(dimethylamino)pyridine (DMAP, ≥99%) and glutathione (GSH, a reduced form) from Sigma Aldrich; DL-dithiothreitol (DTT, 99%) and succinic anhydride (SA, 99%) from Acros Organics; and 1-ethyl-3-(3-dimethylaminopropyl)carbodiimide-HCl salt (EDC) from Matrix Innovation were purchased and used as received. 3,6-Dimethyl-1,4-dioxane-2,5-dione (DL-lactide, LA, 99%) purchased from sigma Aldrich was purified by recrystallization from toluene prior to use. Oligo(ethylene glycol) monomethyl ether methacrylate (OEOMA) with MW= 300 g/mol (#EO = 5, OEOMA-MW300) and MW =475 g/mol (#EO = 7, OEOMA-MW475) were purchased from Sigma-Aldrich Canada and purified by passing through a column filled with basic aluminum oxide to remove inhibitor.

#### 4.2.3. General procedure for ATRP

Initiator, OEOMA, PMDETA, and anisole were added to a 25 mL Schlenk flask. The resulting mixture was deoxygenated by three freeze-pump-thaw cycles. The reaction flask was filled with nitrogen, and then CuBr was added to the frozen mixture. The flask was sealed, purged with vacuum, and backfilled with nitrogen once. The mixture was then thawed and immersed in an oil-bath preheated at 50 °C to start the polymerization. The polymerization was stopped by exposing the reaction mixture to air. For purification, the as-synthesized polymer solution was added dropwise into hexane under magnetic stirring. The precipitate was dissolved in THF and passed through a column filled with basic aluminum oxide to remove the copper species. After the solvent was removed by rotary evaporation, the formed polymer was dried in a vacuum oven at room temperature overnight.

**Synthesis:** Br-AC-SS-OH (125.0 mg, 0.31 mmol), OEOMA-MW300 (2.9 g, 9.5 mmol), PMDETA (23.0 mg, 0.13 mmol), CuBr (18.3 mg, 0.13 mmol), and anisole (14 mL) for P1; P5 (250.0 mg, 0.25 mmol), OEOMA-MW475 (520 mg, 1.0 mmol), PMDETA (1.6 mg, 0.13 mmol), CuBr (1.3 mg, 8.7 μmol) and anisole (14 mL) for P6.

#### 4.2.4. General procedure for a tin-catalyzed ROP of LA

Initiator, LA, Sn(EH)<sub>2</sub> and anhydrous toluene were added to a 10 mL schlenk flask. Three freeze-pump-thaw cycles were performed, then the flask was purged with nitrogen at last and immersed in an oil bath preheated at 120 °C to start the polymerization. The polymerization was stopped after 3 hrs and cooled to room temperature. For purification, the as-synthesized polymer solution was precipitated from cold methanol and dried in vacuum oven for 12 hrs at room temperature.

**Synthesis:** P1 (POEOMA-AC-SS-OH) (0.6 g, 88 μmol), LA (0.7 g, 4.8 mmol), Sn(EH)<sub>2</sub> (1.7 mg, 4 μmol), and toluene (0.4 mL) were used in an attempt to synthesize P2 and small molecule initiators (Py-OH, Br-SS-OH, and Br-AC-SS-OH, 0.5 mmol), LA (34 mmol), Sn(EH)<sub>2</sub> (24 μmol) and anhydrous toluene (3 mL) for P3, P4 and P5.

#### 4.2.5. Synthesis of P6 by reaction of P5 with SA

An organic solution of P5 (0.5 g, 51 μmol) dissolved in anhydrous THF (10 mL) was mixed with an organic solution containing SA (25 mg, 0.25 mmol) and DMAP (3.1 mg, 25 μmol) dissolved in anhydrous THF (10 mL). After an addition of Et<sub>3</sub>N (36 μL, 0.25 mmol) using a syringe under nitrogen flow, the resulting mixture was allowed to stir for 48 hrs. THF was evaporated using rotary evaporation. The product was precipitated from aqueous HCl solution to remove excess (unreacted) SA and the precipitate was dissolved in chloroform. The procedure was repeated three times and then the product was dried over sodium sulfate. Chloroform was removed by rotary evaporation, the product was dried in a vacuum oven set at room temperature for 12 hrs; Yield = 0.41 g (83 %).

#### 4.2.6. Synthesis of P7 by reaction of P6 with Br-AC-SS-OH

An organic solution containing P6 (0.61 g, 55 μmol), EDC (31 mg, 0.16 mmol), and DMAP (40 mg, 0.33 mmol) dissolved in anhydrous dichloromethane (10 mL) was mixed with Br-AC-SS-OH (25 mg, 66 μmol) under stirring at room temperature for 24 hrs. The product was washed with an aqueous sodium bicarbonate solution and water twice. After the removal of dichloromethane, the product was precipitated from cold methanol and then dried in vacuum oven at room temperature for 12 hrs; Yield = 0.36 g (58 %).

#### 4.2.7. Determination of critical micellar concentration (CMC)

A stock solution of NR in THF at 1 mg/mL and two stock solutions of the purified dried copolymer in THF at 1 mg/mL and 10  $\mu$ g/mL were prepared. A series of organic solutions were prepared by mixing the different amounts of the copolymer solutions with the same amount of the NR stock solution (0.5 mL, 0.5 mg NR). The resulting mixtures were mixed with water (10 mL) under stirring for 12 hrs to remove THF. They were then subjected to filtration using 0.45  $\mu$ m PES filters to remove excess NR to prepare a series of NR-loaded micelles at various concentrations of copolymer ranging from 10<sup>-6</sup> to 0.1 mg/mL. Their fluorescence spectra were recorded at  $\lambda_{\text{ex}} = 480$  nm.

#### 4.2.8. Aqueous micellization

Aliquots of the purified, dried copolymers (10 mg) dissolved in THF (2 mL) were mixed with PBS solution (10 mL, pH = 7.4). The resulting dispersion was then stirred at room temperature overnight to evaporate THF, yielding nanoassemblies at 1 mg/mL.

#### 4.2.9. Investigation of acidic pH/reduction-responsive degradation

For copolymers dissolved in DMF (homogeneous solution), aliquots of the copolymers (10 mg) dissolved in DMF (2 mL) were mixed with HCl (20  $\mu$ L) for acidic degradation and DTT (2.3 mg, 15 mmol) for reductive degradation under stirring at room temperature. After 48 hrs of incubation time, the resulting mixtures were analyzed for molecular weights and their distribution by GPC.

For nanoassemblies, aliquot of aqueous nanoaggregate solution (1 mL, 1 mg/mL) was mixed with 3 mL of PBS buffer with GSH (10 mM) at pH 5.4, under stirring at room temperature.

### 4.3. Results and discussion

**4.3.1. An initial unsuccessful approach involving a tin-catalyzed ROP initiated with an acetal initiator.** Figure 4.2a depicts our initial approach in an attempt to synthesize PLA-SS-AC-POEOMA P2 diblock copolymer labeled with both acetal and disulfide linkages at the block junction. The approach utilizes combined ATRP and tin-catalyzed ROP techniques with a double-

head dual function initiator (Br-AC-SS-OH) labelled with both disulfide and acetal linkages as well as dual terminal Br (for ATRP) and OH (for ROP) initiating sites. The synthesis and characterization of Br-AC-SS-OH are described in our previous publication<sup>211</sup> and further in supporting information (Figure 4.S2 for <sup>1</sup>H-NMR analysis).

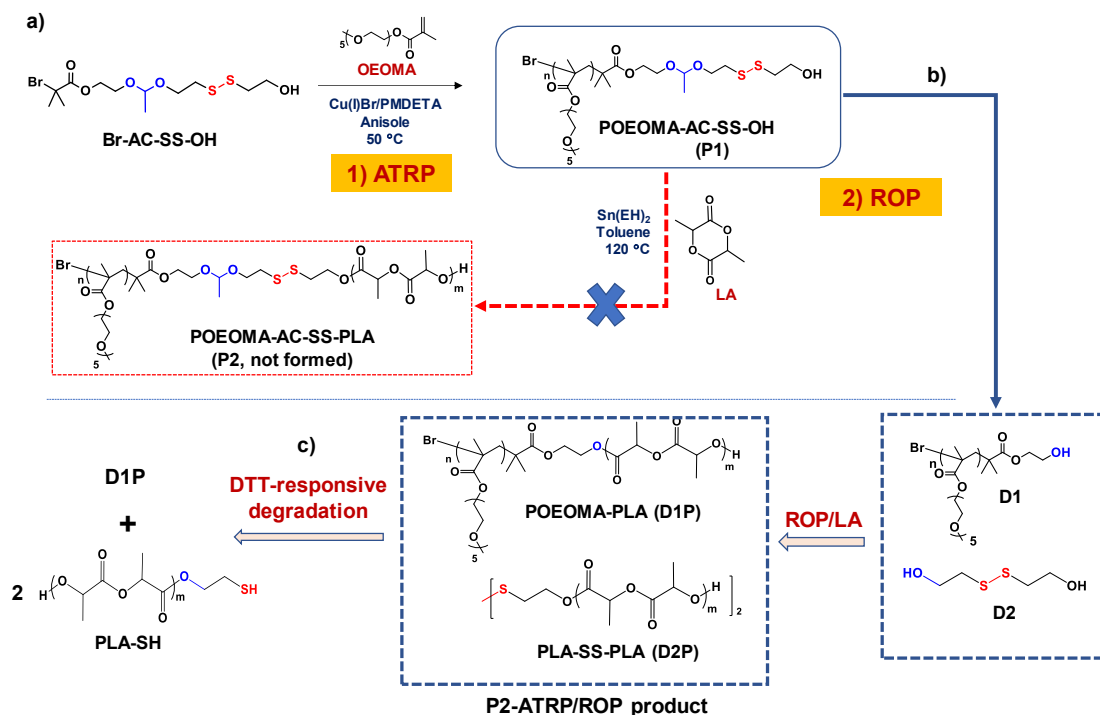


**Figure 4.2.** Schematic illustration of an initial unsuccessful approach utilizing combined ATRP and tin-catalyzed ROP techniques in the presence of a double-head initiator (Br-AC-SS-OH) in an attempt to synthesize POEOMA-AC-SS-PLA P2 diblock copolymer (a); possible cleavage of acetal linkages of P1 precursor during ROP of LA with Sn(EH)<sub>2</sub> at 120 °C resulting in the formation of P2-ATRP/ROP product composed of D1P and D2P (b) and its possible reductive degradation with DTT (c).

The first step of the approach is the ATRP of OEOMA initiated with Br-AC-SS-OH initiator to synthesize well-controlled POEOMA-AC-SS-OH homopolymer (P1). Active Cu(I)Br/PMDETA complex was used in anisole at 50 °C, with the initial mole ratio of [OEOMA]<sub>0</sub>/[Br-AC-SS-OH]<sub>0</sub> = 30/1 as the target degree of polymerization (DP) = 30 at complete monomer conversion. At 63% OEOMA conversion, the resultant product after purification was characterized for structural analysis by <sup>1</sup>H-NMR (Figure 4.S3a) and molecular weight by GPC (Figure 4.S4). These results, along with <sup>1</sup>H-NMR analysis confirming the presence of acetal and

disulfide linkages, suggest a success in the synthesis of well-controlled POEOMA-AC-SS-OH (P1) homopolymer with the number average molecular weight  $M_n = 8.9$  kg/mol and  $M_w/M_n = 1.18$ .

Given the success in ATRP as the first step, the second step of the approach involves the use of the formed P1 as a macroinitiator for tin-catalyzed ROP of LA in toluene at 120 °C.  $\text{Sn}(\text{EH})_2$  is a common catalyst used for most ROP of LA due to its low sensitivity to air, high conversion yield, and low catalytic loadings. With the  $[\text{LA}]_0/[\text{POEOMA-AC-SS-OH}]_0 = 70/1$ , the amount of tin catalyst was set as  $[\text{POEOMA-AC-SS-OH}]_0/[\text{Sn}(\text{EH})_2]_0 = 1/0.05$  (standard) to an attempt to the synthesis of P2. After 3 hrs, the polymerization mixture was purified by precipitation from cold methanol to remove unreacted LA and residual tin catalysts. The formed product (termed P2-ATRP/ROP product) had the  $M_n = 9.2$  kg/mol, which is somewhat larger by 3 kg/mol, compared with its precursor P1 (Figure 4.S4).  $^1\text{H-NMR}$  spectrum in Figure 4.S3b shows the distinct peaks at 1.6 and 5.2 ppm that confirm the formation of PLA block. Using the integrals of the peaks with the  $\text{DP} = 21$  for POEOMA block, the  $\text{DP}$  of PLA block was calculated to be 63. However, the peak at 4.8 ppm corresponding to methine proton in acetal moieties did not appear, suggesting the possible loss of the acetal linkage during the tin-catalyzed ROP step. The formed P2-ATRP/ROP product was further characterized for aqueous micellization. As seen in Figure 4.S5, fluorescence spectroscopy analysis with a NR probe confirms that the product had its CMC to be 15.6  $\mu\text{g/mL}$  in aqueous solution, suggesting that the formed product retains amphiphilicity.

The P2-ATRP/ROP product was subsequently investigated for its acid and reduction-responsive degradation. The expected P2 copolymer contains both acetal and disulfide linkages at the block junctions. As illustrated in Figure 4.1, P2 should degrade to the corresponding POEOMA and PLA homopolymer species upon the cleavage of acetal and disulfide linkages at the block junctions in acidic pH or in the presence of DTT (a reducing agent). Such an acid- or reduction-responsive degradation should result in a significant decrease in molecular weight of the degraded product, which could be monitored by GPC. As seen in Figure 4.3, the GPC diagrams of the degraded products after treatment with acid or reductive reaction were quite different from our anticipation for the degradation of P2 copolymer. After the incubation of an aliquot of the ATRP/ROP product with HCl (20  $\mu\text{L}$ , equivalent to  $[\text{H}^+] = 190$  mM and thus  $\text{pH} = 3.7$ ) in DMF, its molecular weight distribution of the remained unchanged up to 72 hrs (Figure 4.3a). This result suggests the absence of junction acetal linkages in the P2-ATRP/ROP product. Further, upon the

incubation with excess DTT (15 equivalents to disulfides), its molecular weight did not significantly decrease. Interestingly, a new small peak appeared in low molecular weight region with  $M_n \approx 2.5$  kg/mol, which could be attributed to the degraded PLA species (Figure 4.3b). In another set, similar results were obtained with a less amount of tin catalyst as  $[LA]_0/[POEOMA-AC-SS-OH]_0/[Sn(EH)_2]_0 = 70/1/0.03$ .

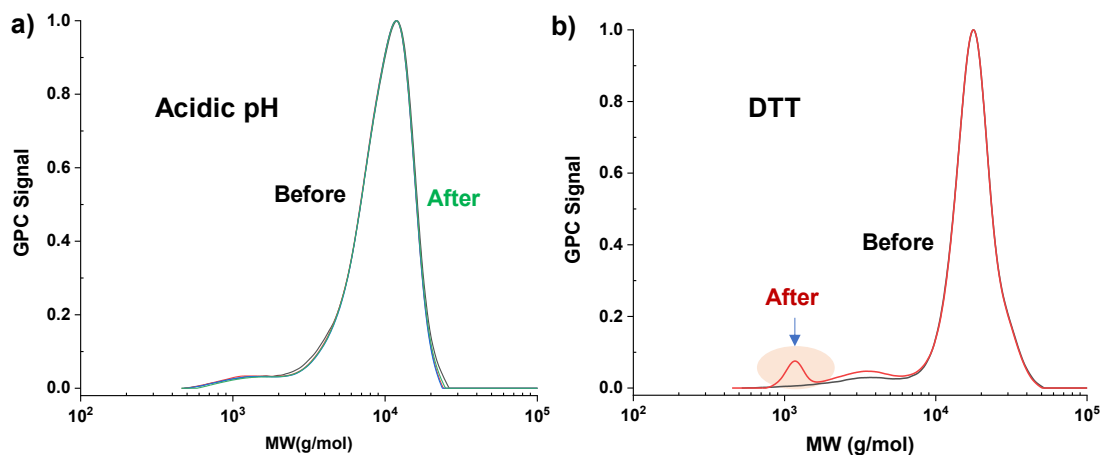


**Figure 4.3.** GPC diagrams of P2-ATRP/ROP product, synthesized by a combination of ATRP of OEOMA with ROP of LA in the presence of Br-AC-SS-OH, before and after being incubated with acid (a) and DTT (b).

The combined results from structural analysis, aqueous micellization, and acid/reduction-responsive degradation suggest the possibility to the cleavage of junction acetal linkage under the ROP conditions with tin catalyst at 120 °C. As illustrated in Figure 4.2b, the unexpected cleavage of acetal linkage can generate D1 (POEOMA-OH) and D2 (HO-ss-OH). These species can initiate the ROP of LA to yield D1P (POEOMA-*b*-PLA with no acetal and disulfide linkages at the block junction) and D2P (PLA-ss-PLA with only disulfide linkage) as P2-ATRP/ROP product. D1P is an amphiphilic diblock copolymer which self-assembles to form micellar aggregates. Further, D1P is inert to both acid and reduction-responsive degradation and thus exhibit no change in molecular weight distribution in response to acid or reductive reaction. D2P is a PLA homopolymer labeled with a single disulfide linkage. Its reductive degradation can generate PLA-SH, which corresponds to the new peak appeared in lower molecular weight region as seen in Figure 4.2c.

To further investigate the possibility of the cleavage of the junction acetal linkage under tin-catalyzed ROP condition, small molecule Br-AC-SS-OH with an acetal linkage was examined for ROP of LA under similar condition, along with other OH-bearing initiators with no acetal linkages: Py-OH and Br-SS-OH (Figure 4.4). The synthesis of Br-SS-OH is reported elsewhere.<sup>150</sup> After purification, the formed PLA homopolymers were characterized by <sup>1</sup>H-NMR (Figure 4.S6 and 4.S7) and GPC (Figure 4.5a).

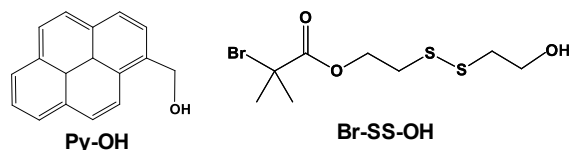


**Figure 4.4.** Small molecule OH-bearing initiators labeled without an acetal linkage examined under a tin-catalyzed ROP condition.

**Table 4.1.** Characteristics and properties of functional PLA homopolymers synthesized by ROP of LA with small molecule OH-bearing initiators with no acetal linkage.<sup>a)</sup>

PLA-OH	Initiator	DP <sup>b)</sup>	M <sub>n</sub> (kg/mol) <sup>c)</sup>	M <sub>w</sub> /M <sub>n</sub> <sup>c)</sup>	Distribution <sup>c)</sup>
P3	Py-OH	63	18	1.1	Monomodal
P4	Br-SS-OH	65	13	1.2	Monomodal
P5	Br-SS-AC-OH	-	6	1.6	Bimodal

a) Conditions for ROP of LA: [LA]<sub>0</sub>/[initiator]<sub>0</sub>/[Sn(EH)<sub>2</sub>]<sub>0</sub> = 70/1/0.05 in toluene at 120 °C; LA/toluene = 1.4/1 wt/wt; b) by NMR; and c) by GPC with PSt standards

As summarized in Table 4.1, the formed P3 (from Py-OH) and P4 (Br-SS-OH) homopolymers had the M<sub>n</sub> = 13 -18 kg/mol with monomodal and narrow molecular weight distribution (M<sub>w</sub>/M<sub>n</sub> = 1.1-1.2), which is typical results for ROP of LA initiated with a tin catalyst in toluene at 120 °C.<sup>21, 147-150, 155, 207</sup> However, P5 synthesized with Br-AC-SS-OH bearing the acetal linkage had a smaller M<sub>n</sub> = 6.0 kg/mol. Its molecular weight distribution was relatively broader with M<sub>w</sub>/M<sub>n</sub> = 1.6 and multimodal, suggesting that the formed product had more than two species. When the product was subjected to reductive degradation for 24 hrs, its GPC diagram was not only shifted to lower molecular weight region with a decreasing M<sub>n</sub> = 2.3 kg/mol, but also became monomodal and narrow (M<sub>w</sub>/M<sub>n</sub> = 1.2) (Figure 4.5b). The plausible reason is illustrated in Figure 4.6. Similar to the ROP of LA with P1 precursor, the acetal linkage in Br-AC-SS-OH can be cleaved under tin-catalyzed ROP condition. Such a cleavage generates D3 (Br-OH) and D4 (HO-ss-OH) as degraded

products. These OH-bearing species can initiate the ROP of LA to yield P5-ROP product composed of D3P (Br-PLA) and D4P (PLA-ss-PLA), thus causing multimodal molecular weight distribution. While Br-PLA is inert to reductive cleavage, PLA-SS-PLA degrades to the corresponding PLA-SH upon the cleavage of the disulfide linkage. Again, these results suggest the possible cleavage of the acetal linkage under tin-catalyzed ROP conditions.

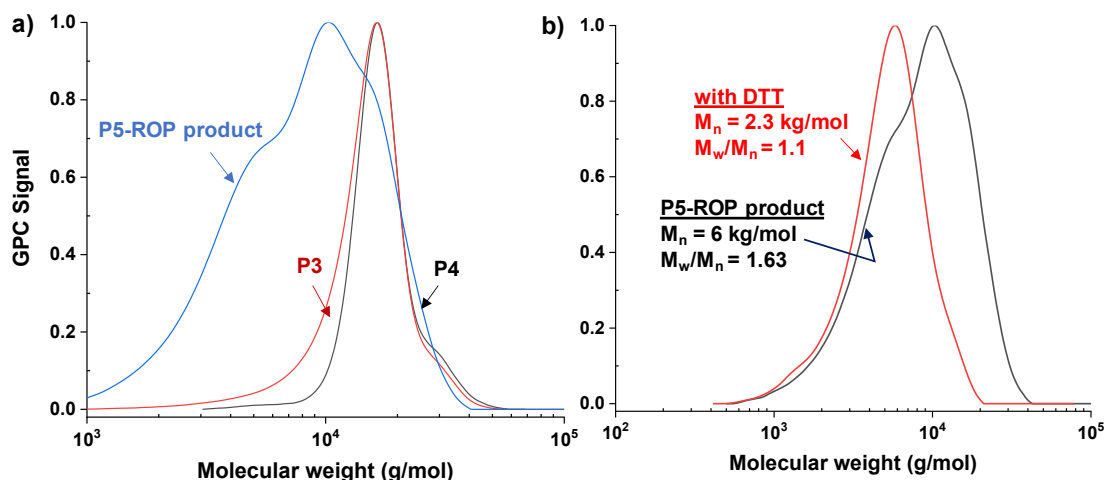


**Figure 4.5.** GPC diagrams of PLA homopolymers (a) and P5-ROP product synthesized by ROP of LA with Br-AC-SS-OH before and after being incubated with DTT in DMF (b).

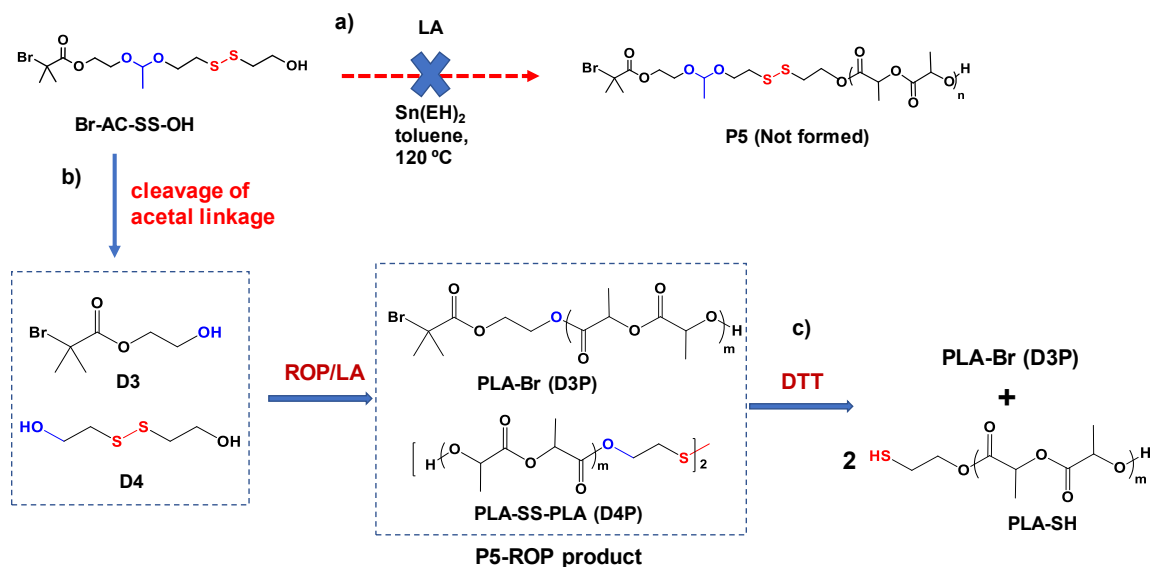


**Figure 4.6.** Schematic illustration of ROP of LA with Br-AC-SS-OH initiator (a) and possible cleavage of acetal linkages on the course of tin-catalyzed ROP of LA, yielding undesired P5-ROP product composed of D3P and D4P (b), and their possible reductive degradation in the presence of DTT (c).

In another set, we have conducted a control experiment using  $^1\text{H-NMR}$  technique to investigate the stability of the acetal linkage under tin-catalyzed ROP condition. An aliquot of Br-AC-SS-OH and  $\text{Sn}(\text{EH})_2$  was dissolved in toluene- $d_8$  and heated at  $100\text{ }^\circ\text{C}$  (slightly lower than  $120\text{ }^\circ\text{C}$ ) for 4 h. To mimic the ROP condition for LA, the same amounts of Br-AC-SS-OH,  $\text{Sn}(\text{EH})_2$ , and toluene as well as time were used. Figure 4.S8 compares  $^1\text{H-NMR}$  spectrum of Br-AC-SS-OH/ $\text{Sn}(\text{EH})_2$  mixture with those of individual  $\text{Sn}(\text{EH})_2$  and Br-AC-SS-OH. The peak at 1.9 ppm (e) corresponds to two methyl groups in the bromine initiating moiety and the peak at 4.8 ppm (d) corresponds to methine group in the acetal moiety. The integral ratio of the two peaks decreased by 25%, which is attributed to the cleavage of the acetal linkage under the ROP condition.

**4.3.2. Alternative approach to synthesis of well-controlled PLA-SS-AC-POEOMA block copolymer.** Given the possible cleavage of the acetal linkage during tin-catalyzed ROP of LA initiated with an acetal-bearing initiator at an elevated temperature, we have developed an alternative new approach that avoids the tin-catalyzed ROP condition in the presence of acetal-bearing initiating species. Figure 4.7 depicts this approach that leads to the success in the synthesis of the PLA-SS-AC-POEOMA diblock copolymer.

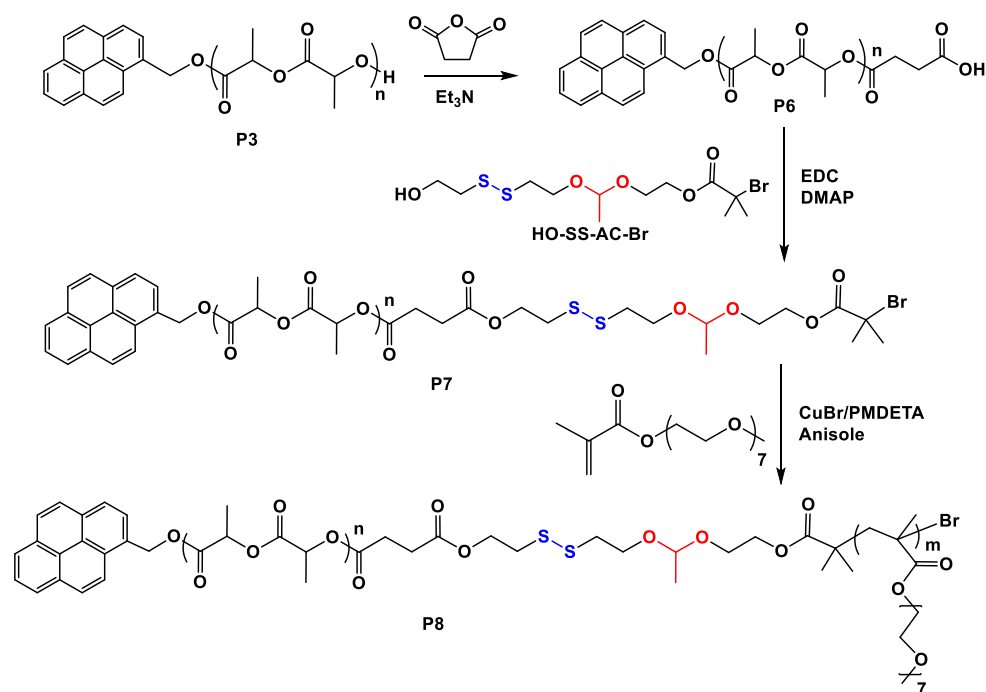


**Figure 4.7.** Schematic illustration of an alternative approach designed with the conjugation of Br-AC-SS-OH with a COOH-terminated PLA and subsequent ATRP to synthesize PLA-SS-AC-POEOMA diblock copolymer.

The approach began with the tin-catalyzed ROP of LA in the presence of small molecule OH-bearing initiators. Here, Py-OH was selected as a typical ROP initiator because the fluorescence of pyrene groups at the end of the resultant block copolymer can be used for cellular imaging to study endocytosis as well as excimer formation/dissociation. The ROP of LA with the  $[LA]_0/[Py-OH]_0 = 70/1$  yielded well-controlled Py-PLA-OH (P3). The P3 was characterized with  $DP = 64$  by  $^1H$ -NMR (Figure 4.S6) and  $M_n = 18$  kg/mol with  $M_w/M_n = 1.12$  by GPC (Table 4.1). The second step involves the conjugation of P3 with SA in the presence of a base.  $^1H$ -NMR spectrum in Figure 4.8 shows the peak at 2.5 ppm corresponding to two methylene protons in SA moieties, confirming the synthesis of PLA terminated with carboxylic acid (COOH) (Py-PLA-COOH, P6). In the following step, the formed P6 reacted with Br-AC-SS-OH through an EDC-mediated coupling reaction, yielding Py-PLA-SS-AC-Br (P7), as confirmed by  $^1H$ -NMR analysis.

The last step is the chain extension of P7 with POEOMA by ATRP of OEOMA in the presence of the formed P7 macroinitiator. With the initial mole ratio of  $[OEOMA]_0/[P5]_0 = 50/1$ , ATRP was conducted under the conditions of  $[PLA-SS-AC-Br]_0/[Cu(I)Br]_0/[PMDTA]_0 = 1/0.4/0.42$  in anisole as OEOMA/anisole = 1.4/1 wt/wt at 50 °C. The polymerization was stopped at 72 % conversion; the product was purified by precipitation from hexane to remove residual OEOMA and treatment with basic aluminum oxide to remove copper species.  $^1H$ -NMR spectrum shows the presence of POEOMA and PLA blocks. From their integral ratio, the DP of POEOMA block was determined to be 40. GPC diagram of the product shows the clear shift of molecular weight distribution to the high molecular weight region with  $M_n = 33$  kg/mol and  $M_w/M_n = 1.27$  (Figure 4.9a). Meanwhile, a low-molecular-weight shoulder peak, which has similar molecular weight as P3, is noticed. It should correspond to the polymer chains that did not undergo successful chain extension from P3 or experienced chain breaking reaction during the 1st ROP step.

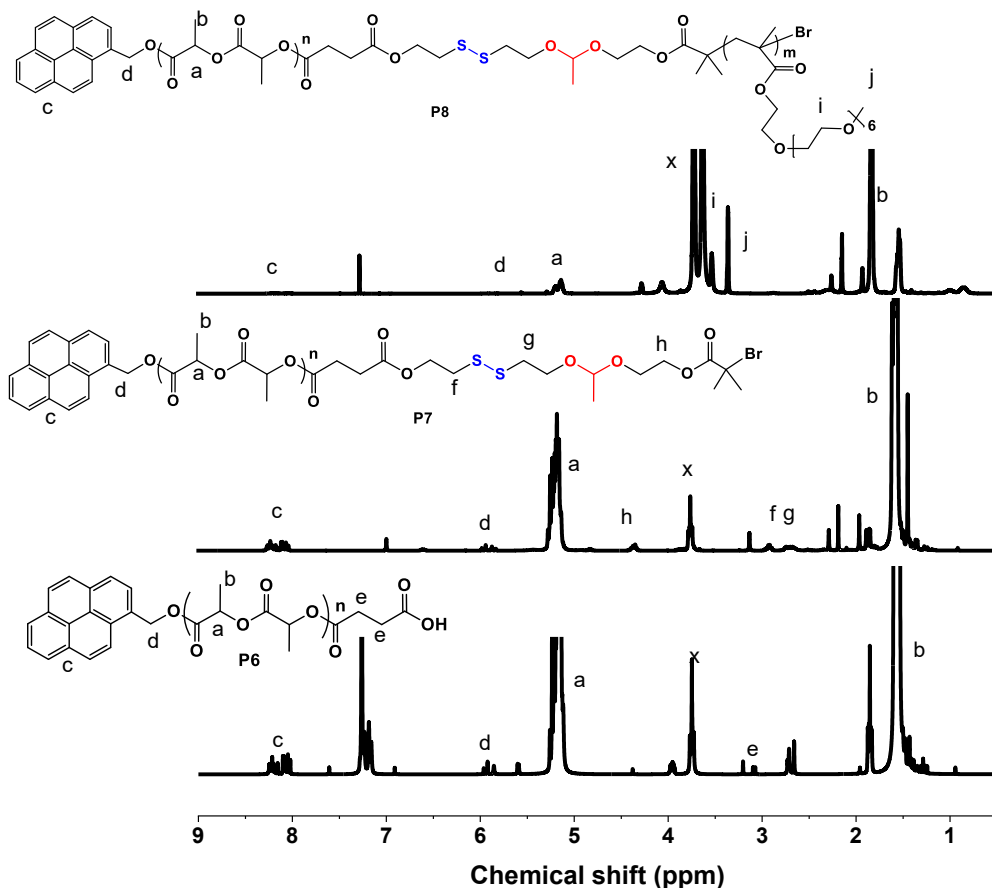


**Figure 4.8.**  $^1\text{H-NMR}$  spectra of Py-PLA-COOH (P6), Py-PLA-SS-AC-Br (P7), and POEOMA-AC-SS-PLA (P8) in  $\text{CDCl}_3$ . Conditions:  $[\text{OEOMA}]_0/[\text{P7}]_0/[\text{CuBr}]_0/[\text{PMDETA}]_0 = 50/1/0.4/0.42$  with OEOMA/anisole = 1.4/1 wt/wt at  $50^\circ\text{C}$  for ATRP.

Following the structural analysis by  $^1\text{H-NMR}$  technique, we then tested the acid- and reduction-responsive cleavage of the P8 copolymer in DMF. GPC technique was used to follow the change in molecular weight distribution. As seen in Figure 4.9a, the molecular weight distribution of P8 after incubation with acid (HCl) was shifted to lower molecular weight region with  $M_n = 23 \text{ kg/mol}$  and  $M_w/M_n = 1.24$ . Importantly, a shoulder in low molecular weight overlapped with that of P3 Py-PLA-OH precursor. Similar results are observed when the P8 was incubated with DTT (to evaluate reduction-responsiveness). As illustrated in Figure 5.9b, these results are attributed to the cleavage of the acetal and disulfide linkages at the block junction, resulting in the generation of degraded products: Py-PLA-SS-OH and HO-POEOMA for acid degradation and Py-PLA-SH and HS-AC-POEOMA for reductive degradation. These results,

combined with those from structural analysis, confirm the presence of acetal and disulfide linkages at the junction, thus the formation of well-controlled POEOMA-AC-SS-PLA P8 diblock copolymer.

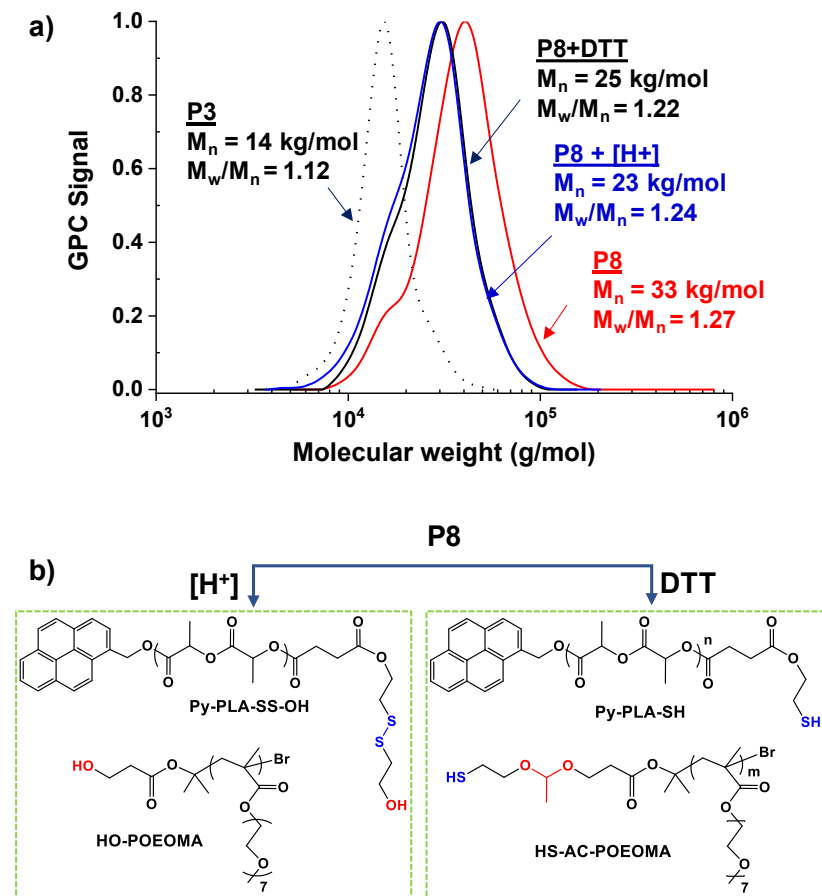


**Figure 4.9.** GPC diagrams of P8 before and after treatment with HCl and DTT, compared with P3 (Py-PLA-OH) precursor (a) and schematic illustration of degraded products of P8 upon the cleavage of the junction acetal and disulfide linkages in response to acid and reduction (b).

**4.3.3. Investigation of aqueous micellization and acid/reduction-responsive degradation.** The formed P8 diblock copolymer is amphiphilic with hydrophilic POEOMA block and hydrophobic PLA block with acetal and disulfide linkages. The solvent evaporation method using THF was examined for micellization through self-assembly in aqueous solution to form nanoassemblies with both acetal and disulfide linkages located at interfaces of PLA core and POEOMA coronas in aqueous solution. DLS analysis shows the z-average diameter of 187 nm for the formed nanoassemblies with monomodal distribution (Figure 4.10a). Their TEM images show that most

of the nanoassemblies are spherical but some of them are irregularly-shaped. Their average diameter was estimated to be  $335 \pm 92$  nm, suggesting a broader size distribution (Figure 4.10b).

To preliminarily investigate the acid-/reduction-responsive degradation, the nanoassemblies were incubated with 10 mM GSH and at pH = 5.4. As seen in Figure 4.10c, the volume distribution by DLS was shifted to larger size range with an increasing z-average diameter to 283 nm by DLS. TEM analysis also confirms an increase in average diameter to  $359 \pm 31$  nm along with the observation of some residues with degraded nanoaggregates, which evidences the degradation of the nanoassemblies in response to both stimuli (Figure 4.10d-f). Besides, the presence of large aggregates in forms of solid precipitates is visibly observed in vials. Such results can be attributed, as illustrated in Figure 4.1, to the cleavage of interfacial acetal and disulfide linkages in response to acidic pH and GSH, causing the detachment of POEOMA coronas at core/corona interfaces. It can be anticipated that such shell-shedding can promote the enhanced release of encapsulated biomolecules, particularly hydrophobic anticancer drugs such as doxorubicin, paclitaxel, etc. from the hydrophobic PLA cores of P8-based nanoaggregates.

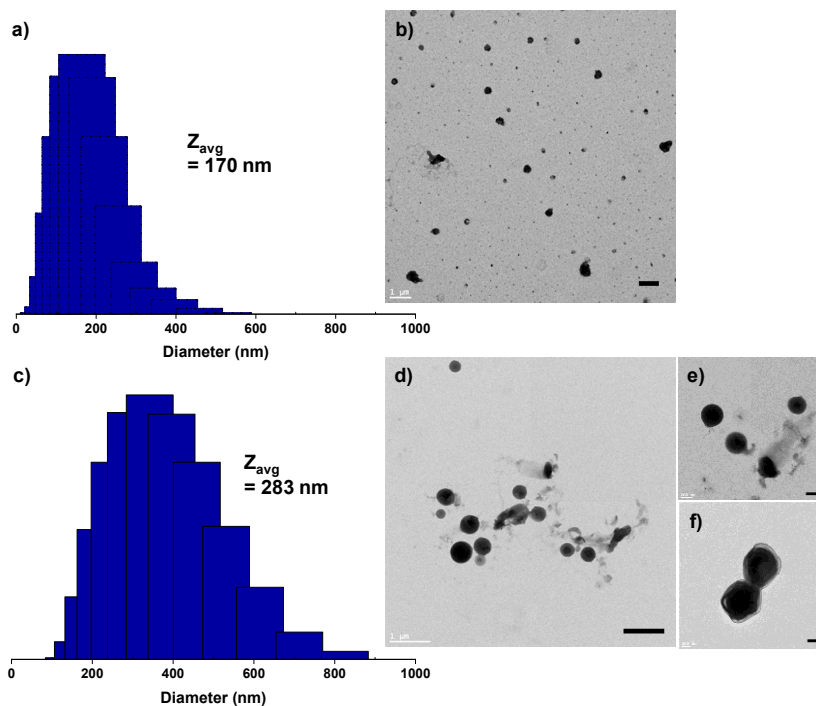


**Figure 4.10.** For P8-based nanoaggregates, DLS intensity distributions (a, c) and TEM images (b, d, scale bar = 1 μm and e-f, scale bar = 200 nm) before (a-b) and after (c-f) treatment with pH = 5.4 and 10 mM GSH in aqueous solution.

#### 4.4. Conclusion

An initial approach utilizing a double-head dual function initiator (Br-AC-SS-OH) for combined ATRP and ROP was unsuccessful in the synthesis of a POEOMA-AC-SS-PLA diblock copolymer. Although ATRP initiated with Br-AC-SS-OH enables to synthesize well-controlled POEOMA-AC-SS-OH with acetal and disulfide linkages (P1), a tin-catalyzed ROP in the presence of the formed P1 as well as Br-AC-SS-OH at elevated temperature did not render the targeted PLA-based products. The plausible reason is the unexpected instability of acetal linkages under ROP condition based on our systematic investigations with structural analysis, dual acid-/reduction-responsive degradation, and control experiments. Promisingly, the alternative approach designed without tin-catalyzed ROP of LA in the presence of Br-AC-SS-OH enables the synthesis of well-controlled PLA-SS-AC-POEMA diblock copolymer bearing both acetal and disulfide linkages at the block junction. The synthesized copolymer is amphiphilic and thus self-assembles in aqueous solutions. The formed aqueous nanoaggregates degrade in acidic solutions or in the presence of GSH, thus exhibiting acid-/reduction-responses at PLA core/POEOMA corona interfaces.

#### 4.5. Supplementary Information

##### I) Synthesis of Br-AC-SS-OH

A1 (4.6 g, 29.8 mmol) was added dropwise to a clear solution containing 2-hydroxyethyl disulfide (7.1 g, 29.8 mmol), PPTS (0.74 g, 2.98 mmol), and anhydrous dichloromethane (100 mL) in an ice bath for 20 min. The reaction mixture was stirred vigorously overnight at room temperature, and then quenched by the addition of trimethylamine (1 mL). After being washed with PBS (pH 7.4, 100 mL) three times, the product was purified by silica gel column chromatography using hexane/ethyl acetate (6/4 v/v). The product, yellow oil, was collected as the second of the total two bands off a silica gel column, yielding 6.4 g (55%);  $R_f = 0.33$  on silica (6/4 v/v hexane/ethyl acetate).

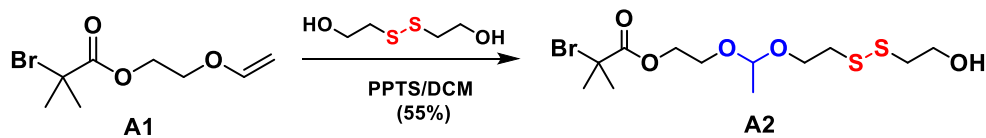


**Figure 4.S1.** Reaction scheme to synthesize A2.

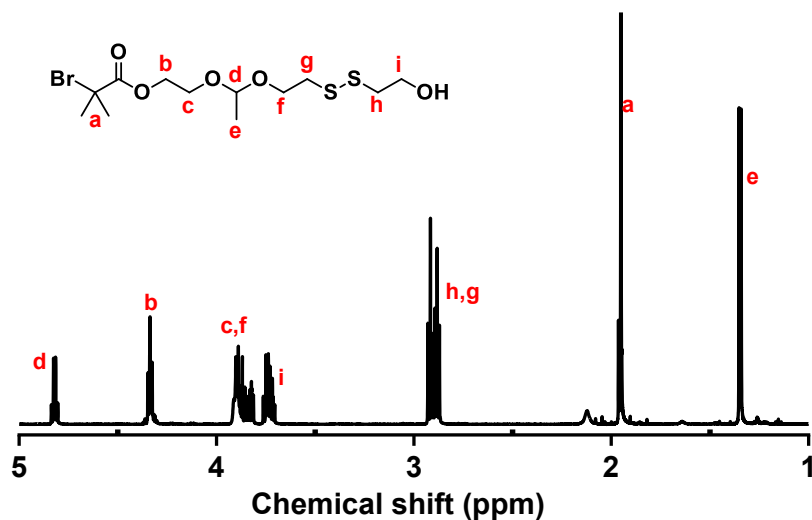


Figure 4.S2.  $^1\text{H-NMR}$  spectrum of Br-AC-SS-OH in  $\text{CDCl}_3$ .

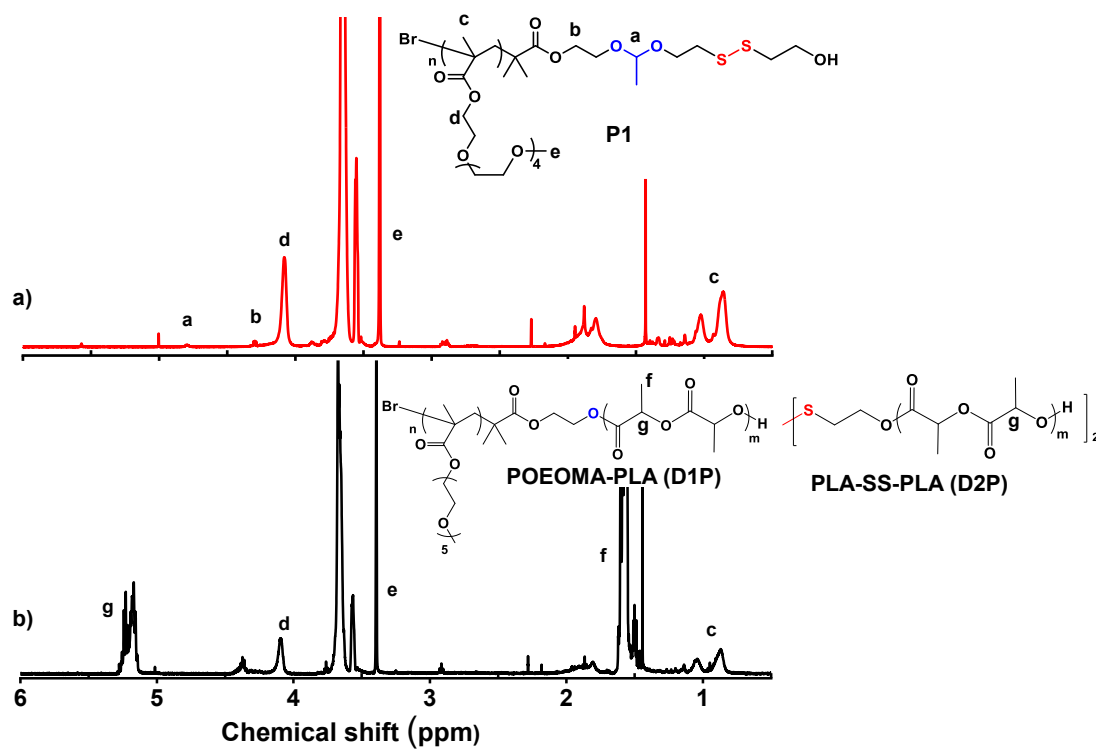
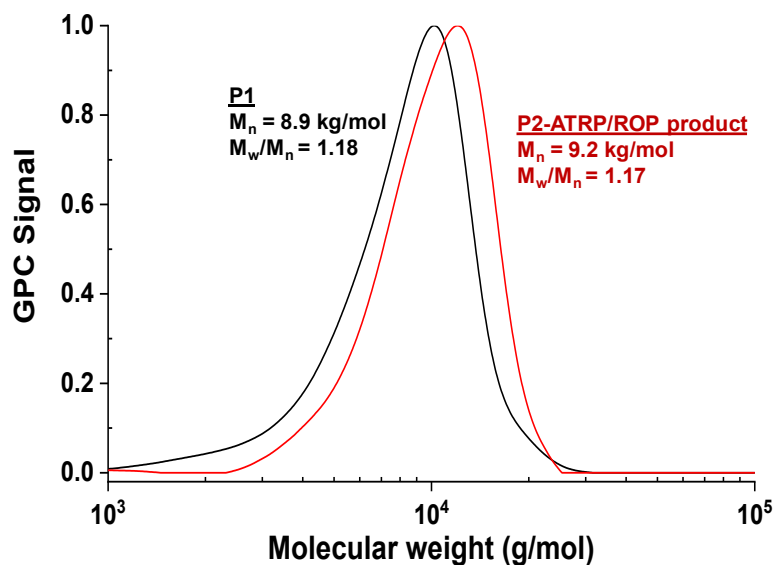


Figure 4.S3.  $^1\text{H-NMR}$  spectra of POEOMA-AC-SS-OH (P1) precursor (a) and P2-ATRP/ROP product (b) in  $\text{CDCl}_3$ .

Conditions:  $[\text{OEOMA}]_0/[\text{Br-AC-SS-OH}]_0/[\text{Cu(I)Br}]_0/[\text{PMDETA}]_0 = 30/1/0.4/0.42$  with OEOMA-MW300/anisole = 1.4/1 wt/wt at 50 °C for ATRP and  $[\text{LA}]_0/[\text{P1}]_0/[\text{Sn(EH)}_2]_0 = 70/1/0.05$  with LA/toluene = 1.9/1 wt/wt at 120 °C for ROP.

The peaks at 0.8-1.1 ppm, 3.3 ppm, and 3.5-3.8 ppm correspond to POEOMA. Using the integral ratio of the peaks (b and c), the DP of POEOMA was determined to be 21, which is somewhat larger than the calculated DP = 18 based on monomer conversion. The peak at 4.7 ppm corresponds to a methine proton in acetal moiety and the peak at 2.9 ppm is equivalent to methylene protons adjacent to disulfide linkage.



**Figure 4.S4.** GPC traces of POEOMA-AC-SS-OH precursor (P1) and P2-ATRP/ROP product (b).

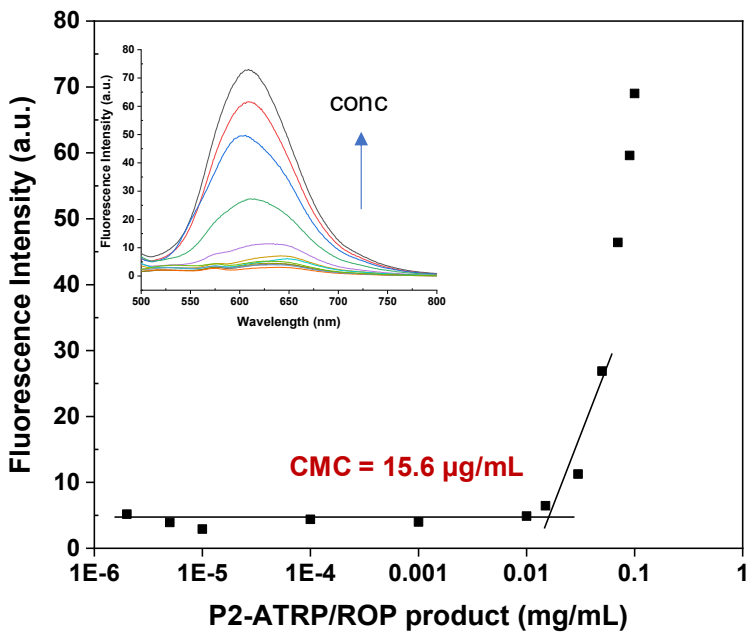


**Figure 4.S5.** Maximum fluorescence intensity of NR over concentration of the formed P2-ATRP/ROP product to determine CMC with a NR probe.

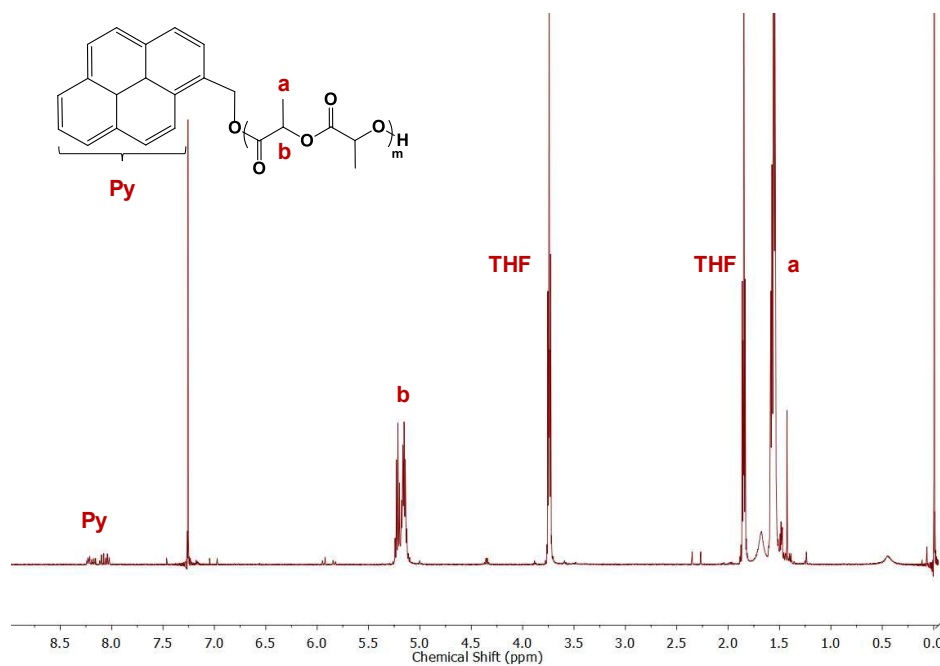


**Figure 4.S6.** <sup>1</sup>H-NMR spectrum in CDCl<sub>3</sub> of P3 synthesized by ROP of LA with Py-OH.

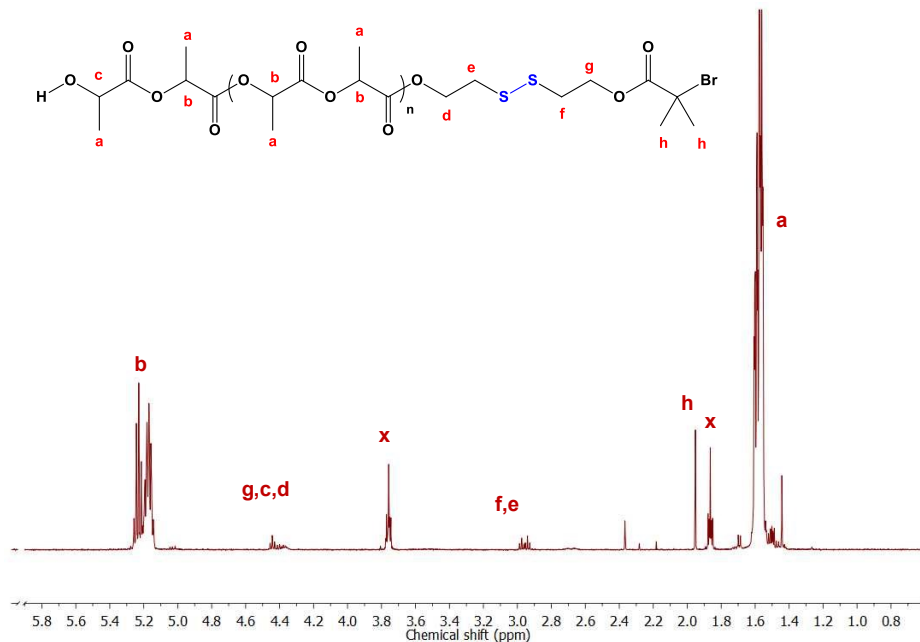


**Figure 4.S7.** <sup>1</sup>H-NMR spectrum in CDCl<sub>3</sub> of P4 synthesized by ROP of LA with Br-SS-OH.

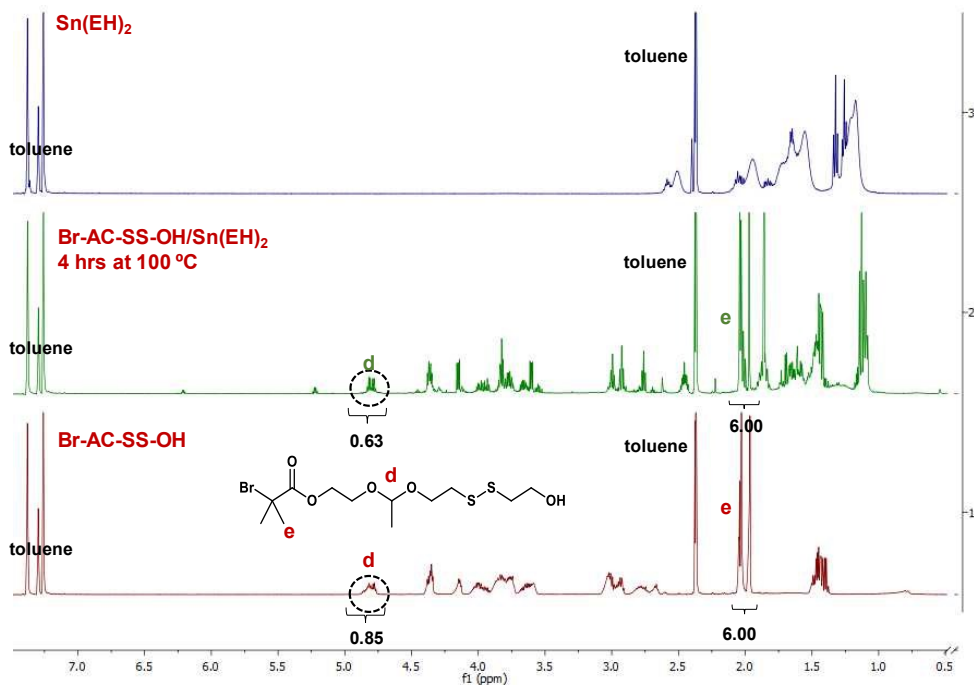


**Figure 4.S8.** <sup>1</sup>H-NMR spectrum of Br-AC-SS-OH incubated with Sn(EH)<sub>2</sub> for 4 hrs at 100 °C, compared with those of Sn(EH)<sub>2</sub> and Br-AC-SS-OH in toluene-d<sub>8</sub>.

## Chapter 5

### Synthetic method and drug release evaluation of GSH-degradable PEG-SS-PLA block copolymer nanoassemblies

#### 5.1. Introduction

Amphiphilic block copolymer-based nanoassemblies have gained significant attention as effective drug delivery nanocarriers, due to their unique properties such as nanoscaled size, high surface-to-volume ratio, and favorable physico-chemical characteristics.<sup>212-214</sup> Particularly, PEG-based PLA block copolymers (named PEG-b-PLA) have been extensively explored as tumor targeting intracellular drug delivery nanocarriers.<sup>215-217</sup> PEG is a hydrophilic or water-soluble polymer which offers various features such as non-immunogenicity, low polydispersity and non-protein adsorption.<sup>218, 219</sup> PLA is a hydrophobic biodegradable and biocompatible polyester that is approved by FDA for clinical use. Due to these features, PEG-b-PLA nanoassemblies loaded with PTX have been approved in South Korea under the name of Genexol<sup>®</sup>-PM for the treatment of breast, lung and ovarian cancers.<sup>220, 221</sup> However, this formulation uses diffusion-controlled mechanism to release encapsulated PTX in tumor sites<sup>222</sup>, which is not specific to tumor tissues and hence can ultimately result in poor therapeutic efficacy.

Numerous reports describe that SRD-based nanoassemblies exhibit controlled/enhanced release of encapsulated drug upon the cleavage of labile linkages in response to biological stimuli. Particularly, GSH-responsive degradable nanoassemblies are promising as disulfide can be cleaved to thiols in reducing environment. In biological systems, GSH is a cellular reducing agent, found at increased concentration in intracellular compartments and further at elevated levels in tumor tissues in comparison to healthy cells.<sup>223</sup> Given these features, we have investigated novel strategies that allow for the synthesis of PEG-PLA block copolymers labelled with disulfide linkages at PEG and PLA block junction (PEG-SS-PLA). Two approaches to synthesize macroinitiator for ROP of LA were proposed: a) click type azido-alkyne cycloaddition reaction and, b) protection/deprotection with acid-labile ketal chemistry. An interesting trend was observed correlating the amount of LA monomer and the DP of PLA during ROP. The formed PEG-SS-PLA block copolymer was evaluated for aqueous micellization as well as GSH-responsive PTX release *in vitro*.

## 5.2. Experimental

**5.2.1. Materials.** 2-Hydroxy ethyl disulfide (ssDOH, 99.5%), chloroacetic acid ( $\geq 99\%$ ), 4-(N,N-dimethylamino)pyridine (DMAP,  $\geq 99\%$ ), sodium azide ( $\text{NaN}_3$ ,  $\geq 99.5\%$ ), propiolic acid (95%), N,N'-dicyclohexylcarbodiimide (DCC, 99 %), anhydrous diethyl ether, N,N,N',N'',N''-pentamethyldiethylenetriamine (PMDETA,  $>98\%$ ), copper (I) bromide ( $\text{CuBr}$ ,  $>99.99\%$ ), 2-methoxypropene (97%), triethylamine ( $\text{Et}_3\text{N}$ , 99.5%), pyridinium p-toluenesulfonate (PPTS, 98%), 1,8-diazabicyclo[5.4.0]undec-7-ene (DBU), hydrochloric acid ( $\text{HCl}$ , 37%), 3,6-dimethyl-1,4-dioxane-2,5-dione (DL-lactide, LA, 99%), tin(II) 2-ethylhexanoate ( $\text{Sn}(\text{EH})_2$ , 95%), doxorubicin (Dox,  $-\text{NH}_3^+\text{Cl}^-$  forms,  $>98\%$ ), Nile red (NR), 1,4-dithiothreitol (DTT), 1,1'-carbonyldiimidazole solution (CDI), and glutathione (GSH, a reduced form) from Sigma Aldrich Canada and ethyl-3-(3-dimethylaminopropyl)carbodiimide-HCl salt (EDC) from Matrix Innovation were purchased and used as received. Methoxy poly(ethylene glycol) with MW = 5000 g/mol (PEG-OH) was donated by Advanced Polymer Materials (APM) Inc. located in Dorval, Quebec Province, Canada. Dichloromethane (DCM), dimethylformamide (DMF), tetrahydrofuran (THF), and toluene were distilled to be anhydrous. LA was recrystallized to remove residual moisture from toluene and stored under vacuum until use.

**5.2.2. Synthesis of PEG-Cl (A1).** A solution of EDC (0.32 g, 0.12 mmol) in DCM (DCM, 10 mL) was added dropwise to a solution containing PEG-OH (2 g, 0.4 mmol), chloroacetic acid (0.18 g, 1.6 mmol) and DMAP (14.6 mg, 0.12 mmol) dissolved in DCM (50 mL) in an ice bath under stirring. The mixture was stirred at room temperature for 13 hrs, washed with brine solution twice, and precipitated from cold diethyl ether. The precipitate was isolated by vacuum filtration and dried in a vacuum oven at room temperature 12 hrs. Yield = 1.3 g (60%).

**5.2.3. Synthesis of PEG-N3 (A2).** The purified, dried A1 (0.5 g, 0.1 mmol) was dissolved in DMF (10 mL) and mixed with  $\text{NaN}_3$  (0.16 g, 2.5 mmol) under stirring at 60 °C for 12 hrs. After the removal of solvents, the residue was dissolved in DCM (50 mL). The mixture was washed with brine solution twice, dried over sodium sulfate, and then precipitated from cold diethyl ether. The precipitate was isolated by vacuum filtration and dried in vacuum oven at room temperature for 12 hrs. Yield = 0.5 g (80%).

**5.2.4. Synthesis of A3.** A solution of propiolic acid (2.3 g, 33.3 mmol) dissolved in THF (THF, 10 mL) was added dropwise to an organic solution consisting of ssDOH (6.2 g, 40 mmol), DCC (14.6 mg, 0.12 mmol) and DMAP (0.2 g, 1.67 mmol) in THF (80 mL) in an ice bath under stirring. After the mixture was stirred at room temperature for 12 hrs, the solvent was evaporated by rotary evaporation. The product was purified by silica gel column chromatography with ethyl acetate/hexane (1/4 v/v). The product as a pink oil was collected as the second band of total four bands. Yield= 1.3 g (15%);  $R_f$  on silica = 0.6 (ethyl acetate/hexane 1/4 v/v).

**5.2.5. Synthesis of PEG-SS-OH/I.** The mixture containing A2 (6.2 g, 40 mmol), Alkyne-SS-OH (14.6 mg, 0.12 mmol) and PMEDTA (0.2 g, 1.6 mmol) and THF (6 mL) in a 15 mL Schlenk flask was purged with nitrogen for 30 min. CuBr (0.9 mg) was added to initiate reaction and the resulting mixture was stirred at room temperature for 12 hrs. After exposed to air to stop the reaction, the mixture was precipitated from cold diethyl ether. The precipitate was isolated by vacuum filtration and dried in vacuum oven at room temperature for 12hrs, yielding white solids.

**5.2.6. Synthesis of monoprotected 2-hydroxyldisulfide (OH-SS-Ketal, B1).** 2-Methoxypropene (1.7 g, 23.8 mmol) was added dropwise to a mixture containing ssDOH (3.3 g, 21.7 mmol), PPTS (0.32 g, 1.3 mmol) and molecular sieves (35 g) in THF (50 mL) in an ice-bath. The resulting mixture was stirred in an ice-bath for 20 mins and then in room temperature for 2 hrs before it was quenched by the addition of Et<sub>3</sub>N. After the removal of molecular sieves by a vacuum filtration and THF by rotary evaporation, DCM (200 mL) was added. The mixture was washed with aqueous PBS solution (pH = 7.4) twice, and then dried over sodium sulfate. After evaporation of DCM, the product was purified by silica gel column chromatography using hexane/ethyl acetate (3/2 v/v). The product as colorless oil was collected as the second of the total two bands off a silica gel column. Yield = 1.5 g (31%);  $R_f$  = 0.28 on silica (hexane/ethyl acetate = 3/2 v/v).

**5.2.7. Synthesis of PEG-SS-OH/II.** PEG-CDI (2.6 g, 0.52 mmol) was added dropwise to a clear solution containing OH-SS-Ketal (0.70 g, 3.1 mmol), DBU (63.1 mg, 0.41 mmol), and anhydrous

DCM (30 mL) in an ice-bath for 20 min. The reaction mixture was stirred vigorously overnight at room temperature, and then precipitated from cold diethyl ether. The product was collected by filtration and dried in vacuum oven at room temperature for 12 hrs to form PEG-SS-Ketal (B2). In the next step, the formed A2 was dissolved in DCM (30 mL) and mixed with HCl (40  $\mu$ L). The reaction mixture was stirred for 1 hr and then washed with aqueous PBS solution (pH = 7.4) twice. After having passed through sodium sulphate, the product, the mixture precipitated from diethyl ether. The product as white solids were collected by vacuum filtration and dried in vacuum oven at room temperature for 12 hrs: Yield = 2.2 g (83.0 %).

**5.2.8. General procedure for ring opening polymerization (ROP) of LA.** LA, initiator and Sn(EH)<sub>2</sub> mixed with toluene in a Schlenk flask were subject to three freeze-pump-thaw cycles and filled with N<sub>2</sub> at the last cycle. The resulting mixture placed in an oil-bath pre-set at 120 °C to start polymerization. After 20 hrs, the solution was precipitated from cold diethyl ether. The precipitate was dried under vacuum for 12 hrs.

**Synthesis of P1.** LA (1.4 g, 9.7 mmol), PEG-SS-OH/II (0.7 g, 0.14 mmol), Sn(EH)<sub>2</sub> (4.4 mg, 11  $\mu$ mol) and anhydrous toluene (3 mL) for PEG-SS-PLA (P1);

**Synthesis of P1C.** LA (3 g, 20 mmol), PEG-OH (1.48 g, 0.30 mmol), Sn(EH)<sub>2</sub> (9.6 mg, 23  $\mu$ mol) and anhydrous toluene (7 mL) for PEG-PLA (P1C).

**Synthesis of P2.** LA (2 g, 14 mmol), PEG-OH (1 g, 0.19 mmol), Sn(EH)<sub>2</sub> (6.4 mg, 15  $\mu$ mol) and anhydrous toluene (4.5 mL) for PEG-PLA (P2).

**5.2.9. Investigation of reduction-responsive degradation.** For copolymer, P2 (3 mg) was dissolved in DMF/LiBr solution (3 mL), to which, DTT (5  $\mu$ g, 10 equivalents to disulfide bonds) was added. The reaction mixture was stirred at room temperature. Aliquots were periodically withdrawn and analyzed immediately by GPC to determine the extent of cleavage of disulfide bond in the polymer. The control block copolymer PEG-PLA was also analyzed for degradation.

**5.2.10. Determination of CMC using NR probe method.** A stock solution of Nile Red (NR) in THF at 1 mg/mL and a stock solution of PEG-SS-PLA in THF at 1 mg/mL were prepared. Water (10 mL) was added dropwise into a series of mixtures consisting of the same amount of the stock solution of NR (0.5 mL, 0.5 mg NR) and various amounts of the stock solution in 20 mL vials. The resulting dispersions were stirred for 24 hrs to evaporate THF. The dispersions were then filtered using 0.45  $\mu\text{m}$  PES filters to remove excess NR. A series of NR-loaded micelles at various concentrations of PEG-SS-PLA ranging from  $5 \times 10^{-6}$  to 0.4 mg/mL were formed. Their fluorescence spectra were recorded at  $\lambda_{\text{ex}} = 480 \text{ nm}$ . CMC for the control block copolymer PEG-PLA was determined using similar procedure.

**5.2.11. Aqueous micellization.** P1 (10 mg) was first dissolved in DMF (2 mL) followed by the addition of 10 mL of PBS buffer dropwise using a syringe pump. This solution was then transferred to the dialysis bag with MWCO = 3.5 kDa to remove the DMF and dialyzed against PBS buffer which was changed twice. After 24 hrs, dialysis was stopped, and the micellar dispersion was analyzed for the hydrodynamic diameter using DLS.

**5.2.12. Preparation of PTX-loaded micelles.** The PTX-loaded micelles were prepared using the dialysis method as reported above. Briefly, 10 mg of the polymer and paclitaxel (3 mg) were dissolved in DMF (5 mL) and allowed to stir for 30 mins. After that, polymer solution was added to the dialysis bag with MWCO = 3.5 kDa and dialyzed against PBS (pH 7.4) and outer media was exchanged twice. After 24 hrs, dialysis was stopped, and the resultant solution was centrifuged and passed through PES filter. PTX-loaded micellar solution was evaluated for the size and polydispersity using DLS.

**5.2.13. Determination of loading of PTX in PTX-loaded micelles.** The drug loading efficiency was determined using HPLC. The mobile phase consisted of acetonitrile/water (40:60 v/v). The reverse phase column was ACE 5 C18 (150 x 4.6 mm). The column temperature was maintained at 30 °C. The flow rate was set at 1.0 mL/min and the detection wavelength was 227 nm. Sample solution was injected at a volume of 5  $\mu\text{L}$ . The HPLC was calibrated with standard solutions of 5

to 100 µg/mL of PTX dissolved in acetonitrile. Nanoparticles were dissolved in acetonitrile and vigorously vortexed to get a clear solution. The encapsulation efficiency was defined by the ratio of measured and initial amount of PTX encapsulated in nanoparticles.

$$\text{Drug loading content (\%)} = \frac{\text{Amount of PTX in nanoparticles}}{\text{Amount of PTX in nanoparticles} + \text{total mass copolymer}} \times 100$$

$$\text{Encapsulation efficiency (\%)} = \frac{\text{Amount of PTX in nanoparticles}}{\text{Initial amount of PTX}} \times 100$$

**5.2.14. *In vitro* PTX release.** The drug release was examined using dialysis method. In brief, 2 mL of nps were suspended into the dialysis tube (MWCO = 3.5 kDa) which was immersed in 40 mL of release medium PBS (pH 7.4) without and with 10 mM GSH. Quantitative samples were taken at various intervals for analysis and replaced with fresh medium. The collected samples were dissolved in acetonitrile for analysis by HPLC using above method. The accumulated release of drugs from PTX-loaded nps was plotted against time.

### 5.3. Results and discussion

**5.3.1. Synthesis of PEG-SS-OH.** Two strategies as routes I and II were explored to synthesize PEG-SS-OH. Route I was designed and synthesized by Xiaolei Hu (M.Sc. student in Dr. Oh's lab). It used a click type azido-alkyne cycloaddition reaction, as depicted in Figure 5.1. The route began with an EDC coupling reaction of PEG-OH with an excess chloroacetic acid (4 equiv) to synthesize a chlorine-capped PEG (PEG-Cl) at 60 % yield. The synthesis is followed by the appearance of the characteristic peak (c) at 4.2 ppm corresponding to methylene protons adjacent to Cl atom in its <sup>1</sup>H-NMR spectrum (Figure 5.2a). The formed PEG-Cl reacts with excess NaN<sub>3</sub>(4 equiv) to yield an azido-terminated PEG (PEG-N<sub>3</sub>), which was confirmed by shift of the peak to 3.9 ppm in <sup>1</sup>H-NMR spectrum (Figure 5.2b). Alkyne-SS-OH was synthesized by a DCC coupling reaction of ssDOH with propiolic acid at 70 % yield. Its chemical structure was confirmed by <sup>1</sup>H-NMR (Figure 5.2c). Given the successful synthesis of PEG-N<sub>3</sub> and Alkyne-SS-OH, the azido-alkyne cycloaddition reaction was conducted in the presence of Cu(I) catalyst to synthesize PEG-SS-OH/I. <sup>1</sup>H-NMR in Figure 5.2d showing the triazole peak (d) at 8.4 ppm confirms the synthesis.

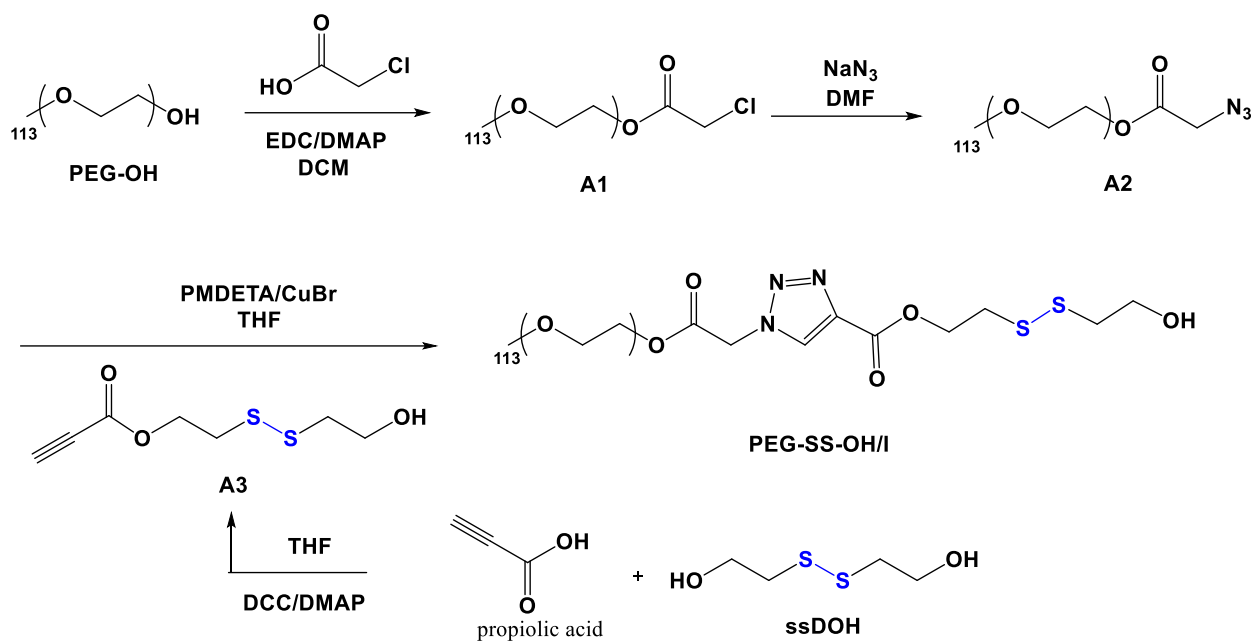


**Figure 5.1.** Route I exploring azido-alkyne cycloaddition reaction to synthesize PEG-SS-OH/I.

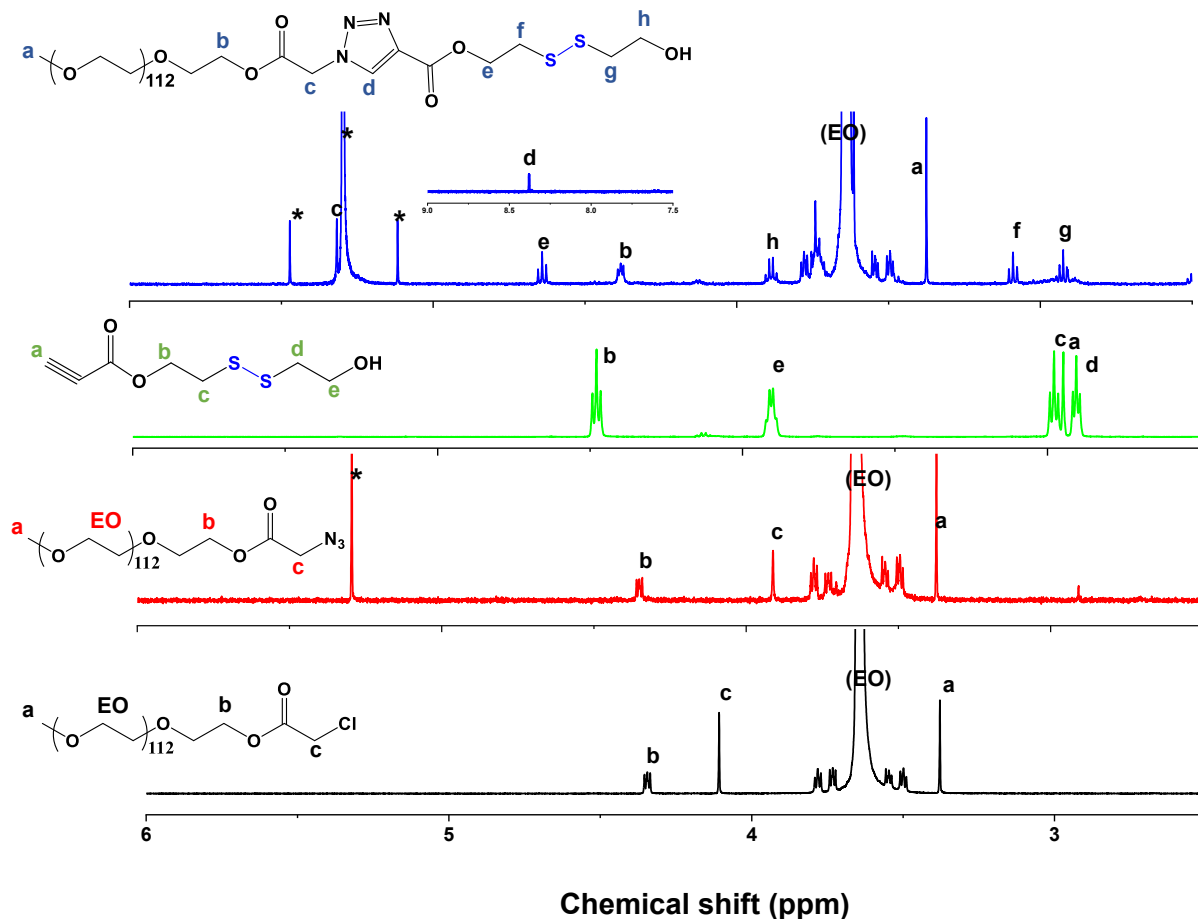


**Figure 5.2.** Overlaid  $^1\text{H-NMR}$  spectra of PEG-Cl a), PEG- $\text{N}_3$  b), Alkyne-SS-OH, and PEG-SS-OH/I in  $\text{CDCl}_3$ .

Route II was designed and carried out by Arman Moini Jazani (PhD student in Dr. John Oh's lab). Route II utilizes the protection/deprotection with acid-labile ketal chemistry as illustrated in Figure 5.3. Route II began with the reaction of ssDOH with 2-methoxypropene to synthesize **B1** bearing a ketal group at one end at 31% yield after being purified by column chromatography. The presence of the peak at 1.3 ppm corresponding to dimethyl group in ketal moiety and the peak at 3.2 ppm for methylene groups adjacent to disulfide group in  $^1\text{H-NMR}$  (Figure 5.4a) confirms the synthesis of **B1**. In the next step, the purified **B1** was used for the coupling reaction with PEG-Cl to yield **B2**. The reaction was performed in presence of DBU as a catalyst and excess of B1 (6 mole equivalent) to ensure their complete coupling.  $^1\text{H-NMR}$  shows the disappearance of aromatic imidazole peaks, confirming quantitative conjugation. With no requirement of purification, the

formed **B2** was subjected to acid-catalyzed hydrolysis for deprotection of the ketal group, forming PEG-SS-OH/II at 83% yield with PEG5000-OH. The reaction was followed by  $^1\text{H-NMR}$  showing no peaks at 3.22 ppm for ketal groups and appearance of the peak at 3.8 ppm equivalent to methylene protons adjacent to the terminal hydroxyl group.

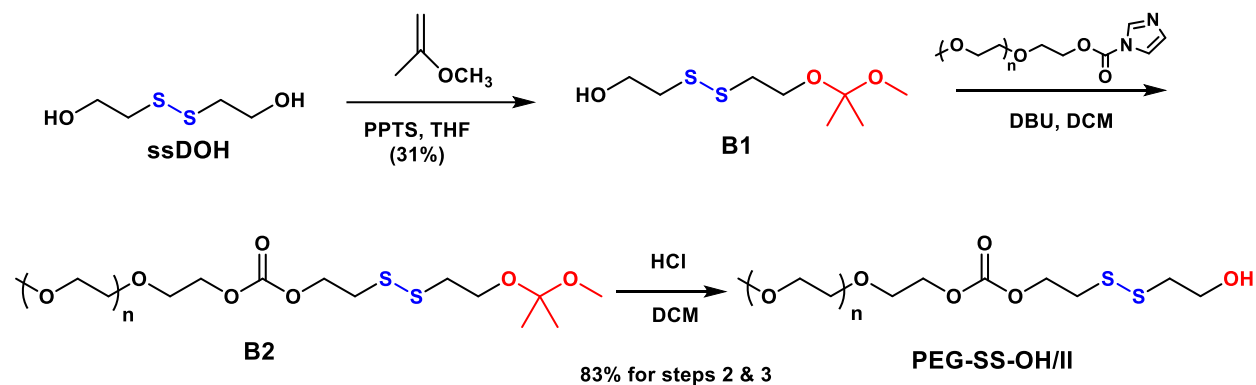


**Figure 5.3.** Route II utilizing the protection-deprotection chemistry with acid-labile ketal group to synthesize PEG-SS-OH/II.

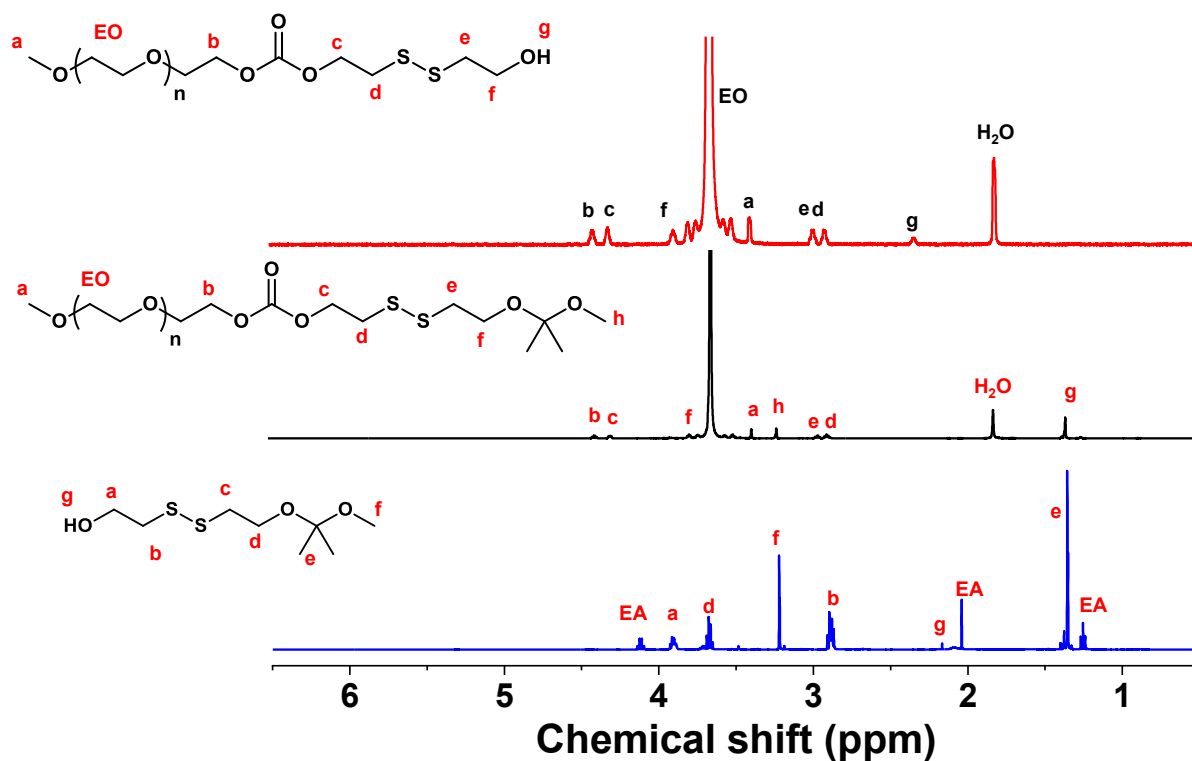


**Figure 5.4.** Overlaid  $^1\text{H-NMR}$  spectra of B1, B2 and PEG-SS-OH/II in  $\text{CDCl}_3$ . EA refers to traces of ethyl acetate.

For comparison, ROP of LA with PEG-OH (no SS) was carried out under similar condition as P1 synthesis. Similarly, their chemical structures and molecular weights were characterized (Figure 5.S1 for  $^1\text{H}$  NMR and GPC). Note that P2 was synthesized with smaller batch size (LA amount).

**5.3.2. Synthesis of PEG-SS-PLA.** Figure 5.5a illustrates our approach to synthesize well-defined PEG-SS-PLA with narrow molecular weight distributions by the ROP of LA under tin-catalyzed condition at 120 °C in toluene. With a choice of PEG5000-SS-OH/II synthesized through Route II, ROP was conducted under conditions of  $[\text{LA}]_0/[\text{PEG-SS-OH}]_0/[\text{Sn}(\text{EH})_2]_0 = 70/1/0.08$  with  $\text{LA}/\text{toluene} = 0.43/1$  wt/wt. The amount of LA monomer as batch size were varied at 1.4 g for P1 and 2 g for P2. After being purified by precipitation from cold diethyl ether to remove unreacted LA and residual tin catalyst, the formed copolymers were characterized for chemical structure by  $^1\text{H}$  NMR and molecular weight by GPC. As an example, with P1,  $^1\text{H}$  NMR spectrum in Figure 5.5b shows the presence of PLA at 5.1 (g) and 1.6 ppm (f) and PEG at 3.62-3.69 ppm (EO protons). The integrals were used to determine the DP which was 61 for PLA block. GPC analysis shows that molecular weight distribution of P1 was shifted to high molecular weight region with  $M_n = 21$  kg/mol and  $\text{Đ} = 1.26$  (Figure 5.5c). Similarly, P2 was characterized with  $\text{DP} = 27$  and  $M_n = 15$  kg/mol and  $\text{Đ} = 1.08$ .

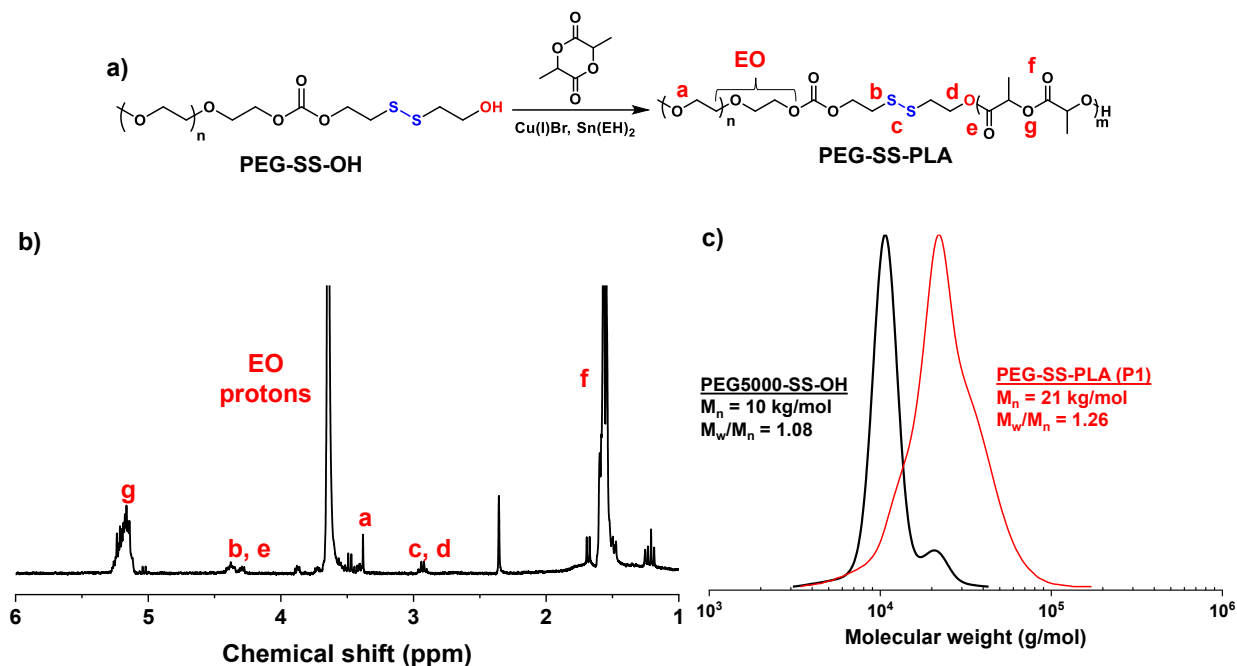


**Figure 5.5.** Synthetic scheme (a), <sup>1</sup>H-NMR spectrum in CDCl<sub>3</sub> (b) of PEG-SS-PLA (P1) by ROP of LA in the presence of PEG-SS-OH/II. Conditions: [LA]<sub>0</sub>/[I]<sub>0</sub>/[Sn(EH)<sub>2</sub>]<sub>0</sub> = 70/1/0.08; LA/toluene = 0.43/1 and GPC diagram of P1, compared with PEG-SS-OH, its macroinitiator c).

In a separate experiment, we investigated the amount of LA as batch size on chemical structure as DP of PLA block. With PEG-OH (MW =5000 g/mol and MW =2000 g/mol) macroinitiators, a series of PEG-b-PLA block copolymers were prepared under the similar condition as described above, thus [LA]<sub>0</sub>/[PEG-OH]<sub>0</sub>/[Sn(EH)<sub>2</sub>]<sub>0</sub> = 70/1/0.08 with LA/toluene = 0.43/1 w/w. Table 5.S1 summarizes the DP of PLA and molecular weight data of PEG-b-PLA copolymers. P1C and P2 polymers represent the PEG-b-PLA copolymers synthesized with PEG5000-OH and PEG2000-OH macroinitiators, respectively. The DP of PLA block over the amount of LA used (as batch size) for P1C and P2C (inset) block copolymers is plotted in Figure 5.S2. The DP sharply increased with the amount of LA up to around 3 g; upon further increase in LA, it gradually increased. This result suggests the importance to consider manufacturing parameters for the synthesis of copolymers.

**5.3.3. Reduction-responsive degradation.** As illustrated in Figure 5.6a, PEG-SS-PLA could be disassembled to the corresponding PEG-SH and PLA-SH upon the cleavage of disulfide linkage

at the block junction. With an example of P2, the aliquots were mixed with the excess DTT (10 mol equivalent to disulfide) in DMF. GPC was used to follow the reduction-responsive degradation in DMF and after 24 hrs of incubation. The molecular weight of P2 ( $M_n$ ) decreased from 15 kg/mol to 4.5 kg/mol, which can be attributed to the degradation of disulfide linkage (Figure 5.6b).

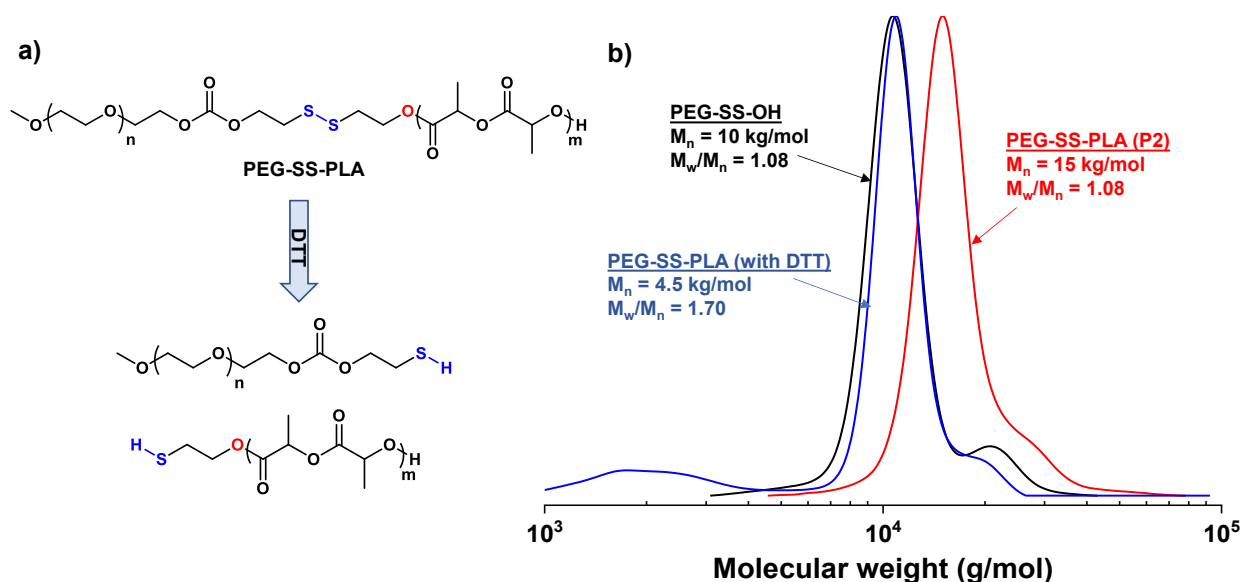


**Figure 5.6.** Schematic illustration of reduction-responsive degradation a) and GPC traces of P2 before and after incubation with DTT b).

**5.3.4. Aqueous micellization.** Self-assembly in water was investigated with a choice of P1. Its CMC was determined using fluorescence spectroscopy method with a NR probe. Figure 5.S3 shows the evolution of the intensity of NR fluorescence over the concentration of P1. Using two linear regressions, CMC was determined to be 8.9  $\mu\text{g/mL}$ , which falls well within the range of polymeric micelles. Due to the amphiphilic nature, PEG-SS-PLA block copolymer self-assembles into micelles through aqueous micellization. Dialysis method was employed to fabricate aqueous nanoassemblies with average hydrodynamic diameter of 69 nm (Figure 5.7). Similar procedure was used, but with PTX to fabricate PTX-loaded nanoassemblies. DLS analysis confirms the diameter to be 62 nm, which is smaller than that of empty micelles.

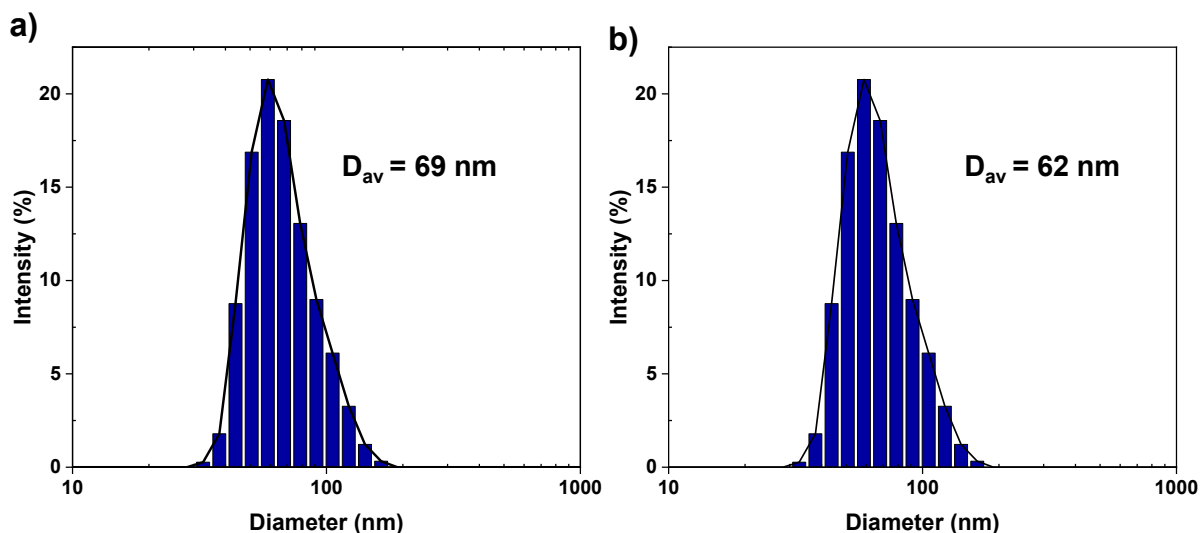


**Figure 5.7.** DLS diagram of empty a) and PTX-loaded P1 micelles b).

**5.3.5. GSH-responsive release of PTX using HPLC technique.** HPLC was used to determine loading efficiency and encapsulation efficiency of PTX in micellar cores. A standard curve of PTX was built in acetonitrile for quantitative analysis (Figure 5.S4). The loading content and encapsulation efficiency were determined to be 1.1 % and 3.5 % respectively. Based on our polymer design which incorporated reduction-responsive disulfide linkages at the junction of hydrophobic and hydrophilic blocks, we hypothesized that the release of PTX would be accelerated in the presence of GSH. The PTX release profiles from the aqueous solutions of the PEG-SS-PLA (P1) contained within dialysis tubing were studied by analyzing the increase in PTX concentration in the release medium over a period of 8 hrs of dialysis against PBS buffer with and without the addition of 10 mM GSH. After every 2 hrs, aliquots of 2 mL of release media were taken out for HPLC analysis and replaced with fresh media. Those aliquots were first evaporated to remove aqueous solution using rotary evaporator and then dissolved in acetonitrile for HPLC analyses. An accelerated drug release profile ca. 70 % PTX release in the presence of GSH compared to no release in normal media was observed (Figure 5.8).

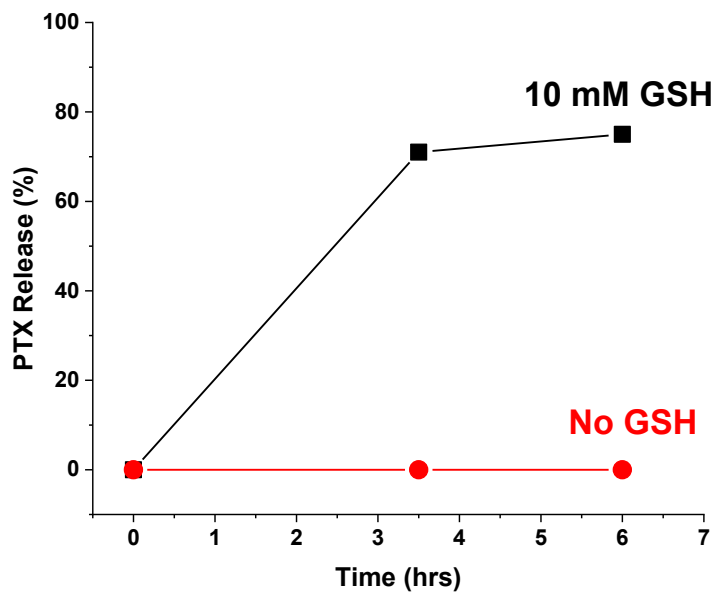


**Figure 5.8.** *In vitro* release profiles of PTX from PTX-loaded micelles incubated with and without 10 mM GSH in PBS solution.

#### 5.4. Conclusion

GSH-responsive PEG-SS-PLA block copolymers were synthesized by ROP of LA with PEG-SS-OH macroinitiator with varying chain lengths successfully. Their low CMC value suggest that they could be colloidally stable upon dilution and during blood circulation. Moreover, their GSH-responsive disassembly and enhanced PTX release demonstrate their potential as promising vehicles for effective intracellular delivery of hydrophobic PTX drugs.

## 5.5. Supporting Figures and Table

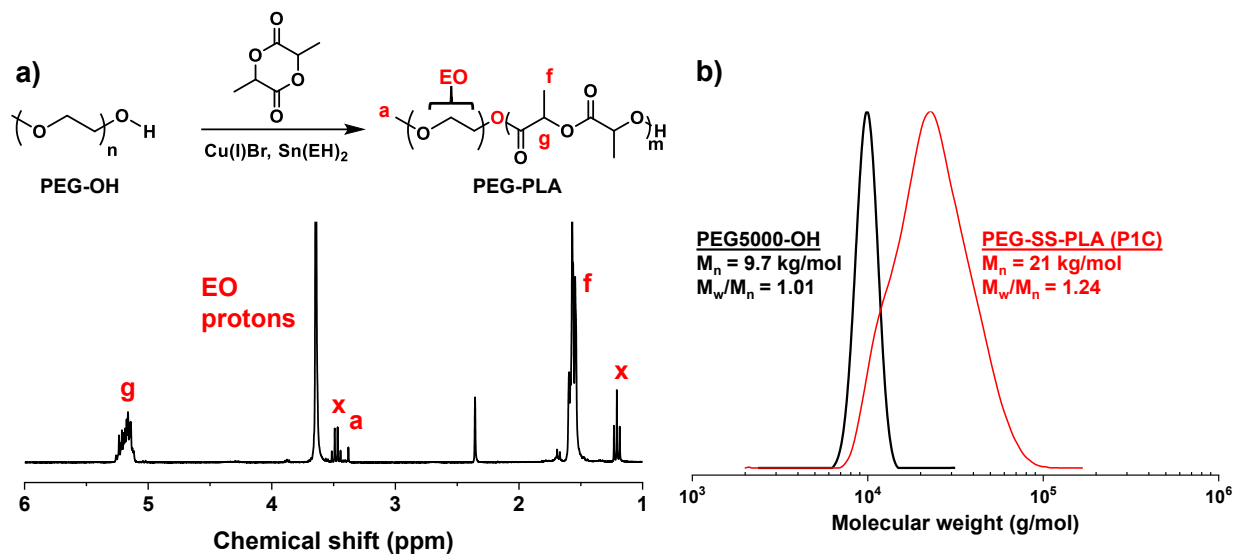


**Figure 5.S1.**  $^1\text{H-NMR}$  of P1C in  $\text{CDCl}_3$  a), GPC diagram of P1C, compared with PEG-OH, its macroinitiator b).

**Table 5.S1.** Characterization data for all control block copolymers synthesized. (P1C and P2C refers to block copolymers synthesized using PEG5000-OH and PEG2000-OH macroinitiators respectively).

Batch	Initiator	LA (g)	DP/PLA	$M_n$ (g/mol)	$\bar{D}$
P1C-0.2	PEG5000-OH	0.2	11	12,380	1.0
P1C-0.5	PEG5000-OH	0.5	40	12,000	1.2
P1C-3	PEG5000-OH	3	52	16,500	1.2
P1C-5	PEG5000-OH	5	61	20,800	1.2
P1C-6	PEG5000-OH	6	58	19,800	1.3
P1C-10	PEG5000-OH	10	63	20,800	1.2
P2C-0.2	PEG2000-OH	0.2	34	6,000	1.3
P2C-0.8	PEG2000-OH	0.8	51	9,000	1.2
P2C-0.4	PEG2000-OH	3.5	68	17,400	1.3
P2C-0.5	PEG2000-OH	10	63	15,400	1.4

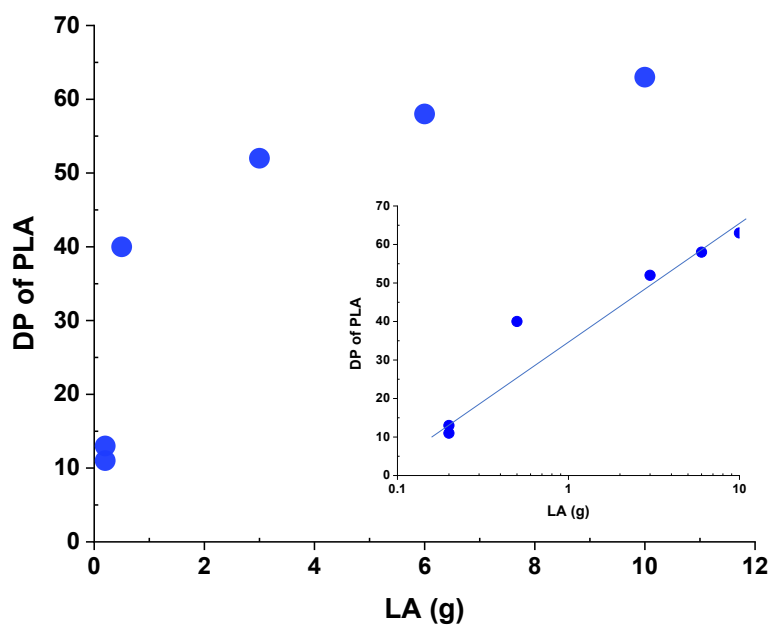


**Figure 5.S2.** DP of PLA block over the amount of LA as batch size for the synthesis of P1C block copolymers [Inset; P2C block copolymers].

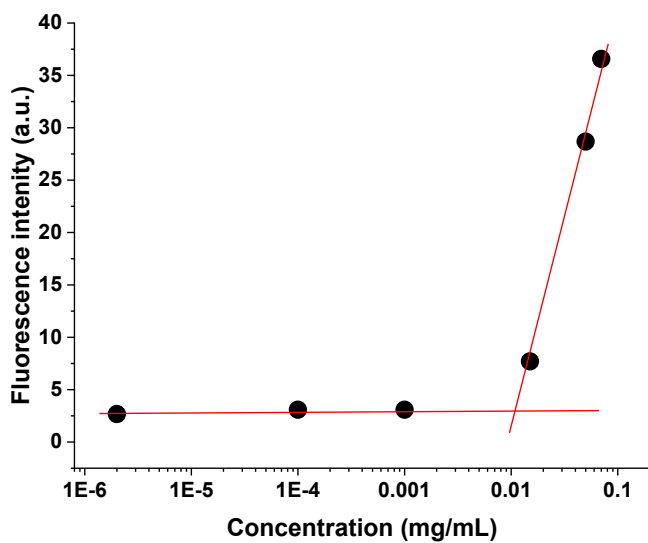


**Figure 5.S3.** Maximum fluorescence intensity of NR over concentration of P1 to determine CMC with a NR probe.

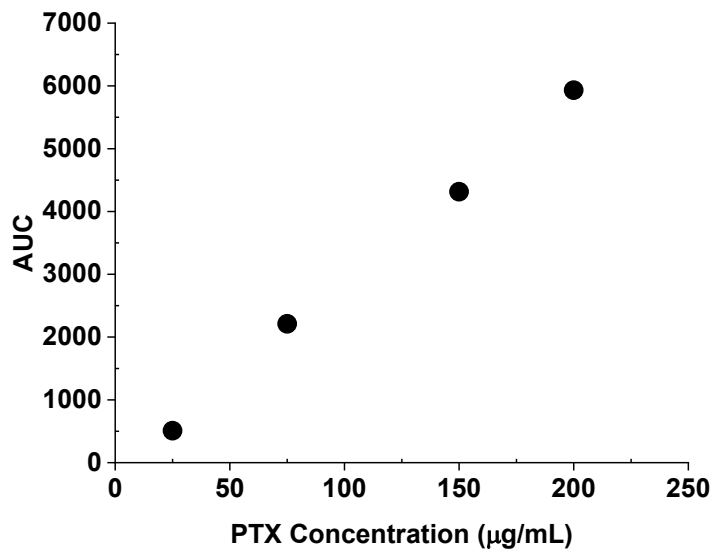


**Figure 5.S4.** Calibration curve for PTX generated using different concentrations of PTX using HPLC.

## Chapter 6

### Summary and recommendations for future work

#### 6.1. Summary of thesis

Tremendous efforts to develop robust ABPs with various architectures and multifunctionalities have advanced our abilities to design, synthesize and characterize nanomaterials. Furthermore, they have fostered effective collaborations in interdisciplinary fields of chemistry, physics, material sciences, and medical sciences. Particularly, SRD-based polymeric nanoassemblies are one of the most promising nanocarriers that delivers various cargoes, not only conventional chemotherapeutic drugs but also biological macromolecules.

The focus of my PhD research was to understand, explore and evaluate PLA-based block copolymers and their nanoassemblies designed with reduction and acidic pH-cleavable linkages for the applications in intracellular drug delivery. The robust synthetic approaches including ROP, ATRP and facile coupling chemistries enabled the preparation of well-defined PLA-containing block copolymers.

*Chapter 3* of this thesis describes the research project focused on the synthesis of DSRD-exhibiting PLA-based triblock copolymer nanoassemblies with the acidic pH-responsive ketal linkages embedded in the hydrophobic block (PLA) and reduction-responsive disulfide linkages positioned between the hydrophilic block POEOMA and hydrophobic PLA block. This triblock copolymer was then characterized for degradation in organic solvent (DMF) using GPC. Furthermore, this triblock copolymer self-assembled to form spherical micelles in aqueous solution with average hydrodynamic diameter of 29 nm at the concentration of 1 mg/mL. These blank micelles showed little cytotoxicity against HeLa cells. Moreover, to evaluate their degradation profile quantitatively, NR was encapsulated, and its release was monitored using fluorescence spectroscopy. A synergistic release was observed under dual acidic pH/redox stimuli conditions in comparison to single stimulus, thereby providing a strong evidence for the feasibility of the system.

*Chapter 4* of this thesis describes the proposed two-step synthetic route for PLA-based diblock copolymer labelled with both reduction-responsive disulfide and acidic pH-responsive acetal

linkages positioned at the junction of hydrophilic and hydrophobic blocks. This two-step synthetic route, however led to the investigation of the stability of acetal linkages under traditional ROP conditions, which was confirmed by control ROPs with initiators without acetal linkages. Therefore, alternative route was then adopted for the synthesis of diblock copolymer, which was characterized using NMR and GPC analyses. In addition, this diblock copolymer was evaluated for the self-assembly properties under the aqueous conditions.

*Chapter 5* describes the synthesis and evaluation of PEG-SS-PLA diblock copolymer as a potential candidate for PTX delivery. This diblock copolymer was synthesized using a PEG-based macroinitiator bearing a terminal -OH group, which allowed for the ROP of LA. Diblock copolymers with varying chain lengths of PLA were synthesized and characterized. Preliminary studies for PTX-loading and its release were also carried out, which showed a burst release within 6 hrs under the reducing (10 mM GSH) conditions in comparison to the control (PBS pH 7.4). Therefore, micelles prepared from the PEG-SS-PLA diblock copolymers hold great potential for PTX loading and delivery.

## **6.2. Future works**

SRD-exhibiting nanoassemblies have been designed meticulously in nanometer range for encapsulation and on-demand release of hydrophobic anticancer drugs in response to biological stimuli. Through my research projects, I was able to demonstrate the feasibility of synthesis and characterization of well-defined SRD-based block copolymers. However, there are additional experiments that are required to examine unmet questions and some outstanding challenges to be resolved.

In Chapter 3, the triblock copolymer contains undesired diblock copolymer (POEOMA-SS-PLA, 40 % by weight). An alternative synthetic route could be used to synthesize pure triblock copolymer which can allow for further studies on encapsulation and release of anticancer drugs such as DOX and PTX. Furthermore, *in vitro* cellular uptake can be studied using CLSM with 2D and 3D-spheroid tumor models.

In Chapter 4, the diblock copolymer synthesized by an alternative approach will be used for comparative studies with control diblock copolymer labelled with either disulfide or acetal linkage.

In addition, pyrene moieties at the terminal end of hydrophobic PLA block can be explored for fluorescence imaging which can impart the properties of theranostic agents to this diblock copolymer.

In Chapter 5, PEG-SS-PLA diblock copolymer will be required for further works including comparative studies where PTX encapsulation and its release will be studied with PEG-SS-PLA block copolymers with varying PLA chain lengths to study the relationship between PTX loading and PLA chain length. In addition, biological studies will be performed including cellular viability, cellular uptake to study *in vitro* cytotoxicity and internalization of PTX-loaded micelles. Depending upon the *in vitro* results, samples will be evaluated for *in vivo* animal models for pharmacokinetics and biodistribution studies.

## References

1. C. F. Thorn, C. Oshiro, S. Marsh, T. Hernandez-Boussard, H. McLeod, T. E. Klein and R. B. Altman, *Pharmacogenet Genomics*, 2011, 21, 440-446.
2. Z. Zhang, L. Mei and S.-S. Feng, *Expert Opinion on Drug Delivery*, 2013, 10, 325-340.
3. M. Liu, H. Du, W. Zhang and G. Zhai, *Materials Science & Engineering C materials for biological applications*, 2017, 71, 1267-1280.
4. C. I. Crucho, *ChemMedChem*, 2015, 10, 24-38.
5. L. L. Tayo, *Biophysical reviews*, 2017, 9, 931-940.
6. C. P. Reis, R. J. Neufeld, A. J. Ribeiro and F. Veiga, *Nanomedicine*, 2006, 2, 8-21.
7. C. Vauthier and K. Bouchemal, *Pharmaceutical research*, 2009, 26, 1025-1058.
8. L. Brannon-Peppas and J. O. Blanchette, *Advanced drug delivery reviews*, 2004, 56, 1649-1659.
9. K. Kataoka, A. Harada and Y. Nagasaki, *Advanced drug delivery reviews*, 2001, 47, 113-131.
10. K. E. Uhrich, S. M. Cannizzaro, R. S. Langer and K. M. Shakesheff, *Chemical reviews*, 1999, 99, 3181-3198.
11. S. Fredenberg, M. Wahlgren, M. Reslow and A. Axelsson, *International journal of pharmaceutics*, 2011, 415, 34-52.
12. N. V. Rao, H. Ko, J. Lee and J. H. Park, *Frontiers in Bioengineering and Biotechnology*, 2018, 6, 110.
13. S. Mura, J. Nicolas and P. Couvreur, *Nature Materials*, 2013, 12, 991-1003.
14. S. Ganta, H. Devalapally, A. Shahiwala and M. Amiji, *Journal of controlled release*, 2008, 126, 187-204.
15. A. P. Gupta and V. Kumar, *European Polymer Journal*, 2007, 43, 4053-4074.
16. M. Vert, G. Schwarch and J. Coudane, *Journal of Macromolecular Science, Part A*, 1995, 32, 787-796.
17. J. Hao, J. Servello, P. Sista, M. C. Biewer and M. C. Stefan, *Journal of Materials Chemistry*, 2011, 21.
18. P. Mainil-Varlet, B. Rahn and S. Gogolewski, *Biomaterials*, 1997, 18, 257-266.
19. N. Kang, M. E. Perron, R. E. Prud'homme, Y. Zhang, G. Gaucher and J. C. Leroux, *Nano letters*, 2005, 5, 315-319.
20. J.-K. Oh, *Soft Matter*, 2011, 7, 5096-5108.
21. N. Chan, S. Y. An and J. K. Oh, *Polymer Chemistry*, 2014, 5, 1637-1649.
22. N. R. Ko and J. K. Oh, *Biomacromolecules*, 2014, 15, 3180-3189.
23. H. R. Kricheldorf, *Chemosphere*, 2001, 43, 49-54.
24. H. R. Kricheldorf and I. Kreiser-Saunders, *Die Makromolekulare Chemie*, 1990, 191, 1057-1066.
25. D. Bourissou, B. Martin-Vaca, A. Dumitrescu, M. Graullier and F. Lacombe, *Macromolecules*, 2005, 38, 9993-9998.
26. H. R. Kricheldorf, M. Berl and N. Scharnagl, *Macromolecules*, 1988, 21, 286-293.
27. X. Wang, K. Liao, D. Quan and Q. Wu, *Macromolecules*, 2005, 38, 4611-4617.
28. F. E. Kohn, J. G. Van Ommen and J. Feijen, *European Polymer Journal*, 1983, 19, 1081-1088.
29. X. D. Feng, C. X. Song and W. Y. Chen, *Journal of Polymer Science: Polymer Letters Edition*, 1983, 21, 593-600.

30. H. R. Kricheldorf and D.-O. Damrau, *Macromolecular Chemistry and Physics*, 1997, 198, 1753-1766.
31. K. Stridsberg, M. Ryner and A.-C. Albertsson, *Macromolecules*, 2000, 33, 2862-2869.
32. J. Kasperczyk and M. Bero, *Polymer*, 2000, 41, 391-395.
33. J. Sun, W. Shi, D. Chen and C. Liang, *Journal of Applied Polymer Science*, 2002, 86, 3312-3315.
34. B. M. Chamberlain, Y. Sun, J. R. Hagadorn, E. W. Hemmesch, V. G. Young, M. Pink, M. A. Hillmyer and W. B. Tolman, *Macromolecules*, 1999, 32, 2400-2402.
35. H. Tsuji, *Macromolecular Bioscience*, 2005, 5, 569-597.
36. J. Ahmed and S. K. Varshney, *International Journal of Food Properties*, 2011, 14, 37-58.
37. A. Stjern Dahl, A. Finne-Wistrand, A. C. Albertsson, C. M. Backesjo and U. Lindgren, *The Journal of Biomedical Materials Research Part A*, 2008, 87, 1086-1091.
38. J. E. Leibner and J. Jacobus, *The Journal of Organic Chemistry*, 1979, 44, 449-450.
39. T. L. Jones-Lepp, K. E. Varner, M. McDaniel and L. Riddick, *Applied Organometallic Chemistry*, 1999, 13, 881-889.
40. G. Baker, E. Vogel and M. Smith, *Polymer Reviews*, 2008, 48, 64-84.
41. S. Y. Kim, I. G. Shin and Y. M. Lee, *Journal of controlled release*, 1998, 56, 197-208.
42. Y. Zhao, Z. Wang, J. Wang, H. Mai, B. Yan and F. Yang, *Journal of Applied Polymer Science*, 2004, 91, 2143-2150.
43. M. Tobío, R. Gref, A. Sánchez, R. Langer and M. J. Alonso, *Pharmaceutical Research*, 1998, 15, 270-275.
44. D. Štular, B. Tomšič, I. Jerman, B. Simončič, M. Mihelčič, L. Noč and I. German Ilić, *Progress in Organic Coatings*, 2018, 124, 213-223.
45. I. Armentano, N. Bitinis, E. Fortunati, S. Mattioli, N. Rescignano, R. Verdejo, M. A. Lopez-Manchado and J. M. Kenny, *Progress in Polymer Science*, 2013, 38, 1720-1747.
46. J. K. Oh, *Polymer Chemistry*, 2019, 10, 1554-1568.
47. L. Liu and P. Liu, *Frontiers of Materials Science*, 2015, 9, 211-226.
48. J. R. Casey, S. Grinstein and J. Orłowski, *Nature reviews. Molecular cell biology*, 2010, 11, 50-61.
49. H. Izumi, T. Torigoe, H. Ishiguchi, H. Uramoto, Y. Yoshida, M. Tanabe, T. Ise, T. Murakami, T. Yoshida, M. Nomoto and K. Kohno, *Cancer Treatment Reviews*, 2003, 29, 541-549.
50. Y. Wang, P. Brown and Y. Xia, *Nature materials*, 2011, 10, 482-483.
51. M. W. Tibbitt, J. E. Dahlman and R. Langer, *Journal of the American Chemical Society*, 2016, 138, 704-717.
52. H. Cabral and K. Kataoka, *Journal of controlled release*, 2014, 190, 465-476.
53. J. K. Oh, R. Drumright, D. J. Siegwart and K. Matyjaszewski, *Progress in Polymer Science*, 2008, 33, 448-477.
54. M. A. van Dongen, C. A. Dougherty and M. M. Banaszak Holl, *Biomacromolecules*, 2014, 15, 3215-3234.
55. S. S. Kelkar and T. M. Reineke, *Bioconjugate Chemistry*, 2011, 22, 1879-1903.
56. A. Blanazs, S. P. Armes and A. J. Ryan, *Macromolecular Rapid Communications*, 2009, 30, 267-277.
57. A. S. Mikhail and C. Allen, *Journal of controlled release*, 2009, 138, 214-223.
58. X.-B. Xiong, A. Falamarzian, S. M. Garg and A. Lavasanifar, *Journal of controlled release*, 2011, 155, 248-261.

59. L. Li, K. Raghupathi, C. Song, P. Prasad and S. Thayumanavan, *Chemical Communications*, 2014, 50, 13417-13432.
60. A. Harada and K. Kataoka, *Progress in Polymer Science*, 2006, 31, 949-982.
61. N. Nishiyama and K. Kataoka, *Advances in Polymer Science*, 2006, 193, 67-101.
62. C. Allen, D. Maysinger and A. Eisenberg, *Colloids and Surfaces, B: Biointerfaces*, 1999, 16, 3-27.
63. N. Nishiyama and K. Kataoka, in *Polymer Therapeutics II*, Springer, 2006, pp. 67-101.
64. A. S. Mikhail and C. Allen, *J Control Release*, 2009, 138, 214-223.
65. X. B. Xiong, A. Falamarzian, S. M. Garg and A. Lavasanifar, *Journal of controlled release*, 2011, 155, 248-261.
66. L. Dai, J. Liu, Z. Luo, M. Li and K. Cai, *Journal of Materials Chemistry B*, 2016, 4, 6758-6772.
67. S. Taurin, H. Nehoff and K. Greish, *Journal of controlled release*, 2012, 164, 265-275.
68. L. Zhang, Y. Li and J. C. Yu, *Journal of Materials Chemistry B*, 2014, 2, 452-470.
69. J. W. Nichols and Y. H. Bae, *Nano Today*, 2012, 7, 606-618.
70. D. Klinger and K. Landfester, *Polymer*, 2012, 53, 5209-5231.
71. K. E. Uhrich, S. M. Cannizzaro, R. S. Langer and K. M. Shakesheff, *Chemical Reviews (Washington, DC, United States)*, 1999, 99, 3181-3198.
72. R. E. Drumright, P. R. Gruber and D. E. Henton, *Advanced Materials*, 2000, 12, 1841-1846.
73. O. Dechy-Cabaret, B. Martin-Vaca and D. Bourissou, *Chemical reviews*, 2004, 104, 6147-6176.
74. G. B. Jacobson, R. Shinde, C. H. Contag and R. N. Zare, *Angewandte Chemie International Edition* 2008, 47, 7880-7882.
75. S. Kaihara, S. Matsumura, A. G. Mikos and J. P. Fisher, *Nature Protocols*, 2007, 2, 2767-2771.
76. S. M. Guillaume, *European Polymer Journal*, 2013, 49, 768-779.
77. S. Penczek, M. Cypryk, A. Duda, P. Kubisa and S. Slomkowski, *Progress in Polymer Science*, 2007, 32, 247-282.
78. H. R. Kricheldorf, I. Kreiser-Saunders and A. Stricker, *Macromolecules*, 2000, 33, 702-709.
79. H. R. Kricheldorf, I. Kreiser-Saunders and C. Boettcher, *Polymer*, 1995, 36, 1253-1259.
80. A. Kowalski, A. Duda and S. Penczek, *Macromolecular Rapid Communications*, 1998, 19, 567-572.
81. D. E. Borchmann, N. ten Brummelhuis and M. Weck, *Macromolecules* 2013, 46, 4426-4431.
82. M. Huo, J. Yuan, L. Tao and Y. Wei, *Polymer Chemistry*, 2014, 5, 1519-1528.
83. M. R. Molla and S. Ghosh, *Macromolecules* 2012, 45, 8561-8570.
84. R. Dorresteyn, N. Billecke, M. Schwendy, S. Puetz, M. Bonn, S. H. Parekh, M. Klapper and K. Muellen, *Advanced Functional Materials*, 2014, 24, 4026-4033.
85. R. Dorresteyn, R. Ragg, G. Rago, N. Billecke, M. Bonn, S. H. Parekh, G. Battagliarin, K. Peneva, M. Wagner, M. Klapper and K. Muellen, *Biomacromolecules*, 2013, 14, 1572-1577.
86. N. Kang, M.-E. Perron, R. E. Prud'homme, Y. Zhang, G. Gaucher and J.-C. Leroux, *Nano letters*, 2005, 5, 315-319.

87. Z. Li, D. Yuan, G. Jin, B. H. Tan and C. He, *ACS Applied Materials & Interfaces*, 2016, 8, 1842-1853.
88. W.-L. Chen, S.-J. Liu, C.-H. Leng, H.-W. Chen, P. Chong and M.-H. Huang, *Biomaterials*, 2014, 35, 1686-1695.
89. R. Fenyves, M. Schmutz, I. J. Horner, F. V. Bright and J. Rzayev, *Journal of the American Chemical Society*, 2014, 136, 7762-7770.
90. W.-L. Chen, Y.-F. Peng, S.-K. Chiang and M.-H. Huang, *International Journal of Nanomedicine*, 2015, 10, 2815-2822.
91. Z. Yue, Z. You, Q. Yang, P. Lv, H. Yue, B. Wang, D. Ni, Z. Su, W. Wei and G. Ma, *Journal of Materials Chemistry B*, 2013, 1, 3239-3247.
92. D. P. Y. Chan, S. C. Owen and M. S. Shoichet, *Bioconjugate Chemistry*, 2013, 24, 105-113.
93. A. Basu, K. R. Kunduru, J. Katzhendler and A. J. Domb, *Advanced drug delivery reviews*, 2016, 107, 82-96.
94. H. Yu, X. Shen, Y. Li and Y. Duan, *Journal of Macromolecular Science - Pure and Applied Chemistry*, 2010, 47, 230-234.
95. H. Lee, J. B. Park and J. Y. Chang, *Journal of Polymer Science, Part A: Polymer Chemistry*, 2011, 49, 2859-2865.
96. M. Motornov, Y. Roiter, I. Tokarev and S. Minko, *Progress in Polymer Science*, 2010, 35, 174-211.
97. N. Rapoport, *Progress in Polymer Science*, 2007, 32, 962-990.
98. C. Alexander and K. M. Shakesheff, *Advanced Materials*, 2006, 18, 3321-3328.
99. D. Roy, J. N. Cambre and B. S. Sumerlin, *Progress in Polymer Science*, 2010, 35, 278-301.
100. H. G. Schild, *Progress in Polymer Science*, 1992, 17, 163-249.
101. M. A. Ward and T. K. Georgiou, *Polymers (Basel, Switzerland)*, 2011, 3, 1215-1242.
102. D. Kurzbach, M. J. N. Junk and D. Hinderberger, *Macromolecular Rapid Communications*, 2013, 34, 119-134.
103. H. Ringsdorf, J. Venzmer and F. M. Winnik, *Macromolecules*, 1991, 24, 1678-1686.
104. A. W. Jackson and D. A. Fulton, *Polymer Chemistry*, 2013, 4, 31-45.
105. C. J. F. Rijcken, O. Soga, W. E. Hennink and C. F. van Nostrum, *Journal of controlled release*, 2007, 120, 131-148.
106. Y. Wang, H. Xu and X. Zhang, *Advanced Materials*, 2009, 21, 2849-2864.
107. K. Loomis, K. McNeeley and R. V. Bellamkonda, *Soft Matter*, 2011, 7, 839-856.
108. M. D. Rikkou and C. S. Patrickios, *Progress in Polymer Science*, 2011, 36, 1079-1097.
109. M. H. Lee, Z. Yang, C. W. Lim, Y. H. Lee, D. Sun, C. Kang and J. S. Kim, *Chemical reviews*, 2013, 113, 5071-5109.
110. C. Deng, Y. Jiang, R. Cheng, F. Meng and Z. Zhong, *Nano Today*, 2012, 7, 467-480.
111. H. Wei, R.-X. Zhuo and X.-Z. Zhang, *Progress in Polymer Science*, 2013, 38, 503-535.
112. J. F. Quinn, M. R. Whittaker and T. P. Davis, *Polymer Chemistry*, 2017, 8, 97-126.
113. S. Binauld and M. H. Stenzel, *Chemical Communications*, 2013, 49, 2082-2102.
114. G. Kocak, C. Tuncer and V. Butun, *Polymer Chemistry*, 2017, 8, 144-176.
115. M.-H. Xiong, Y. Bao, X.-J. Du, Z.-B. Tan, Q. Jiang, H.-X. Wang, Y.-H. Zhu and J. Wang, *ACS Nano*, 2013, 7, 10636-10645.

116. I. Rosenbaum, A. J. Harnoy, E. Tirosh, M. Buzhor, M. Segal, L. Frid, R. Shaharabani, R. Avinery, R. Beck and R. J. Amir, *Journal of the American Chemical Society*, 2015, 137, 2276-2284.
117. A. J. Harnoy, I. Rosenbaum, E. Tirosh, Y. Ebenstein, R. Shaharabani, R. Beck and R. J. Amir, *Journal of the American Chemical Society*, 2014, 136, 7531-7534.
118. Y. Zhao, *Macromolecules* 2012, 45, 3647-3657.
119. G. Liu, W. Liu and C.-M. Dong, *Polymer Chemistry*, 2013, 4, 3431-3443.
120. H. Zhao, E. S. Sterner, E. B. Coughlin and P. Theato, *Macromolecules* 2012, 45, 1723-1736.
121. R. Cheng, F. Feng, F. Meng, C. Deng, J. Feijen and Z. Zhong, *Journal of controlled release*, 2011, 152, 2-12.
122. A. Russo, W. DeGraff, N. Friedman and J. B. Mitchell, *Cancer research*, 1986, 46, 2845-2848.
123. J. Yu, X. Chu and Y. Hou, *Chemical Communications*, 2014, 50, 11614-11630.
124. C. Alvarez-Lorenzo and A. Concheiro, *Chemical Communications*, 2014, 50, 7743-7765.
125. R. Li and Y. Xie, *Journal of controlled release*, 2017, 251, 49-67.
126. G. K. Such, Y. Yan, A. P. R. Johnston, S. T. Gunawan and F. Caruso, *Advanced Materials*, 2015, 27, 2278-2297.
127. Q. Zhang, S. Aleksanian, A. Cunningham and J. K. Oh, *ACS symposium series. American Chemical Society*, 2012, 1101, 287-302.
128. Q. Zhang, N. R. Ko and J. K. Oh, *Chemical Communications*, 2012, 48, 7542-7552.
129. S. Aleksanian, B. Khorsand, R. Schmidt and J. K. Oh, *Polymer Chemistry*, 2012, 3, 2138-2147.
130. A. Nelson-Mendez, S. Aleksanian, M. Oh, H.-S. Lim and J. K. Oh, *Soft Matter*, 2011, 7, 7441-7452.
131. D. Han, X. Tong and Y. Zhao, *Macromolecules*, 2011, 44, 437-439.
132. N. Ma, Y. Li, H. Xu, Z. Wang and X. Zhang, *Journal of the American Chemical Society*, 2010, 132, 442-443.
133. Q. Zhang, S. Aleksanian, S. M. Noh and J. K. Oh, *Polymer Chemistry*, 2013, 4, 351-359.
134. B. Khorsand, G. Lapointe, C. Brett and J. K. Oh, *Biomacromolecules*, 2013, 14, 2103-2111.
135. J.-H. Ryu, R. T. Chacko, S. Jiwpanich, S. Bickerton, R. P. Babu and S. Thayumanavan, *Journal of the American Chemical Society*, 2010, 132, 17227-17235.
136. J.-H. Ryu, S. Jiwpanich, R. Chacko, S. Bickerton and S. Thayumanavan, *Journal of the American Chemical Society*, 2010, 132, 8246-8247.
137. Z. Jia, L. Wong, T. P. Davis and V. Bulmus, *Biomacromolecules*, 2008, 9, 3106-3113.
138. K. Rahimian, Y. Wen and J. K. Oh, *Polymer*, 2015, 72, 387-394.
139. D. Biswas, S. Y. An, Y. Li, X. Wang and J. K. Oh, *Molecular Pharmaceutics*, 2017, DOI: 10.1021/acs.molpharmaceut.6b01146, Ahead of Print.
140. N. Chan, S. Y. An, N. Yee and J. K. Oh, *Macromolecular Rapid Communications*, 2014, 35, 752-757.
141. N. Chan, B. Khorsand, S. Aleksanian and J. K. Oh, *Chemical Communications*, 2013, 49, 7534-7536.
142. N. Chan, N. R. Ko, S. Y. An, B. Khorsand and J. K. Oh, *ACS symposium series. American Chemical Society*, 2015, 1188, 273-291.

143. A. Klaikherd, C. Nagamani and S. Thayumanavan, *Journal of the American Chemical Society*, 2009, 131, 4830-4838.
144. W. Chen, P. Zhong, F. Meng, R. Cheng, C. Deng, J. Feijen and Z. Zhong, *Journal of controlled release*, 2013, 169, 171-179.
145. N. Song, M. Ding, Z. Pan, J. Li, L. Zhou, H. Tan and Q. Fu, *Biomacromolecules*, 2013, 14, 4407-4419.
146. T. Sun, P. Li and J. K. Oh, *Macromolecular Rapid Communications*, 2015, 36, 1742-1748.
147. N. R. Ko, K. Yao, C. Tang and J. K. Oh, *Journal of Polymer Science, Part A: Polymer Chemistry*, 2013, 51, 3071-3080.
148. N. R. Ko, G. Sabbatier, A. Cunningham, G. Laroche and J. K. Oh, *Macromolecular Rapid Communications*, 2014, 35, 447-453.
149. N. R. Ko, J. Cheong, A. Noronha, C. J. Wilds and J. K. Oh, *Colloids and Surfaces, B: Biointerfaces*, 2015, 126, 178-187.
150. B. Khorsand Sourkahi, A. Cunningham, Q. Zhang and J. K. Oh, *Biomacromolecules*, 2011, 12, 3819-3825.
151. S.-X. Li, L. Liu, L.-J. Zhang, B. Wu, C.-X. Wang, W. Zhou, R.-X. Zhuo and S.-W. Huang, *Polymer Chemistry*, 2016, 7, 5113-5122.
152. A. Cunningham and J. K. Oh, *Macromolecular Rapid Communications*, 2013, 34, 163-168.
153. A. Cunningham, N. R. Ko and J. K. Oh, *Colloids and Surfaces, B: Biointerfaces*, 2014, 122, 693-700.
154. H.-C. Kim, E. Kim, T.-L. Ha, S. W. Jeong, S. G. Lee, S. J. Lee and B. Lee, *Colloids and Surfaces, B: Biointerfaces*, 2015, 127, 206-212.
155. N. R. Ko and J. K. Oh, *Biomacromolecules*, 2014, 15, 3180-3189.
156. J. Liu, Y. Pang, W. Huang, X. Huang, L. Meng, X. Zhu, Y. Zhou and D. Yan, *Biomacromolecules*, 2011, 12, 1567-1577.
157. Y. Guo, B. Niu, Q. Song, Y. Zhao, Y. Bao, S. Tan, L. Si and Z. Zhang, *Journal of Materials Chemistry B*, 2016, 4, 2338-2350.
158. X. Guo, X. Wei, Y. Jing and S. Zhou, *Advanced Materials*, 2015, 27, 6450-6456.
159. S. V. Lale, A. Kumar, S. Prasad, A. C. Bharti and V. Koul, *Biomacromolecules*, 2015, 16, 1736-1752.
160. Q. Yang, L. Bai, Y. Zhang, F. Zhu, Y. Xu, Z. Shao, Y.-M. Shen and B. Gong, *Macromolecules* 2014, 47, 7431-7441.
161. C. He, Z. Zhang, Q. Yang, Q. Chang, Z. Shao, B. Gong, Y.-M. Shen, B. Liu and Z. Zhu, *Polymer Chemistry*, 2016, 7, 4352-4366.
162. Q. Yang, C. He, Y. Xu, B. Liu, Z. Shao, Z. Zhu, Y. Hou, B. Gong and Y.-M. Shen, *Polymer Chemistry*, 2015, 6, 1454-1464.
163. Q. Yang, C. He, Z. Zhang, L. Tan, B. Liu, Z. Zhu, Z. Shao, B. Gong and Y.-M. Shen, *Polymer*, 2016, 90, 351-362.
164. W. Hu, C. He, L. Tan, B. Liu, Z. Zhu, B. Gong, Y.-M. Shen and Z. Shao, *Polymer Chemistry*, 2016, 7, 3145-3155.
165. Y. Cao, M. Gao, C. Chen, A. Fan, J. Zhang, D. Kong, Z. Wang, P. Dan and Y. Zhao, *Nanotechnology*, 2015, 26, 115101/115101-115101/115109.
166. Y. Guo, P. Zhang, Q. Zhao, K. Wang and Y. Luan, *Macromolecular Bioscience*, 2016, 16, 420-431.

167. F. Zhu, Q. Yang, Y. Zhuang, Y. Zhang, Z. Shao, B. Gong and Y.-M. Shen, *Polymer*, 2014, 55, 2977-2985.
168. S. Li, K. Hu, W. Cao, Y. Sun, W. Sheng, F. Li, Y. Wu and X.-J. Liang, *Nanoscale*, 2014, 6, 13701-13709.
169. Z. Zhang, Q. Lv, X. Gao, L. Chen, Y. Cao, S. Yu, C. He and X. Chen, *ACS Applied Materials & Interfaces*, 2015, 7, 8404-8411.
170. N. Liu, B. Li, C. Gong, Y. Liu, Y. Wang and G. Wu, *Colloids and Surfaces, B: Biointerfaces*, 2015, 136, 562-569.
171. Z. Hami, M. Amini, M. Ghazi-Khansari, M. Rezayat Seyed and K. Gilani, *Colloids and surfaces. B, Biointerfaces*, 2014, 116, 309-317.
172. Y. Yu, C.-K. Chen, W.-C. Law, H. Sun, P. N. Prasad and C. Cheng, *Polymer Chemistry*, 2015, 6, 953-961.
173. M. N. Ganivada, P. Kumar, P. Kanjilal, H. Dinda, J. D. Sarma and R. Shunmugam, *Polymer Chemistry*, 2016, 7, 4237-4245.
174. Y. Zhang Can, Q. Yang You, X. Huang Tu, B. Zhao, D. Guo Xin, F. Wang Ju and J. Zhang Li, *Biomaterials*, 2012, 33, 6273-6283.
175. X. Zhang, D. Chen, S. Ba, J. Zhu, J. Zhang, W. Hong, X. Zhao, H. Hu and M. Qiao, *Biomacromolecules*, 2014, 15, 4032-4045.
176. R. Liu, B. He, D. Li, Y. Lai, J. Z. Tang and Z. Gu, *Macromolecular Rapid Communications*, 2012, 33, 1061-1066.
177. L. Wu Xiang, H. Kim Jong, H. Koo, M. Bae Sang, H. Shin, S. Kim Min, B.-H. Lee, R.-W. Park, I.-S. Kim, K. Choi, C. Kwon Ick, K. Kim and S. Lee Doo, *Bioconjugate Chemistry*, 2010, 21, 208-213.
178. Y. Gao, Y. Zhou, L. Zhao, C. Zhang, Y. Li, J. Li, X. Li and Y. Liu, *Acta Biomaterialia*, 2015, 23, 127-135.
179. V. M. Gaspar, P. Baril, E. C. Costa, D. de Melo-Diogo, F. Foucher, J. A. Queiroz, F. Sousa, C. Pichon and I. J. Correia, *Journal of Controlled Release*, 2015, 213, 175-191.
180. K. Hu, H. Zhou, Y. Liu, Z. Liu, J. Liu, J. Tang, J. Li, J. Zhang, W. Sheng, Y. Zhao, Y. Wu and C. Chen, *Nanoscale*, 2015, 7, 8607-8618.
181. S.-Y. Lee, J. Y. Tyler, S. Kim, K. Park and J.-X. Cheng, *Molecular Pharmaceutics*, 2013, 10, 3497-3506.
182. S.-Y. Lee, S. Kim, J. Y. Tyler, K. Park and J.-X. Cheng, *Biomaterials*, 2013, 34, 552-561.
183. X. Du, S. Yin, F. Zhou, X. Du, J. Xu, X. Gu, G. Wang and J. Li, *International journal of pharmaceutics*, 2018, 550, 1-13.
184. V. M. Gaspar, P. Baril, E. C. Costa, D. de Melo-Diogo, F. Foucher, J. A. Queiroz, F. Sousa, C. Pichon and I. J. Correia, *Journal of controlled release*, 2015, 213, 175-191.
185. J. He and Y. Zhao, *Dyes and Pigments*, 2011, 89, 278-283.
186. C. Zhao, S. Shuai, S. Zhou, Y. Liu, W. Huo, H. Zhu, Z. Rao, Y. Li, K. Zhou, W. Ge and J. Hao, *Materials Letters*, 2020, 261.
187. S. H. Sadr, S. Davaran, E. Alizadeh, R. Salehi and A. Ramazani, *Journal of Drug Delivery Science and Technology*, 2018, 45, 240-254.
188. Y. Zhu, C. Chen, Z. Cao, S. Shen, L. Li, D. Li, J. Wang and X. Yang, *Theranostics*, 2019, 9, 8312-8320.
189. Y. Shen, B. Cao, N. R. Snyder, K. M. Woeppel, J. R. Eles and X. T. Cui, *Journal of nanobiotechnology*, 2018, 16, 13.

190. J. Zhu, M. Qiao, Q. Wang, Y. Ye, S. Ba, J. Ma, H. Hu, X. Zhao and D. Chen, *Biomaterials*, 2018, 162, 47-59.
191. M. T. Gambles, B. Fan, A. Borecki and E. R. Gillies, *ACS Omega*, 2018, 3, 5002-5011.
192. K. Knop, R. Hoogenboom, D. Fischer and U. S. Schubert, *Angewandte Chemie International Edition* 2010, 49, 6288-6308.
193. S. Mura, J. Nicolas and P. Couvreur, *Nature Materials*, 2013, 12, 991-1003.
194. G. Saito, J. A. Swanson and K.-D. Lee, *Advanced drug delivery reviews*, 2003, 55, 199-215.
195. K. K. Bawa and J. K. Oh, *Molecular Pharmaceutics*, 2017, 14, 2460-2474.
196. I. F. Tannock and D. Rotin, *Cancer research*, 1989, 49, 4373-4384.
197. S. Liu, R. J. Ono, C. Yang, S. Gao, J. Y. Ming Tan, J. L. Hedrick and Y. Y. Yang, *ACS Applied Materials & Interfaces*, 2018, 10, 19355-19364.
198. A. M. Jazani and J. K. Oh, *Macromolecules*, 2017, 50, 9427-9436.
199. K. Matyjaszewski and J. Xia, *Chemical reviews*, 2001, 101, 2921-2990.
200. Y. Ding, C. Du, J. Qian, L. Zhou, Y. Su, R. Zhang and C.-M. Dong, *Polymer Chemistry*, 2018, 9, 3488-3498.
201. Y. Li, Y. Li, W. Ji, Z. Lu, L. Liu, Y. Shi, G. Ma and X. Zhang, *Journal of the American Chemical Society*, 2018, 140, 4164-4171.
202. X. Zeng, X. Zhou, M. Li, C. Wang, J. Xu, D. Ma and W. Xue, *Journal of Materials Science: Materials in Medicine*, 2015, 26, 1-12.
203. B. S. Bolu, R. Sanay and A. Sanyal, *Molecules*, 2018, 118, 3965-3991.
204. V. Delplace and J. Nicolas, *Nature Chemistry*, 2015, 7, 771-784.
205. A. Russo, W. DeGraff, N. Friedman and J. B. Mitchell, *Cancer research*, 1986, 46, 2845-2848.
206. P. Kuppusamy, H. Li, G. Ilangovan, A. J. Cardounel, J. L. Zweier, K. Yamada, M. C. Krishna and J. B. Mitchell, *Cancer research*, 2002, 62, 307-312.
207. K. K. Bawa, A. M. Jazani, C. Shetty and J. K. Oh, *Macromolecular Rapid Communications*, 2018, 39, n/a.
208. C. Nehate, A. A. Moothedathu Raynold, V. Haridas and V. Koul, *Biomacromolecules*, 2018, 19, 2549-2566.
209. L. Xiao, L. Huang, F. Moingeon, M. Gauthier and G. Yang, *Biomacromolecules*, 2017, 18, 2711-2722.
210. S. Petrova, E. Jager, R. Konefal, A. Jager, C. G. Venturini, J. Spevacek, E. Pavlova and P. Stepanek, *Polymer Chemistry*, 2014, 5, 3884-3893.
211. A. M. Jazani, N. Arezi, K. Maruya-Li, S. Jung and J. K. Oh, *ACS Omega*, 2018, 3, 8980-8991.
212. G. S. Kwon and K. Kataoka, *Advanced Drug Delivery Reviews*, 1995, 16, 295-309.
213. G. S. Kwon and T. Okano, *Advanced Drug Delivery Reviews*, 1996, 21, 107-116.
214. A. Zimmer and J. Kreuter, *Advanced Drug Delivery Reviews*, 1995, 16, 61-73.
215. W. C. Lee, Y. C. Li and I. M. Chu, *Macromolecular Bioscience*, 2006, 6, 846-854.
216. A. K. Jain, A. K. Goyal, N. Mishra, B. Vaidya, S. Mangal and S. P. Vyas, *International journal of pharmaceutics*, 2010, 387, 253-262.
217. J. Matsumoto, Y. Nakada, K. Sakurai, T. Nakamura and Y. Takahashi, *International journal of pharmaceutics*, 1999, 185, 93-101.
218. A. J. Bradley, K. L. Murad, K. L. Regan and M. D. Scott, *Biochimica et biophysica acta*, 2002, 1561, 147-158.

219. R. Gref, M. Lück, P. Quellec, M. Marchand, E. Dellacherie, S. Harnisch, T. Blunk and R. H. Müller, *Colloids and surfaces. B, Biointerfaces*, 2000, 18, 301-313.
220. J. Wang, S. Li, Y. Han, J. Guan, S. Chung, C. Wang and D. Li, *Frontiers in Pharmacology*, 2018, 9, 202.
221. S. C. Kim, D. W. Kim, Y. H. Shim, J. S. Bang, H. S. Oh, S. W. Kim and M. H. Seo, *Journal of Controlled Release*, 2001, 72, 191-202.
222. M. E. Werner, N. D. Cummings, M. Sethi, E. C. Wang, R. Sukumar, D. T. Moore and A. Z. Wang, *International Journal of Radiation Oncology\*Biophysics*, 2013, 86, 463-468.
223. A. Vazquez, J. J. Kamphorst, E. K. Markert, Z. T. Schug, S. Tardito and E. Gottlieb, *Journal of cell science*, 2016, 129, 3367-3373.